NBS BUILDING SCIENCE SERIES 73

U.S. DEPARTMENT OF COMMERCE / National Bureau of Standards

Structural Performance of Masonry Walls Under Compression and Flexure

The Building Science Series

The Building Science Series disseminates technical information developed at the National Bureau of Standards on building materials, components, systems, and whole structures. The Series presents research results, test methods, and performance criteria related to the structural and environmental functions and the durability and safety characteristics of building elements and systems.

These publications, similar in style and content to the NBS Building Materials and Structures Reports (1938-59), are directed toward the manufacturing, design, construction, and research segments of the building industry, standards organizations, and officials responsible for building codes.

The material for this Series originates principally in the Center for Building Technology of the NBS Institute for Applied Technology. The publications are divided into three general groups: Building Systems and Processes; Health, Safety and Comfort; and Structures and Materials. For further information regarding these publications please contact the Program Planning and Liaison Unit, Center for Building Technology, Institute for Applied Technology, National Bureau of Standards, Washington, D.C. 20234.

[See mailing list announcement on last page]

Structural Performance of Masonry Walls Under Compression and Flexure

S. G. Fattal and L. E. Cattaneo

Center for Building Technology
Institute for Applied Technology
National Bureau of Standards
Washington, D.C. 20234

Sponsored by

Brick Institute of America
1750 Old Meadows Rd.
McLean, Va. 22101
National Concrete Masonry Assoc.,
1800 North Kent Street
Arlington, Va. 22209
The Departments of the Army, the Navy,
and the Air Force

and

The National Bureau of Standards

U.S. DEPARTMENT OF COMMERCE, Rogers C. B. Morton, *Secretary*

James A. Baker, III, *Under Secretary*

Dr. Betsy Ancker-Johnson, *Assistant Secretary for Science and Technology*

NATIONAL BUREAU OF STANDARDS, Ernest Ambler, *Acting Director*

Issued June 1976

Library of Congress Cataloging in Publication Data
Fattal, S G
Structural performance of masonry walls under compression and flexure.
(NBS Building Science Series ; 73)
Bibliography: p.
Supt. of Docs. No.: C 13.29/2:73.
1. Masonry--Testing. 2. Walls--Testing. I. Cattaneo, L. E., joint author. II. Brick Institute of America. III. Title. IV. Series: United States.
National Bureau of Standards. Building Science Series ; 73.
TA435.U58 no. 73 [TA670] 690'.08s [693.2'1] 75-619305

National Bureau of Standards Building Science Series 73

Nat. Bur. Stand. (U.S.), Bldg. Sci. Ser. 73, 65 pages (June 1976)
CODEN: BSSNBV

U.S. GOVERNMENT PRINTING OFFICE
WASHINGTON: 1976

For sale by the Superintendent of Documents, U.S. Government Printing Office, Washington, D.C. 20402 (Order by SD Catalog No. C13.29/2:73). Price $1.25. (Add 25 percent additional for other than U.S. mailing).
Stock No. 003-003-01479-6

Contents

Notation

A	Area of net section
a	Flexural compressive strength coefficient
af'_m	Flexural compressive strength of masonry
b	Width of wall
c	Distance from centroid to outer fiber
E	Modulus of elasticity in compression normal to bed joint
E_i	Initial tangent modulus of elasticity
EI	Flexural rigidity of masonry at failure
e	Eccentricity relative to centroid of section
e_k	Distance from centroid to edge of kern
f'_m	Compressive strength of masonry determined from axial prism tests
f'_t	Tensile strength of masonry determined from modulus of rupture tests
g	Coefficient in the evaluation of M_e
h	Unsupported height of wall
I, I_n	Moment of inertia of section based on uncracked net section
L	Height of wall between lateral supports
M	Resultant moment on cross section
M_e	Maximum moment capacity, computed using linear stress gradients
M_k	Moment developed by P_k applied at the edge of the kern
M_0	Maximum moment capacity exclusive of slenderness effect
m	Ratio of elastic moduli in composite section
P	Resultant compressive force on cross section
P_{cr}	Critical buckling load for walls with pinned supports
P_k	Vertical load capacity when load is applied at the edge of the kern of a wall section
P_0	Short-wall axial load capacity determined on the basis of prism strength
t	Thickness of wall
w	Distributed transverse load
Δ	Maximum transverse deflection

SI Conversion Units

In view of present accepted practice in this technological area, U.S. customary units of measurement have been used throughout this report. It should be noted that the U.S. is a signatory to the General Conference on Weights and Measures which gave official status to the metric SI system of units in 1960. Readers interested in making use of the coherent system of SI units will find conversion factors in ASTM Standard Metric Practice Guide, ASTM Designation E 380–72 (available from American Society for Testing and Materials, 1916 Race Street, Philadelphia, Pennsylvania 19103). Conversion factors for units used in this paper are:

Length

1 in = 0.0254* meter
1 ft = 0.3048* meter

Area

1 $in^2 = 6.4516 \times 10^{-4}$ $meter^2$
1 $ft^2 = 9.2903 \times 10^{-2}$ $meter^2$

Force

1 lb (lbf) = 4.448 newton
1 kip = 4448 newton

Pressure, Stress

1 psi = 6895 pascal
1 psf = 47.88 pascal

Mass/Volume

1 lb/ft^3 (lbm/ft^3) = 16.02 $kilogram/meter^3$

Moment

1 lbf-ft = 1.3558 newton-meter
1 lbf-in = 0.1130 newton-meter

Temperature

°C = 5/9 (Temperature °F − 32)

*Exactly.

Structural Performance of Masonry Walls Under Compression and Flexure*

S. G. Fattal and L. E. Cattaneo

Ninety-five prisms and 56 walls of brick, concrete block and composite brick and block masonry construction were tested under various combinations of compressive and transverse loads. Constitutive relations for masonry are developed from test results. By using rational analysis it is shown that prism strength can be predicted on the basis of linear behavior at failure. It is also shown that wall strength can be predicted on the basis of prism strength when an appropriate allowance is made for the effect of wall slenderness on sectional capacity.

Key words: Brick; buckling; composite walls; compressive strength; concrete block; constitutive relations; flexural strength; masonry; masonry walls; mortar; slenderness ratio; standards; stiffness; structural stability; walls.

1. Introduction and Objective

An analytical approach recently proposed [1, 2, 17],[1] was used to demonstrate that the strength of masonry walls can be predicted by using the strength of prisms of similar construction together with moment-amplification factors to account for the slenderness of the walls.

The objective of this investigation was to expand and supplement the earlier study by exploiting new experimental evidence on constitutive relationships and the strength of masonry prism and wall specimens of brick, concrete block and composite brick and block construction.

The results of tests of prisms and walls of various types of masonry construction are reported in sections 1 through 6. The interpretation of test results and the analytical approach to predict the strength of masonry walls on the basis of experimental evidence is presented in section 7. Conclusions and recommendations are summarized in section 8.

On the basis of available test results from many different types of masonry construction, it is reasonable to assume that the consistent rational procedure, which is corroborated by the experimental evidence obtained in this and other programs, can be applied to types of masonry construction not yet tested, with appropriate allowance for their physical and mechanical characteristics.

2. Scope

Tests were conducted on prisms and walls having the following nominal thicknesses and material compositions:

1. 4-in brick
2. 6-in hollow concrete block
3. 10-in brick and block composite.

All specimens were constructed using portland cement-lime mortar. For each type of construction, a minimum of 30 prisms and 14 walls were tested. In order to obtain correlation between prism and wall strengths, companion prism specimens were constructed for each wall tested, using similar cross-sectional dimensions and masonry composition, and were tested under similar support conditions. As indicated in table 2.1, a total of 95 prisms and 56 walls were tested.

The prisms were subjected to vertical compressive loads applied at various equal, top and bottom eccentricities with respect to the centroid of the cross section. Prisms were also tested in bending, using uniformly distributed transverse load; one-third point, transverse loading; and in accordance with the ASTM E149–66 [3] standard test method. Walls were tested under transverse load, and different combinations of transverse and vertical load.

TABLE 2.1. *Scope and number of tests*

Type of specimen	Vertical loading		Transverse loading	Vertical and transverse loading	Number of specimens
	Centerline	Eccentric			
Brick prisms	8	12	10	–	30
Hollow concrete block prisms	8	12	10	5	35
Brick-block composite prisms	7	13	10	–	30
Brick walls	4	6	2	2	14
Hollow concrete block walls	4	14	2	6	26
Brick block composite walls	2	6	4	4	16
Total number of specimens					151

*This work was partly supported by financial grants from the Brick Institute of America, National Concrete Masonry Association and the Tri-Service Building Materials Investigational Program (Office of the Chief of Engineers; Naval Facilities Engineering Command; Headquarters, U.S. Air Force).

[1] Figures in brackets indicate the literature references at the end of this paper.

3. Materials

All materials used in the construction of test specimens were commercially available and were typical of those commonly used in building construction.

3.1. Brick Units

One type of brick was used; its dimensions and physical properties are given in table 3.1. The brick were extruded, wire-cut units with three round cores as shown in figure 3.1.

3.2. Concrete Block Units

The concrete block units were nominally 6 × 8 × 18-in two-core hollow block. The units are shown in figure 3.1 and their dimensions and physical properties are given in table 3.2. Two shapes of hollow units were used in the test specimens: kerf block and corner block (two square ends). The kerf block units were cut into two pieces and used at the ends of courses requiring a half-unit.

3.3. Mortar

The mortar used in all specimens was type *S* mortar, mixed in accordance with the proportion specifications of ASTM C270–68 [6]. Type I port-

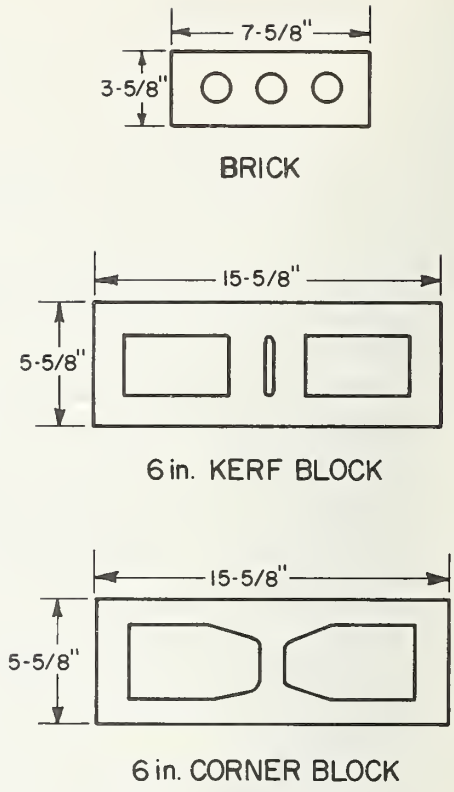

FIGURE 3.1. *Masonry units.*

TABLE 3.1. *Dimensions and physical properties of brick* [a]

Width in	Length in	Height in	Gross area in²	Net solid area percent	Compressive strength (gross area) psi	Absorption percent		Saturation coefficient	Initial rate of absorption g/30 in²/min
						24-h cold	5-h boil		
3.56	7.62	2.25	27.13	79.7	13,085	7.1	9.1	0.76	21.1

[a] Brick was tested in accordance with ASTM C67–66 [4]. Each value in the table represents the average of the results for five specimens.

TABLE 3.2. *Dimensions and physical properties of concrete masonry units* [a]

Unit	Width in	Height in	Length in	Minimum thickness in		Gross area in	Net area percent	Compressive strength psi		Oven dry weight lb	Concrete weight lb/cu ft	Water absorption lb/cu ft
				Face shell	Web			Gross area	Net area			
Corner block	5.60	7.60	15.60	1.05	1.05	87.36	56.3	1243	2210	23.06	106.95	12.97
Kerf block	5.60	7.62	15.60	1.05	1.05	87.36	60.2	1462	2429	25.56	110.37	11.31

[a] Concrete masonry units were tested in accordance to ASTM C140–70 [5]. Each value in the table represents the average of the results for five specimens.

TABLE 3.3. *Compressive strength of mortar cubes for prism specimens*[a]

Batch test number	Age days	Specimen number	Average compressive strength psi
1[b]	—	1A, 2A	—
2	44	3A	1530
3	44	3A	1621
4	58	1B	1541
5	58	1B, 2B	1534
6	76	3B	1478
7	76	3B	1528
8	76	3B	1641
9[b]	—	3B	—
10[b]	—	3B, 1C	—
11[b]	—	1C, 2C	—
12	41	3C1–3	1676
13	41	3C4, 5	1593
14	56	1B6–10	1510
15	56	2B6–10	1501
16	75	3B6, 7	1638
17	75	3B6–9	1559
18	75	3B8, 9	1602
19	74	1C6–10, 3B10	1509
20	37	2D1–5, 1C6–10	1494
21	36	3C6–10	1419
22	36	3C6–10	1455
23	59	1B11–15	1532
24	36	2B11–15, 1B15	1467
25	72	3B11, 12	1335
26	72	3B11–14	1425
27	76	3B13, 14	1368
28	76	3B15	1344
			Avg. 1513

[a] Each value of mortar cube strength represents the average of three test results.
[b] Test data not available.

land cement (ASTM C150–70) [7], type S hydrated lime (ASTM C207–49) [8] and sand were proportioned 1 : ½ : 4½ by volume. Sieve analysis of the sand showed that its fineness modulus which ranged from 1.6 to 1.8 conformed to the requirements of ASTM C144–70 [9]. Although the mortar was proportioned by volume, the measurement of materials used in each batch of mortar was by weight. The mixer used was electrically driven and had rotating blades on a horizontal axis. It was used at half its capacity of 3-ft^3. Upon discharge from the mixer, flow of the mortar was determined in accordance with ASTM Method C185–59 [10]. The values of mortar flow averaged 133.8 percent between the limits of 119.4 percent and 154.3 percent. Air content of the freshly mixed mortar was determined by the pressure method in ASTM Method C231–68 [11] and averaged 7.7 percent between limits of 5.8 percent and 9.5 percent.

A total of 111 batches of mortar were made during the fabrication of prism and wall specimens. Two-inch mortar cubes were made for each batch of mortar used in the prisms and walls, and were air-eured in the laboratory under the same conditions (73° F, 50% R.H.) as the masonry specimens. The mortar cubes were tested at approximately the same age as respective prism and wall specimens. Compressive strengths of the mortar cubes and the identification of the specimens to which they apply are given in tables 3.3 and 3.4 for the respective prism and wall specimens. The average strength of mortar was 1513 psi (between the limits of 1335 and 1676 psi) for the prisms, and 1562 psi (between the limits of 1198 and 2360 psi) for the walls.

Since several batches of mortar were required to construct the walls, the mortar strength varied at different levels in the wall.

3.4. Ties

Galvanized steel ties were used to bond the brick and concrete block wythes of composite masonry specimens. These were of a continuous truss design and consisted of two parallel longitudinal rods welded to a continuous, diagonally folded, cross rod as shown in figure 3.2. The configuration had an outside width of 8 inches and was prefabricated with No. 9 gauge wire.

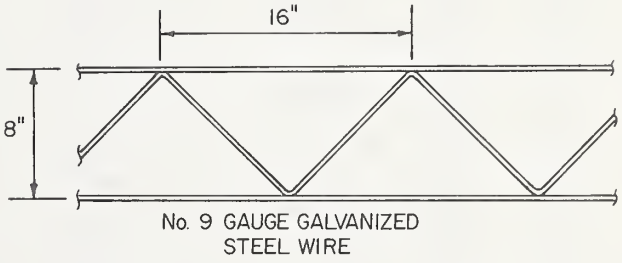

FIGURE 3.2. *Steel ties used in composite construction.*

4. Test Specimens

This section describes the wall and prism specimens and the method of their fabrication. The designations, dimensions, masonry composition, and support conditions of all test specimens are listed in table 4.1. In this table and in the text of the report, the specimens are identified by their nominal dimensions. Actual cross-sectional dimensions are shown in figure 4.1. The net cross-sectional area and the net moment of inertia of each section are given in the same figure. To calculate these properties, a mortar joint thickness of ⅜ in, and a minimum face shell and web thickness of 1.05 in for the hollow block have been assumed.

4.1. Description and Fabrication of Prisms

The prism and wall specimens were fabricated in the same laboratory using similar construction

593-885 O - 76 - 2

TABLE 3.4. *Compressive strength of mortar cubes for prism specimens* [a]

Batch number	Age days	Specimen number	Average compressive strength psi
29	95	4A1	1455
30	95	4A1, 4B1	1422
31	119	4B1, 4C1	1382
32	118	4C1	1373
33	118	4C1	1332
34	94	4A2	1372
35	118	4A2, 4B2	1228
36	115	4C2	1198
37	115	4C2	1264
38	115	4C2, 4A3	1363
39	115	4A3	1257
40	115	4A3	1236
41	109	4B3, 4C3	1499
42	116	4C3	1450
43	116	4C3	1417
44	108	4C3, 4A4	1486
45	111	4A4, 4B4	1323
46	114	4B4, 4C4	1379
47	114	4C4	1315
48	114	4C4	1383
49	133	4A5	1492
50	133	4A5	1631
51	134	4B5, 4C5	1584
52	134	4C5	1555
53	134	4C5	1612
54	133	4A6	1478
55	133	4A6, 4B6	1475
56	133	4B6, 7	1587
57	130	4C6	1527
58	130	4C6	1639
59	135	4C6, 4A7	1602
60	161	4A7	1447
61	160	4A7, 4C7	1602
62	160	4C7	1722
63	160	4C7, 4A8	1516
64	160	4A8	1612
65	162	4A8	1640
66	161	4C8, 4B8	1386
67	161	4C8	1452
68	161	4C8	1509
69	160	4A9	1406
70	160	4A9, 4B9	1393
71	150	4A10	1645
72	149	4A10	1459
73	149	4A11	1468
74	148	4A12	1501
75	148	4A12, 13	1396
76	154	4A13	1535
77	153	4A14	1549
78	153	4A14, 15	1399
79	153	4A15	1671
80	71	4B10, 11	1458
81	71	4B12, 13	1419
82	71	4B14, 15	1476
83	83	4B16, 17	1435
84	83	4B18, 19	1423
85	90	4B20, 21	1521
86	90	4B22, 23	1474
87	94	4B24, 25	1642
88	97	4B26, 27	1548
89	105	4C9, 10	2015
90	100	4C9, 10	2100
91	100	4C9, 10	1946
92	100	4C9, 10	1922
93	100	4C9, 10	1820
94	111	4C11	1460
95	111	4C11	1604
96	111	4C11	1792
97	110	4C12	2360
98	110	4C12	2142
99	110	4C12	2222
100	112	4C13	2192
101	112	4C13	1765
102	112	4C13	1824
103	111	4C14	1524
104	111	4C14	1494
105	111	4C14	1551
106A	112	4C15	1587
106B	112	4C15	1648
107A	112	4C15	1591
107B	112	4C15	1710
108A	112	4C15	1609
108B	112	4C15	1743
			Avg. 1562

[a] Each value of mortar cube strength represents the average of three test results.

methods, workmanship, types of masonry units and mortar. For each of the three types of masonry walls described in section 4.2 (brick, block and brick-block composite), there correspond 15 prisms of the same nominal cross-sectional dimensions as the respective wall types. In table 4.1 these prisms are identified by the letter B appearing in their designation.

At the time of testing, there was no standard ASTM test for determining the compressive strength of masonry prisms. The Brick Institute of America (BIA, formerly Structural Clay Products Institute) [12] at that time recommended a prism not less than 12 inches in height with a height-to-thickness ratio of not more than 5 nor less than 2. Similar recommendations are currently provided by ASTM Standard E 447-72 [14] which was issued after the completion of this testing program. The $4 \times 8 \times 16$-in brick prisms identified by the symbol 1A in their designation were built in stacked bond [2] using six units in as many courses. This gave a height of 15.5 in and a height-to-thickness ratio of 4.4. The $6 \times 16 \times 24$-in hollow concrete block prisms identified by the symbol 2A in their designation were built in stacked bond using three units in as many courses. The National Concrete Masonry Association (NCMA) [13] at the time of testing recommended a prism height not less than 16 in and a height-to-thickness ratio not less than 2. The 23.6-in height and 4.2 height-to-thickness ratio satisfied the NCMA recommendation. The $10 \times 16 \times 32$-in composite

[2] Units in adjacent courses do not overlap, so that all head joints are in vertical alinement.

TABLE 4.1. *Description and number of test specimens*

Type of specimen	Designation	Nominal dimensions in	Nominal height in	Vertical load at eccentricity					Transverse loads	Transverse and vertical loads	End condition	No. of specimens
				0	$t/12$	$t/6$	$t/4$	$t/3$				
Brick prisms	1A1 to 1A5	4× 8×16	16	5							[m]Flat	5
	1B1 to 1B15	4×32×16	16	3	3	3	3	3			Pin	15
	1C1 to 1C10	4× 8×27	24						10		Pin	10
Hollow concrete block prisms	2A1 to 2A5	6×16×24	24	5							Flat	5
	2B1 to 2B15	6×32×24	24	3	3	3	3	3			Pin	15
	2C1 to 2C5	6×16×16	16							5	Pin	5
	2D1 to 2D10	6×16×32	32						10		Pin	10
Brick-block composite prisms	3A1 to 3A5	10×16×32	32	[a]5							Flat	5
	3B1 to 3B15	10×32×32	32	[b]2		[c]4	[d]7	[e]2			Pin	15
	3C1 to 3C10	10×16×32	32						10		Pin	10
Brick walls	4A1 to 4A6, 4A9, 4A10	4×32×96	96	2	2	2		2			Pin	8
	4A7, 4A8			2							Flat	2
	4A11, 4A12								2		Pin	2
	4A13, 4A14									2	Pin	2
Hollow concrete block walls	4B1 to 4B6, 4B11 to 4B15	6×32×96	96	2	2	3	2	2			Pin	11
	4B8, 4B9			2							Flat	2
	4B10, 4B16								2		Pin	2
	4B17 to 4B22									[f]6	Pin	6
	4B23, 4B24							[g]2			Pin	2
	4B25, 4B26, 4B27							[h]3			Pin	3
Brick-block composite walls	4C1 to 4C4, 4C7, 4C8	10×32×96	96	[b]2		[i]2		[j]2			Pin	6
	4C5, 4C6					[k]2					Pin	2
	4C2, 4C9 to 4C11								4		Pin	4
	4C12 to 4C15									[l]4	Pin	4

[a] Load applied at mid-thickness of specimen.
[b] Vertical load positioned at the centroid of transformed composite section.
[c] Load applied at 0.82 in from centroid toward the brick face in one prism and at 1.55 in from centroid toward the block face in three prisms.
[d] Loads applied at 1.64 in from centroid toward the brick face in four prisms and at 3.10 in from centroid toward the block face in three prisms.
[e] Load applied at 4.10 in from centroid toward the block face.
[f] On two of the specimens the vertical load was applied with an eccentricity of $t/4$.
[g] Vertical load eccentricities of $t/3$ and 0 at top and bottom, respectively.
[h] Vertical load eccentricities of $t/3$ and $-t/3$ at top and bottom, respectively.
[i] Vertical load applied at 1.55 in from centroid toward the block face.
[j] Vertical load applied at 3.10 in from centroid toward the block face.
[k] Vertical load applied at 0.82 in from centroid toward the brick face.
[l] Two specimens with vertical load applied 0.82 in from centroid toward the brick face.
[m] Flat and pin refer, respectively, to restraint and freedom of end rotation described in section 5.

prisms, designated by the symbol 3A, were fabricated using three courses of hollow block in stacked bond and nine courses of brick in running bond. The procedure followed in the compressive testing of axially loaded prisms was in accordance with ASTM Test Method E447–72 [14].

ASTM Standard E–518 [23] prescribes a horizontal flexural test method for determining bond strength of masonry. Although this document was not available at the time of testing, the procedures therein described are similar to those used in this test program. The 10-brick prisms of stacked bond, designated by the symbol 1C, were convenient to fabricate and test as simply supported beams in order to determine the modulus of rupture of brick masonry. The two-block hollow concrete prisms (designation 2C) were fabricated for testing flexural bond strength according to ASTM Standard E149–66 [3]. The 6×16×32-in hollow block prisms (2D) and 10×16×32-in composite prisms (3C) were constructed and tested in flexure in a manner similar to that used for the brick prisms.

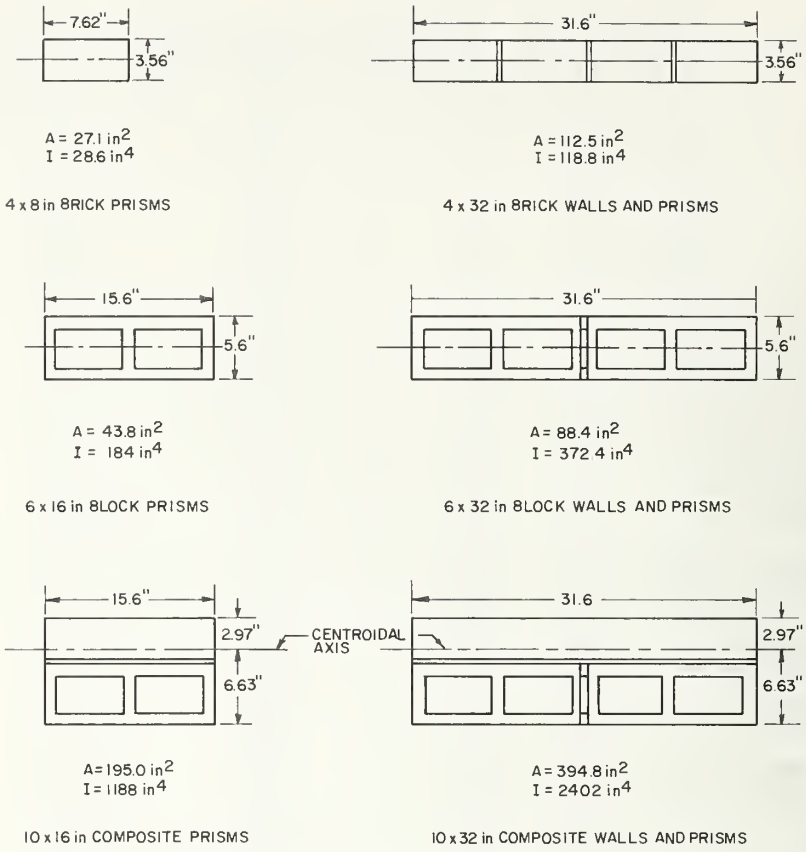

FIGURE 4.1. *Cross-sectional dimensions of test specimens.*

4.2. Description of Walls

All walls were constructed in running bond [3] to a height of approximately 8 ft and were nominally 32-in wide.

The brick walls were of 4-in single-wythe construction with average dimensions of 3.56 × 31.6-in. The brick were laid with full bed and head mortar joints.

The hollow concrete block walls were of 6-in single-wythe construction with average dimensions of 5.6 × 31.6-in. The walls contained 6 × 8 × 16-in whole corner block units having two cores, and half units that were obtained by cutting a kerf block. The bed- and head-joint mortar was applied only to the face shells (face-shell bedding).

The 10-in composite brick and hollow concrete block walls were constructed with 4-in brick facing and 6-in block backing. Full bed and head mortar joints were used in the brick facing and face-shell bedding was used for the horizontal and vertical mortar joints in the hollow block backing. The collar joint was slush-filled with mortar and consolidated in the joint with the aid of a trowel. The brick and block wythes were bonded by continuous truss-type ties (fig. 3.2) imbedded in horizontal joints at a vertical spacing of 16 in. The length of the ties was equal to the width of the specimens.

4.3. Fabrication of Walls

The wall specimens were constructed and air-cured in a laboratory environment maintained at approximately 73° F and 50 percent relative humidity. All specimens were constructed by experienced masons using techniques typical of good workmanship and supervision. The mortar joints on both faces were cut flush and not tooled.

In all wall specimens, the first course was laid directly on a polyethylene sheet placed on the laboratory floor. Walls were erected between wood guides braced in two perpendicular directions to keep them in proper vertical alinement. To control the thickness of bed joints, their locations were marked on the wooden frames at 8-in intervals

[3] Units in adjacent courses overlap by 50 percent and head joints in alternate courses are in vertical alinement.

which corresponded to the height of one block and one 3/8-in joint. Each 8-in interval was further divided into three equal intervals each corresponding to the height of one brick and one joint. Since the average height of the brick units was 2 1/4-inch, the average bed joint thickness for brick specimens was approximately 7/16-inch. The mason kept the outer face of the wall in alinement using a horizontal line and level. The construction of 8-ft wall specimens is shown in figure 4.2.

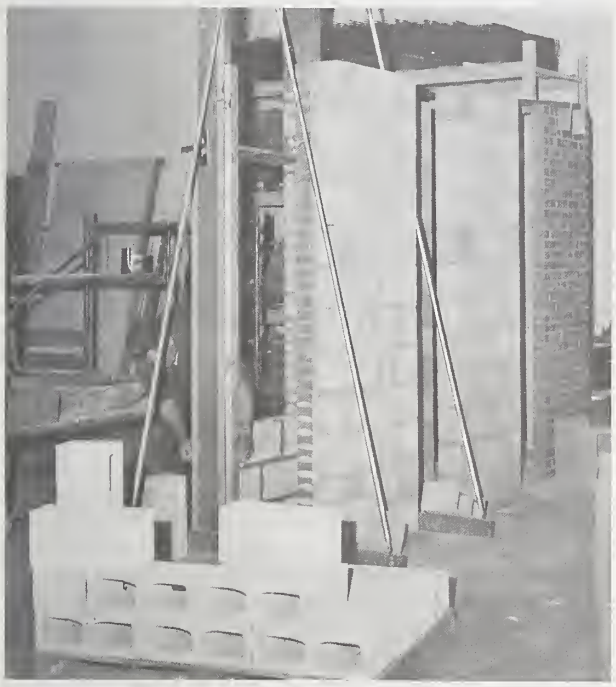

FIGURE 4.2. *Eight-ft brick, hollow concrete block and composite wall specimens.*

5. Test Procedure and Instrumentation

5.1. Prism Tests

All prisms subjected to compressive tests were capped, top and bottom, with high-strength plaster and were tested at a loading rate of 50,000-lb per minute in a 600,000-lb capacity testing machine. The experimental setup used for testing wall panels in vertical compression, as described in greater detail in section 5.3, was closely followed in the compression testing of the prism specimens.

The flexural strength of the masonry prisms was determined by a beam test for brick, concrete block and composite masonry and by a flexural bond test for concrete block masonry. The bond strength in the last test was determined by testing two-block high prisms that were clamped in metal frames at the top and at the bottom of the prism and loaded eccentrically 10 in from the longitudinal centerline of the prism. The test method is described in ASTM Standard E 149–66 [3].

The 10-course brick prisms were tested as beams with the 27-in dimension horizontal. The prisms were supported approximately along the centerline of the two end bricks. The 4-course concrete block prisms were tested as beams with the 32-in dimension horizontal and were supported along lines approximately half a block height from the ends. Equal numbers of these specimens were tested with the concrete face and the brick face in tension, respectively.

Prisms were tested at an average age of approximately 60 days, within a range of 35–75 days.

5.2. Instrumentation for Prism Tests

Test loads on prisms were measured by force transducers of an electrical resistance type or fluid pressure transducers, as required by the various test arrangements.

The prism specimens tested in vertical compression were instrumented with displacement transducers which were linear variable differential transformers (LVDT's) mounted on the specimens to record vertical deformations. The gage length extended between the centers of the top and bottom units and in each case, depended on the height of the specimen. In general, these prisms were instrumented with three LVDT's on each face. The smallest brick prisms ($4 \times 8 \times 16$-in: designation 1A) were instrumented with one LVDT at the centerline of each face and each edge. The output signals from the load transducer and all displacement transducers, except two, were recorded on automatic data-recording equipment for later processing by a digital computer. The signals from two central displacement transducers and the load transducer were monitored by two x-y recorders which provided continuous plots of the load-displacement curves for the opposite sides of the prism.

Two types of transverse loads were separately used on prisms tested in flexure: third-point concentrated loads and uniformly distributed loads induced with an air bag under pressure.

5.3. Wall Tests

A brick wall panel, positioned for testing in vertical compression, is shown in figure 5.1. The experimental setups for compression tests of concrete block walls and composite walls were also similar to that shown in figure 5.1. The vertical load was applied by the head of a hydraulic testing

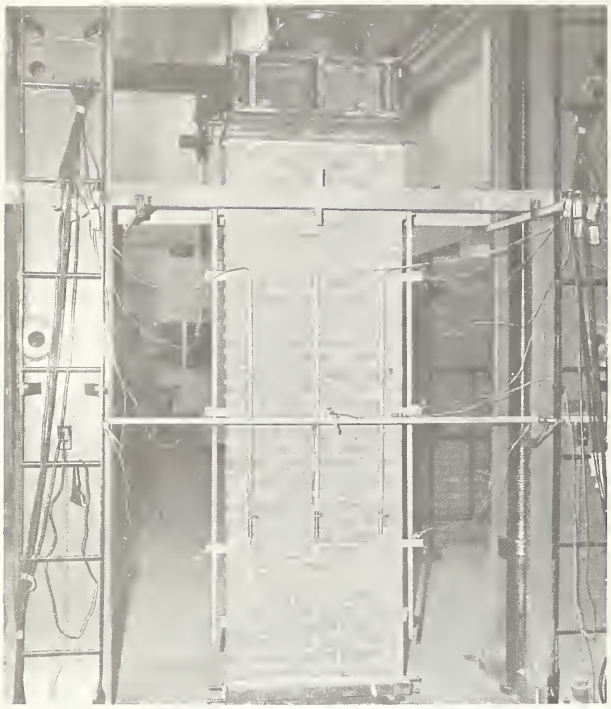

FIGURE 5.1. *Experimental setup for the vertical compression test of a wall free to rotate at its top and base.*

FIGURE 5.2. *Experimental setup for the vertical compression test of a wall in which the rotation at its top and base is prevented.*

machine of 600,000-lb capacity through a 12½-in deep loading beam, a 4½-in diameter half-round steel bar with the flat side toward the loading beam and a 2-in thick steel plate that was bedded in high-strength plaster on the top surface of the wall. In a similar manner, the bottom surface of the wall was seated in plaster on a 2-in thick steel plate positioned over a 4½-in diameter half-round bar with the flat side bearing against the platen of the testing machine. To keep the wall in vertical alinement, temporary wedges were inserted between the bottom steel plate and the floor on opposite sides of the half-round bar. These wedges were removed when the loading head was brought into contact with the loading assembly.

The test setup of figure 5.1 was designed to permit rotation at the top and at the base of the wall. Figure 5.2 shows the setup used for brick and hollow block wall tests designed to prevent end rotation.[4] A concentric vertical load was applied through the loading beam directly to the 2-in thick steel plate attached to the top of the wall. The load was transmitted to the platen through a 2-in thick steel bearing plate at the base of the wall.

The test program included walls tested under uniformly distributed transverse load applied singly or in combination with vertical compressive load. Figure 5.3 shows the test assembly. The transverse load was applied through an air bag, made of 20-mil polyvinyl sheeting, which was 84-in long and extended across the entire width of the wall on one side. The air bag was mounted on a sheet of plywood attached to a steel frame which served as a reaction when the bag was pressurized. The frame was mounted on three wheels for ease of movement. On the opposite side of the wall, upper and lower horizontal reaction bars were spaced with their centerlines 82½-in apart, and attached to another reaction frame on wheels. The two reaction frames were rolled into position on either side of the wall and bolted together near the four corners. A sheet of rubber between the air bag and the specimen provided protection to the bag from abrasion. The reaction bars on the opposite face of the wall were 1-in wide, extended across the entire width of the wall specimen, and were faced with Teflon[5] over leather to provide a quarter-inch thick resilient material. Figure 5.3 shows the assembly with both reaction frames bolted in place, positioned in the 600-kip testing machine which was used to apply the vertical load.

The inlet tube to the air bag was connected to a hand-regulated compressed air line (100 psi maximum pressure). Air pressure was monitored by a piezoresistance pressure transducer connected

[4] The two end conditions described here are called, respectively, "pin end" and "flat end" for brevity in this report.

[5] Trade names are identified in order to adequately specify the experimental procedures. In no case does such identification imply recommendation or endorsement by the National Bureau of Standards, nor does it imply that the material identified is necessarily the best available for the purpose.

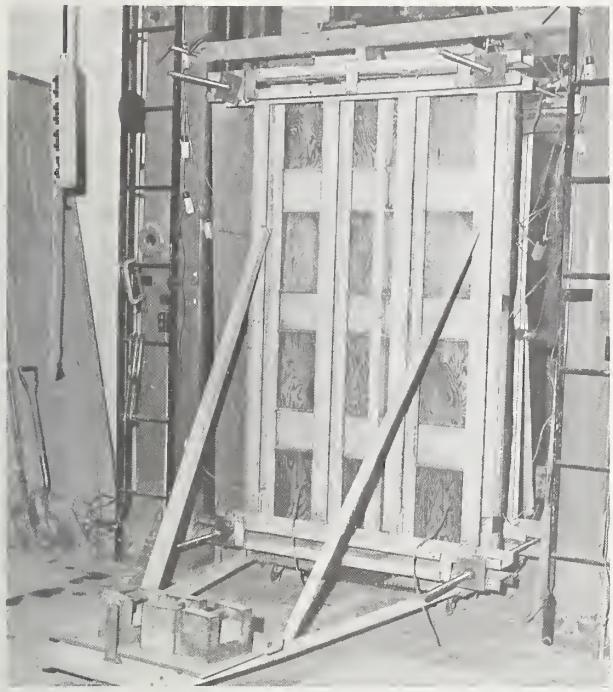

FIGURE 5.3. *Installation of the apparatus for wall tests under transverse uniform load and vertical compressions.*

to the bag outlet tube. Continuous visual monitoring of the air pressure was also accomplished as an alternate backup system, using a mercury manometer which was also connected to the outlet tube. The wall specimens were loaded transversely at a rate of approximately 0.30 to 0.35-psi per minute. In all combined loading tests, the vertical load was applied first, at a rate of 60,000-lb per minute. When the desired vertical load level was reached, it was maintained constant while a transverse load was applied and increased gradually until the specimen failed.

The walls were tested at an average age of approximately 120 days within a range of 70–160 days. They were moved approximately 30 yards from the fabrication area to the testing machine by a fork lift truck. Before moving, the walls were carefully braced with wooden boards strapped to the edges to prevent damage to the specimen.

5.4. Instrumentation for Wall Tests

Vertical loads, transverse loads, vertical deformations, transverse deflections, and transverse strains of the wall specimens were measured and recorded by an automatic electronic multichannel data logging system. The vertical loads were measured with a pressure transducer that was attached to the hydraulic load measuring system of the testing machine. In specimens subjected to transverse uniformly distributed load, the pressure in the air bag was measured with a pressure transducer having a range of 0–50 psi.

Transverse deflections of the wall specimens were measured at 1/4-height, mid-height and 3/4-height with two displacement transducers (LVDT's) at each level, calibrated to read increments of ± 0.0001 in. These LVDT's were attached to 6-ft lengths of 1-in diameter aluminum tubing as shown in figure 5.1. The tubing was attached along the centerline of the two vertical edges of the wall at points 1 ft away from the upper and lower ends of the specimen by hinges to prevent bending of the pipe by out-of-plane rotation of the wall. The lower end of the tubing was allowed to slide in the vertical direction without transverse movement. The ends of the cores of the displacement transducers were attached to aluminum plates that were mounted on the face of the walls at the three levels where deflection measurements were recorded.

Vertical deformations at both faces of the wall specimens were measured with four LVDT's clamped to the lower ends of 1-in diameter aluminum tubing over a 4-ft gage length installed symmetrically with respect to the height and 4 in inside the edges of the specimen. At the upper end, these tubes had a pinned connection to the wall and at the lower end they were attached to a guide which kept the tubes in vertical alinement but permitted them to slide downward when the wall contracted under the load. The centerline of the transducer core was offset at a distance of 1 3/8-in from the face of the wall. Two of the instruments attached to the near face of the wall are shown in figure 5.1.

In the composite wall specimens, 6-in electrical resistance strain gages were attached horizontally across the collar joint at mid-height on both edges to record the transverse strains due to axial compression. In specimens subjected to transverse uniform load, LVDT's for vertical deformation measurement were clamped to the lower ends of the 6-ft aluminum tubing along the edges of the wall since the pressure bag did not permit instrumentation of one face of the wall.

The air-pressure transducer and the displacement transducers provided signals that were recorded on automatic data-recording equipment. Instrument readings were electronically scanned at equal load increments. The tape record was processed by a digital computer. The output consisted of tabulated test results and plotted curves of load versus deformation.

All walls were instrumented with two additional LVDT's which provided an independent set of measurements of the transverse deflection at mid-height and vertical deformation of the specimen. As shown in figure 5.1, the transverse deflection was measured against a stationary cross-bar attached to the legs of the loading frame. The data from these instruments and the corresponding load cell trans-

ducers were monitored with x-y recorders which provided continuous plots of displacement versus applied load.

6. Test Results

6.1. Prism Test Results

A summary of prism test results is given in tables 6.1 through 6.3. Table 6.1 lists results for brick and block prisms tested in vertical compression. Table 6.2 lists results of composite prisms tested in vertical compression. Table 6.3 gives a summary of flexural test results for prisms of the three types of masonry construction.

The compressive strength values in the last column of table 6.1 were calculated using the sectional properties given in figure 4.1 and an assumed linear stress distribution for prisms with the vertical loads applied within the kern eccentricity. For prisms subjected to vertical loads applied at eccentricities greater than the kern eccentricity of the section, the compressive strength was calculated on the basis of sectional properties of the area of contact for the cracked section of the specimen assuming no tensile strength and linear stress distribution. For composite specimens, the last two columns of table 6.2 list the maximum compressive stress at failure in the brick and the block specimens respectively. This stress was calculated on the basis of sectional properties in figure 4.1 for vertical load eccentricities equal to, or less than, the kern eccentricity; or on the basis of cracked-section properties assuming no tensile strength and linear stress distribution for vertical load eccentricities larger than the kern eccentricity. The transformed section was obtained using a modular ratio of 2.6 between brick and concrete masonry (consult sec. 7.2.5). This ratio was obtained from average values of initial elastic moduli derived from the test re-

TABLE 6.1. *Summary of vertical compression tests of brick and hollow block prisms*

Prism designation	Height in	Width in	End conditions	Eccentricity in	Age days	Maximum load kip	Compressive strength [a] psi
4-in Brick prisms							
1A1	15.7	7.6	Flat	0	31	120.0	4423
1A2					31	126.0	4644
1A3					32	122.0	4497
1A4					32	120.0	4423
1A5					32	124.5	4589
Avg						122.5	4515
1B1	15.7	31.6	Pin	0	44	497.0	4418
1B2					45	408.5	3631
1B3					45	450.0	4000
Avg						451.8	4016
1B4	15.7	31.6	Pin	0.297	52	465.0	6200
1B5					52	462.0	6160
1B6					50	495.0	6600
Avg						474.0	6320
1B7	15.7	31.6	Pin	0.593	53	353.0	6275
1B8					53	356.5	6329
1B9					53	331.5	5893
Avg						347.0	6166
1B10	15.7	31.6	Pin	0.890	54	267.0	6329
1B11					57	243.5	5772
1B12					57	267.0	6329
Avg						259.2	6143
1B13	15.7	31.6	Pin	1.187	58	152.0	5404
1B14					58	145.0	5155
1B15					58	151.8	5394
Avg						149.6	5318

sults for axially loaded brick and block prisms. Some of the specimens did not fail under vertical loads applied axially or at low eccentricity, These tests were terminated when the 600-kip capacity of the testing machine was reached.

Figures 6.1 through 6.18 show approximate regression curves through average test data of vertical strain versus vertical load for all prisms tested in vertical compression. For eccentrically loaded specimens, these plots show two curves representing the strains at the two opposite faces of the specimens. It should be noted that vertical deformation measurements actually were recorded at the centerlines of the vertical gages placed 1⅜-in from the faces of the specimens. These data were corrected to provide the strains at the specimen faces by assuming a linear strain distribution between the respective centerlines of the gages at opposite faces of the specimens.

6.2. Prism Failures

In general, the trend of prism failures was similar to those observed in wall specimens of comparable cross section, end conditions and loading configuration. A brief description of prism failures is given in the following sections according to type of specimen.

6.2.1. Brick Prisms

The five-brick stacked bond prisms, tested under axial compression, with flat ends, failed by crushing and splitting in the vertical plane through the circular cores of the units as shown in figure 6.19.

TABLE 6.1. *Summary of vertical compression tests of brick and hollow block prisms*—Continued

Prism designation	Height in	Width in	End conditions	Eccentricity in	Age days	Maximum load kip	Compressive strength [a] psi
6-in Block prisms							
2A1	23.7	15.6	Flat	0	35	54.5	1245
2A2					36	63.4	1448
2A3					37	65.1	1487
2A4					38	75.0	1713
2A5					38	64.5	1473
Avg						64.5	1473
2B1	23.7	31.6	Pin	0	48	127.7	1444
2B2					49	122.5	1385
2B3					49	122.5	1385
Avg						124.2	1405
2B4	23.7	31.6	Pin	0.467	50	120.0	1778
2B5					51	87.8	1300
2B6					49	160.0	2371
Avg						122.6	1816
2B7	23.7	31.6	Pin	0.933	54	115.1	2109
2B8					56	108.9	1996
2B9					56	117.1	2146
Avg						113.7	2084
2B10	23.7	31.6	Pin	1.400	57	82.5	1801
2B11					56	84.4	1843
2B12					56	82.3	1797
Avg						83.1	1814
2B13	23.7	31.6	Pin	1.867	59	62.2	1611
2B14					59	77.0	1994
2B15					62	68.0	1761
Avg						69.1	1789

[a] Based on gross area of brick units and net area of concrete block units.

593-885 O - 76 - 3

TABLE 6.2. *Summary of vertical compression tests of composite prisms*

Prism designation	Height in	Width in	End conditions	Eccentricity in	Age days	Maximum load kip	Maximum compressive stress at failure [a]	
							Brick psi	Block psi
3A1	31.8	15.6	Flat	$e_c^b = 1.230$[c]	42	169.0	899	2024
3A2					44	273.0	1450	3268
3A3					43	190.0	1008	2274
3A4					39	220.8	1172	2644
3A5					43	178.2	951	2133
Avg.						206.2	678	2468
3B1	31.8	31.6	Pin	0	70	> 600	> 1520	> 3951
3B13					76	577.5	1463	3803
Avg.						> 590	> 1491	> 3877
3B1	31.8	31.6	Pin	$e_b^b = 0.820$	70	600.0	5533	1399
3B2					71	600.0	5533	1399
3B3					71	> 600	> 5533	> 1399
Avg.						> 600	> 5533	> 1399
3B4	31.8	31.6	Pin	$e_c = 1.550$	72	341.0	2583	2323
3B5					73	404.0	3060	2752
3B6					74	363.0	2750	2472
Avg.						369.3	2798	2516
3B7	31.8	31.6	Pin	$e_c = 3.100$	75	177.5	1398	1811
3B8					76	150.0	1181	1530
3B9					76	213.5	1681	2178
Avg.						180.3	1420	1840
3B3 [d]	31.8	31.6	Pin	$e_b = 1.640$	71	397.0	6146	325
3B10					74	382.0	5913	313
3B11					75	340.0	5263	278
3B12					75	418.0	6471	342
Avg.						384.2	5948	314
3B14	31.8	31.6	Pin	$e_c = 4.650$	77	117.0	616	1846
3B15					77	100.0	527	1578
Avg.						108.5	572	1712

[a] Values were based on measured net cross-sectional area.
[b] The notation e_c and e_b designates eccentricities of vertical load from the centroid of the composite section toward the concrete block and brick faces, respectively.
[c] Estimated value (basis of derivation explained in sec. 7.3.4).
[d] Specimen which did not fail previously under an axial load equal to the 600-kip capacity of the testing machine was reused for this test.

This failure mode was also observed in axially loaded prisms pinned at the ends. Vertical loads applied at large eccentricities produced specimen failure by crushing at the compression face and by bond separation at the tension face as indicated in figure 6.20. The typical failure of brick prisms tested as beams was by tension in the bond between mortar and brick as shown in figure 6.21.

6.2.2. Block Prisms

The three-block stacked prisms, tested in axial compression, with flat ends, failed by vertical splitting in the web and face shell as shown in figure 6.22. This type of failure was also observed in specimens with pinned ends with vertical loads applied axially or at small eccentricity. As vertical load eccentricity was increased, failure by web splitting was accompanied almost simultaneously by cracking in the horizontal mortar joints on the tensile face of the specimen. This is shown in figure 6.23. Prisms tested as beams failed by tensile cracking in the block as shown in figure 6.24, or, by tensile or bond splitting along the mortar joint.

6.2.3. Composite Prisms

The $10 \times 32 \times 16$-in prisms, tested in vertical compression, failed by vertical splitting in the web of the blocks as shown in figure 6.25. It should be noted that the loading head was positioned symmetrically with respect to the thickness of these specimens, resulting in a vertical load eccentricity toward the block face measured with respect to the centroid of the transformed section. The 600-kip capacity load of the testing machine was not sufficient to cause failure in axially loaded composite prisms.

Vertical eccentric loads applied near the block face produced failures initiated mainly by web splitting in the block for the case of small load eccentricities. At large load eccentricities, failure was initiated by cracking along a mortar bed joint at the brick face accompanied by web splitting and face-shell crushing of the blocks as shown in figure 6.26. Specimens in which the vertical eccentric load was applied near the brick face failed by splitting and crushing of the brick as shown in figure 6.27. Prisms tested as beams failed typically by tensile cracking in the masonry unit or by bond splitting along the mortar joint at the tension face.

TABLE 6.3. *Summary of flexural tests of prisms*

Prism designation	Nominal length of specimen in	Age days	Type and description of maximum load				Flexural modulus of rupture [c] psi
			Transverse uniform lb	Transverse concentrated [d] lb	Axial eccentric [g] lb	Eccentricity in	
4-in Brick prisms							
1C1	27 [f] (24)	29	—	490	—	—	[a] 131
1C2		29	—	488	—	—	130
1C3		29	—	500	—	—	133
1C4		29	—	460	—	—	124
1C5		29	—	452	—	—	122
Avg				478			128
1C6	27 (24)	31	600	—	—	—	[a] 121
1C7		31	664	—	—	—	133
1C8		31	[b] 122	—	—	—	—
1C9		31	516	—	—	—	105
1C10		31	404	—	—	—	84
Avg			546				111
6-in Block prisms							
2C1	16	28	—	—	660	10	81
2C2		28	—	—	630	—	76
2C3		28	—	—	580	—	68
2C4		28	—	—	620	—	74
2C5		28	—	—	662	—	81
Avg					630		76

TABLE 6.3. *Summary of flexural tests of prisms*—Continued

Prism designation	Nominal length of specimen in	Age days	Type and description of maximum load				Flexural modulus of rupture [c] psi
			Transverse uniform lb	Transverse concentrated [d] lb	Axial eccentric [e] lb	Eccentricity in	
2D1	32 (24)	30	—	340	—	—	[c] 24
2D2		30	—	658	—	—	44
2D3		30	—	720	—	—	48
2D4		30	—	700	—	—	47
2D5		30	—	400	—	—	29
Avg				563			38
2D6	32 (24)	30	1332	—	—	—	[c] 64
2D7		30	772	—	—	—	39
2D8		30	1200	—	—	—	59
2D9		30	946	—	—	—	47
2D10		31	918	—	—	—	46
Avg			1032				51
10-in Composite (brick in tension)							
3C1	32 (24)	29	—	8200	—	—	[h] 224
3C2		29	—	8100	—	—	221
3C3		29	—	8640	—	—	234
3C4		32	—	7500	—	—	205
3C5		32	—	7650	—	—	208
Avg				8018			218
10-in. Composite (block in tension)							
3C6	32 (24)	28	—	4490	—	—	[h] 101
3C7		28	—	4160	—	—	99
3C8		28	—	4270	—	—	97
3C9		28	—	4220	—	–	96
3C10		29	—	3700	—	—	89
Avg				4168			96

[a] Includes effect of specimen dead weight (avg. = 48.5 lb).
[b] Excluded from average.
[c] Includes effect of specimen dead weight (avg. = 99 lb).
[d] Represents the sum of two loads positioned at third points.
[e] Based on gross area of brick units and net area of concrete block units.
[f] Bracketed figure represents clear span length.
[g] Tested in accordance to ASTM E149–60 [5].
[h] Includes effect of specimen dead weight (avg. = 235 lb).

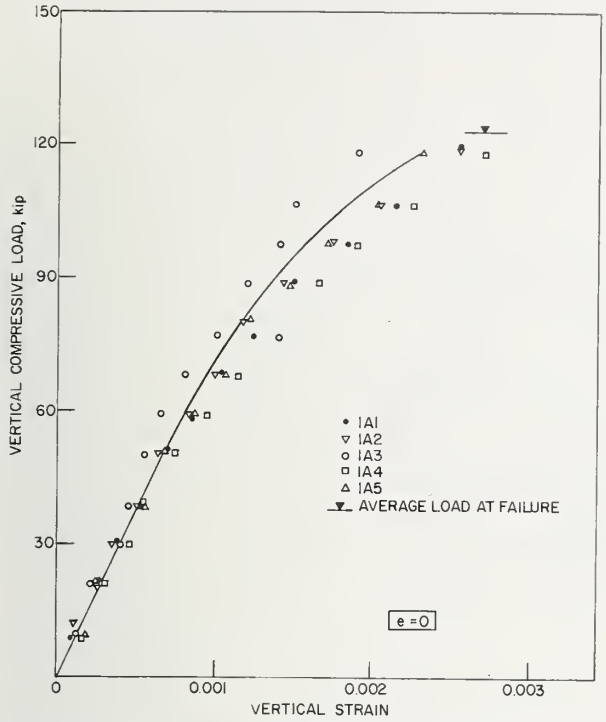

FIGURE 6.1. *Relationship between vertical compressive load and vertical strain for 4 × 8 × 16-in brick prisms at* e = 0.

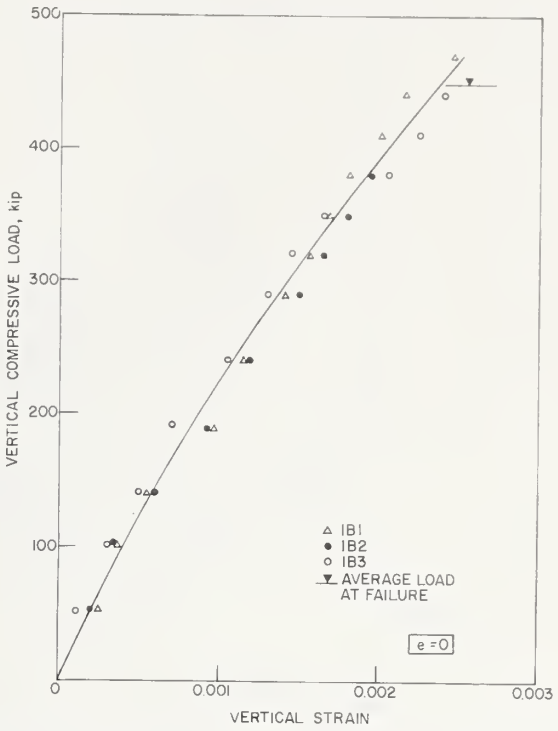

FIGURE 6.2. *Relationship between vertical compressive load and vertical strain for 4 × 32 × 16-in brick prisms at* e = 0.

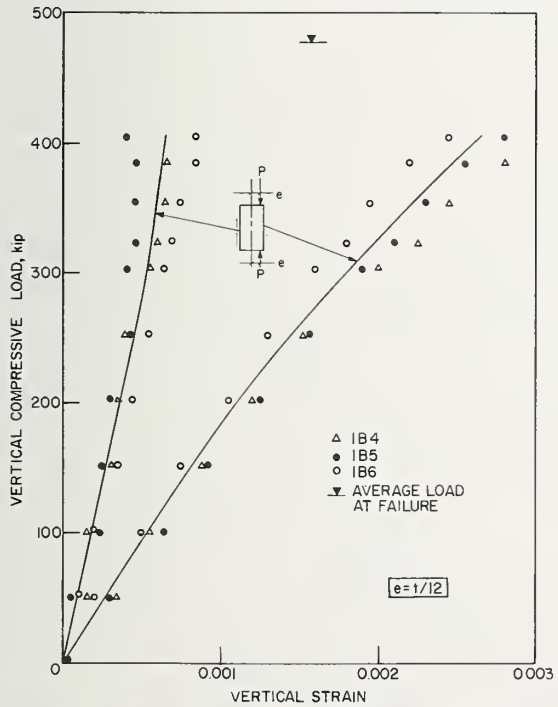

FIGURE 6.3. *Relationship between vertical compressive load and vertical strain for 4 × 32 × 16-in brick prisms at* e = t/12.

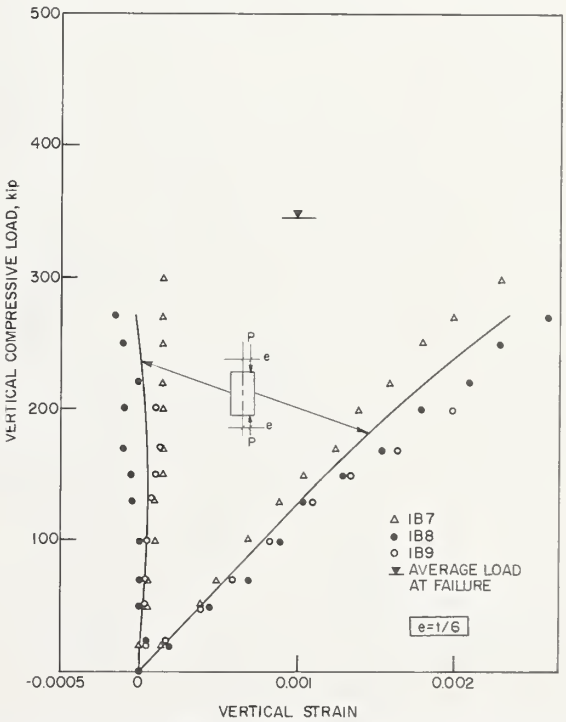

FIGURE 6.4. *Relationship between vertical compressive load and vertical strain for 4 × 32 × 16-in brick prisms at* e = t/6.

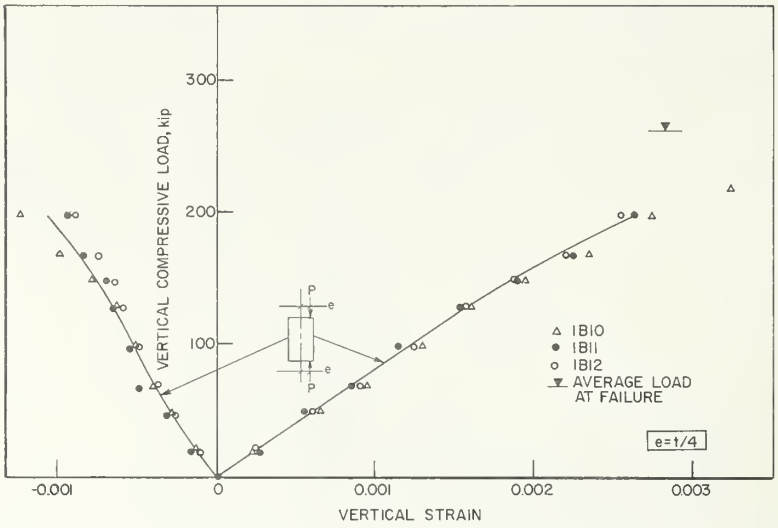

FIGURE 6.5. *Relationship between vertical compressive load and vertical strain for 4 × 32 × 16-in brick prisms at* e = t/4.

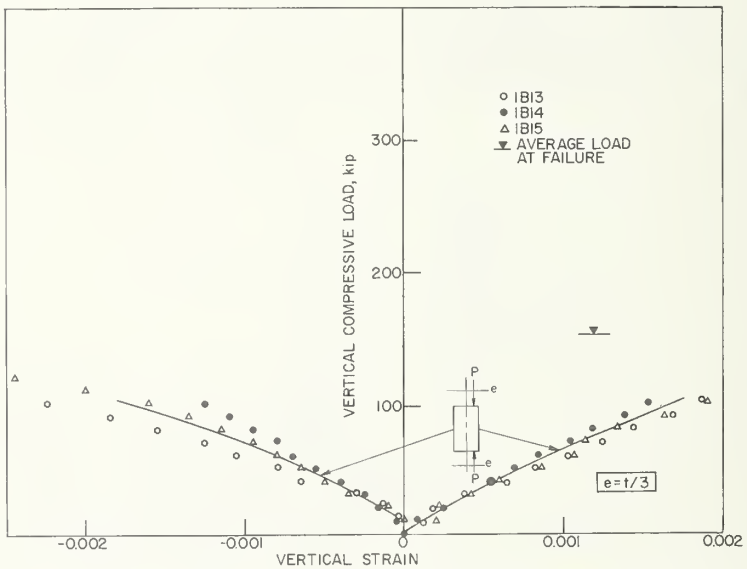

FIGURE 6.6. *Relationship between vertical compressive load and vertical strain for 4 × 32 × 16-in brick prisms at* e = t/3.

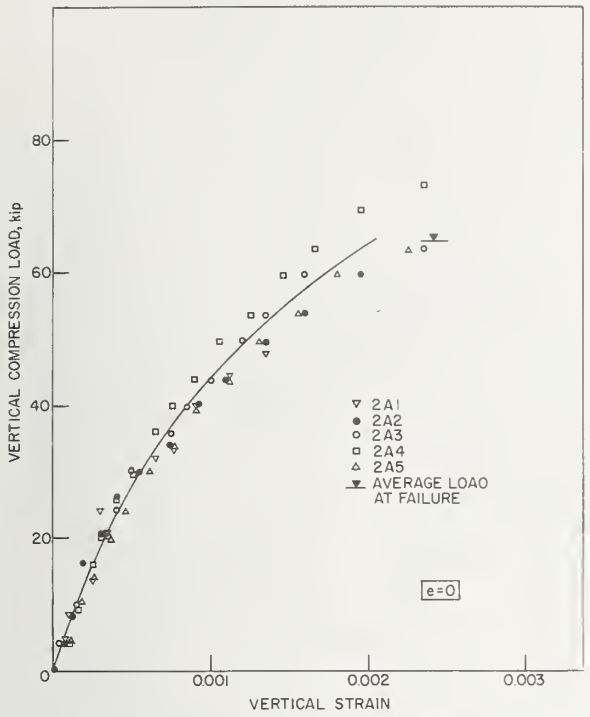

FIGURE 6.7. *Relationship between vertical compressive load and vertical strain for 6 × 16 × 24-in hollow block prisms at* e = 0.

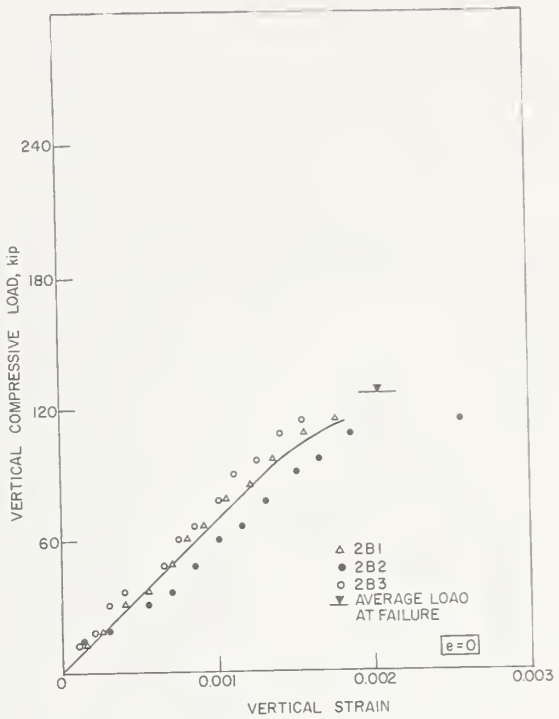

FIGURE 6.8. *Relationship between vertical compressive load and vertical strain for 6 × 32 × 24-in hollow block prisms at* e = 0.

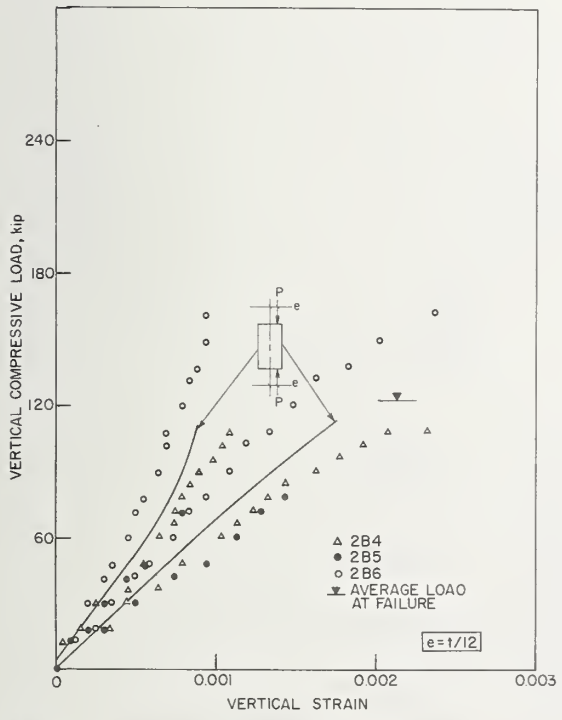

FIGURE 6.9. *Relationship between vertical compressive load and vertical strain for 6 × 32 × 24-in hollow block prisms at* e = t/12.

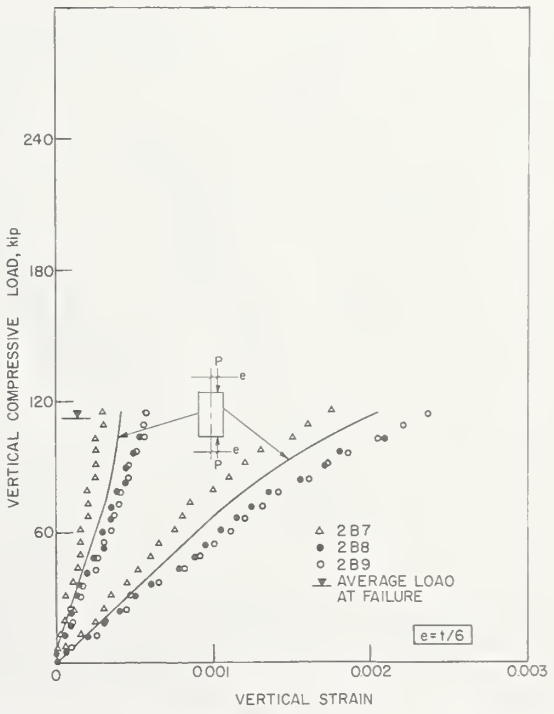

FIGURE 6.10. *Relationship between vertical compressive load and vertical strain for 6 × 32 × 24-in hollow block prisms at* e = t/6.

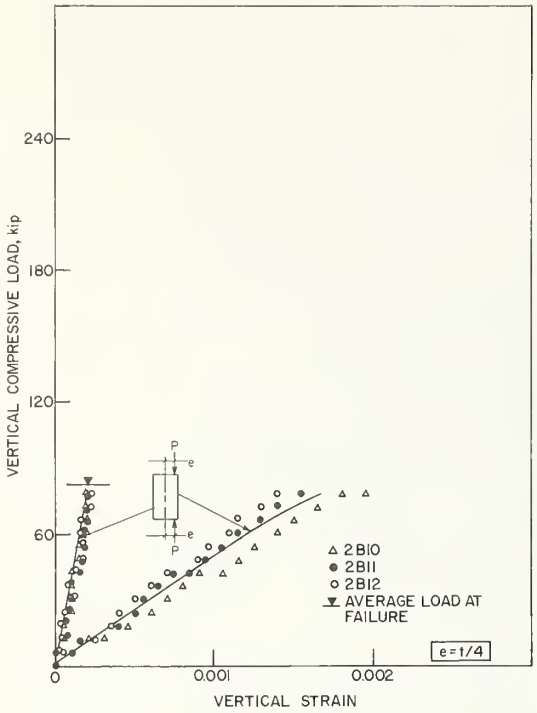

FIGURE 6.11. *Relationship between vertical compressive load and vertical strain for 6×32×24-in hollow block prisms at* e = t/4.

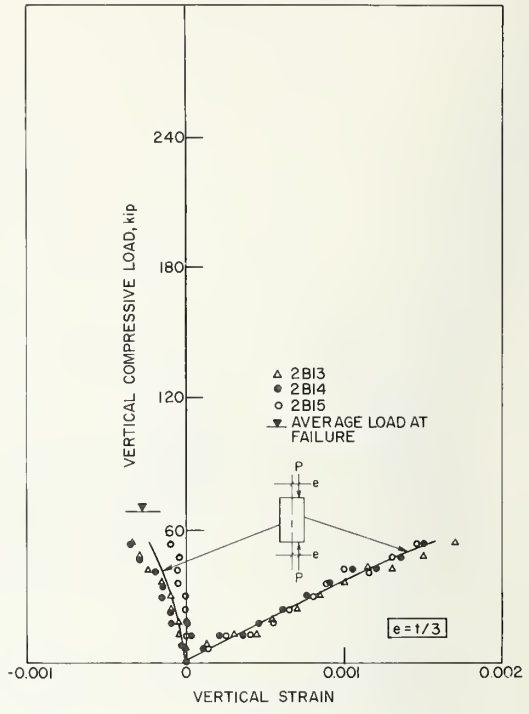

FIGURE 6.12. *Relationship between vertical compressive load and vertical strain for 6×32×24-in hollow block prisms at* e = t/3.

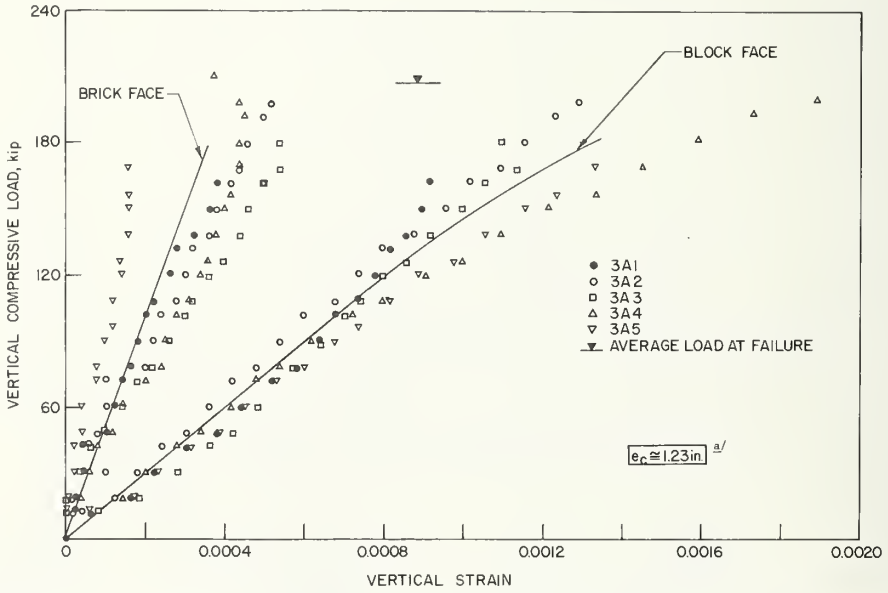

FIGURE 6.13. *Relationship between vertical compressive load and vertical strain for 10×16×32-in composite prisms at* $e_c \simeq 1.23$ *in.*[a]

[a] Estimated on basis discussed in section 7.3.4.

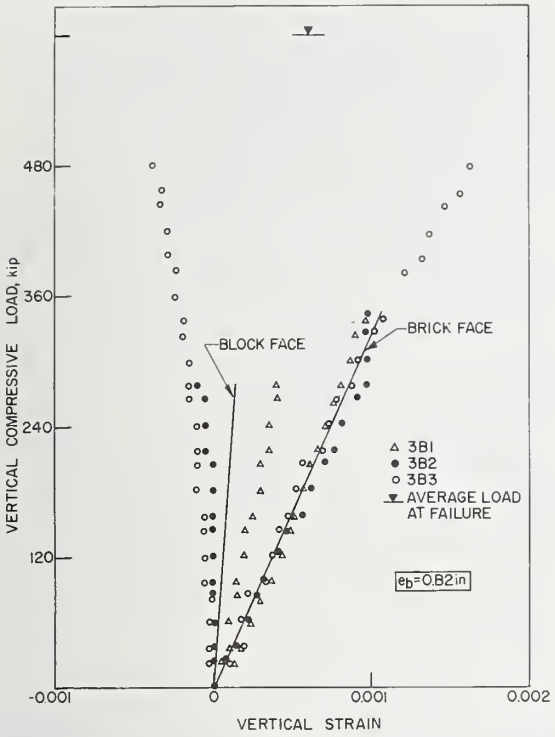

FIGURE 6.14. *Relationship between vertical compressive load and vertical strain for 10×32×32-in composite prisms at* $e_b = 0.82$ *in.*

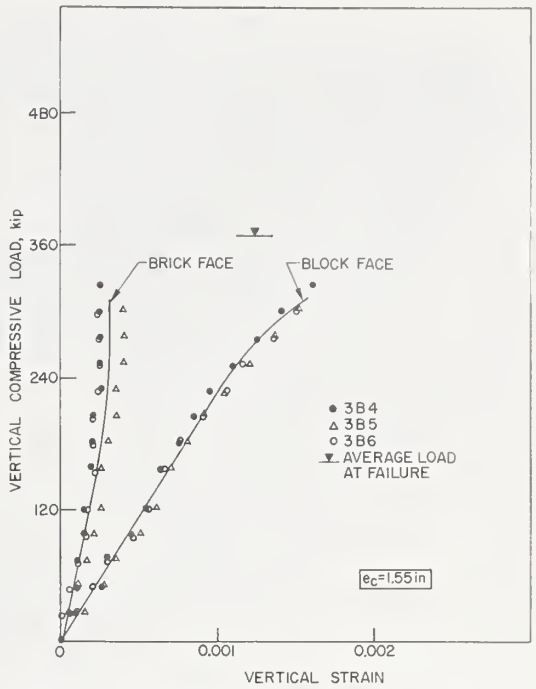

FIGURE 6.15. *Relationship between vertical compressive load and vertical strain for 10×32×32-in composite prisms at* $e_c = 1.55$ *in.*

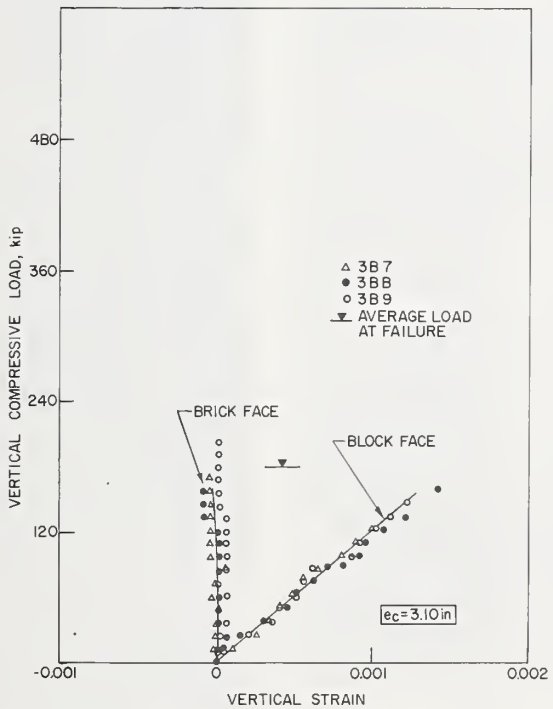

FIGURE 6.16. *Relationship between vertical compressive load and vertical strain for 10×32×32-in composite prisms at* $e_c = 3.10$ *in.*

593-885 O - 76 - 4

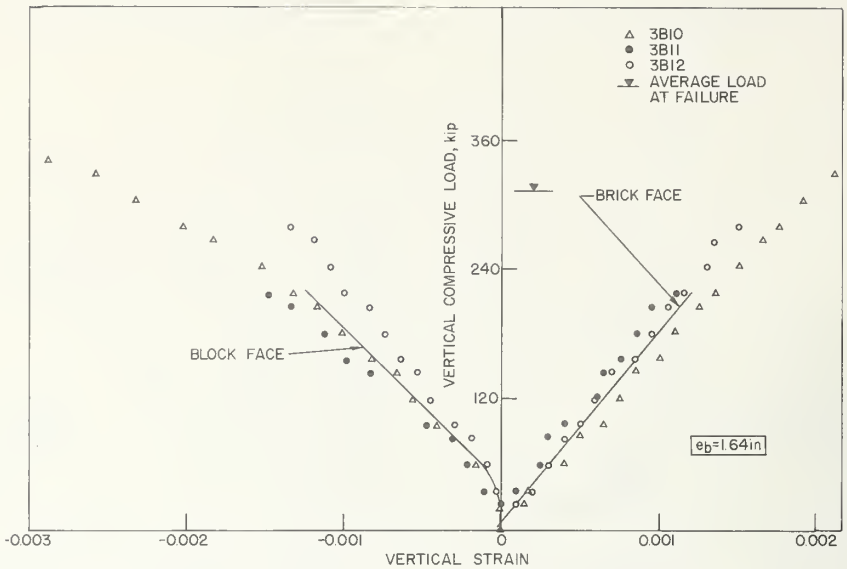

FIGURE 6.17. *Relationship between vertical compressive load and vertical strain for 10 × 32 × 32-in composite prisms at* $e_b = 1.64$ *in.*

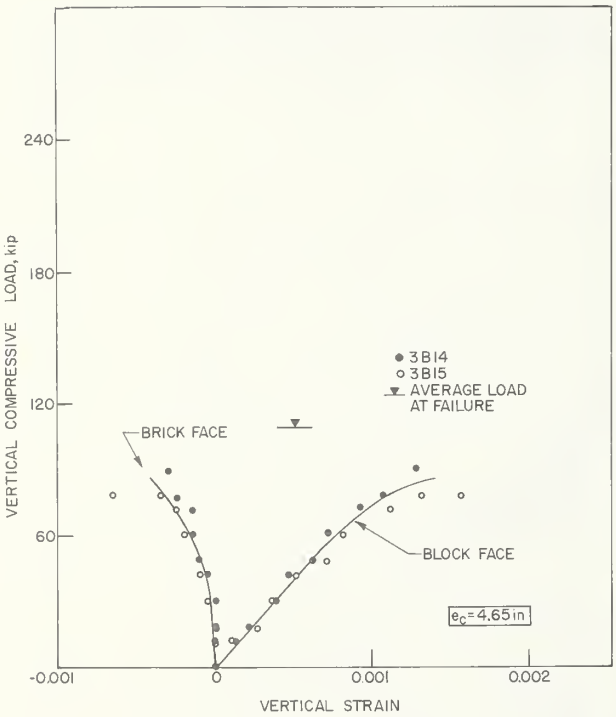

FIGURE 6.18. *Relationship between vertical compressive load and vertical strain for 10 × 32 × 32-in composite prisms at* $e_c = 4.65$ *in.*

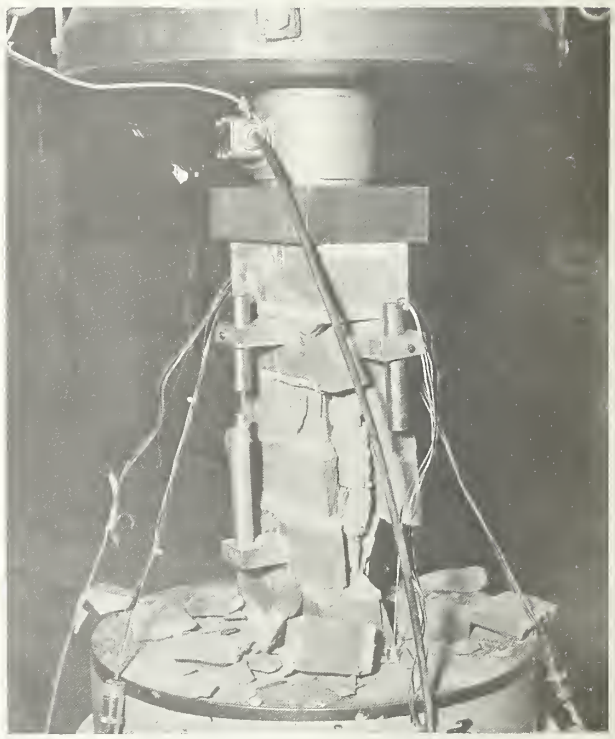

FIGURE 6.19. *Compressive failure of axially loaded brick prism.*

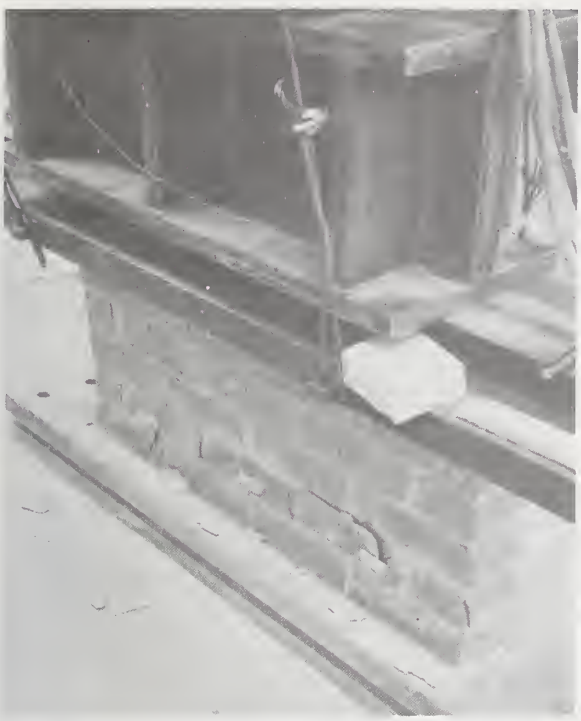

PRISM SPECIMEN 1B15

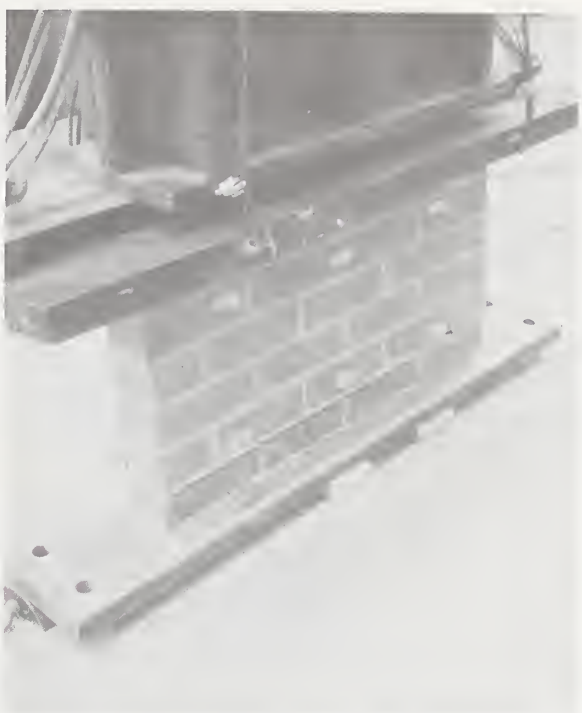

PRISM SPECIMEN 1B15

FIGURE 6.20. *Failure of brick prism under eccentric vertical loading.*

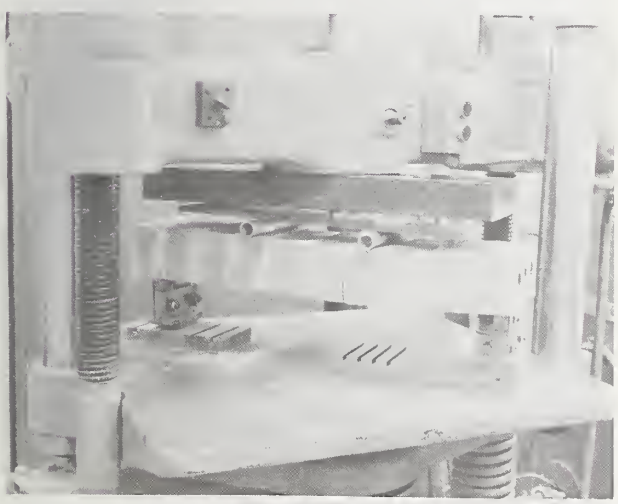

FIGURE 6.21. *Failure of a brick prism tested in flexure.*

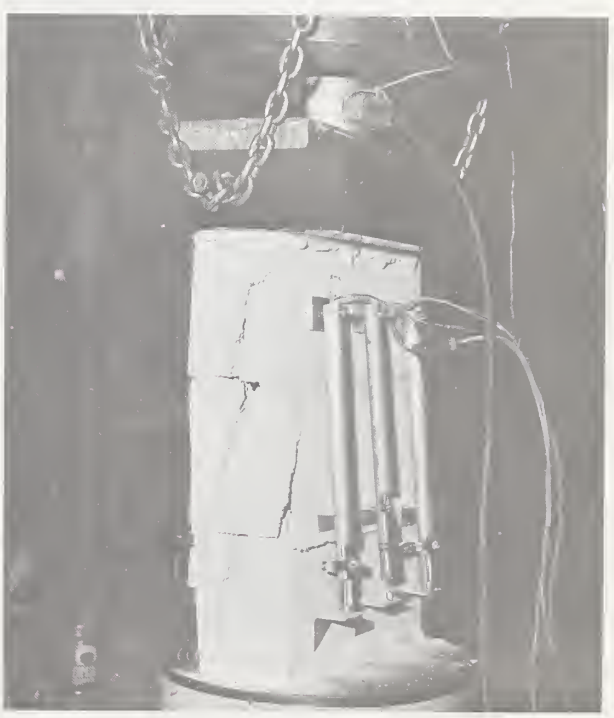

FIGURE 6.22. *Compression failure of hollow concrete block prism.*

FIGURE 6.23. *Failure of hollow block prism under eccentric vertical compressive load.*

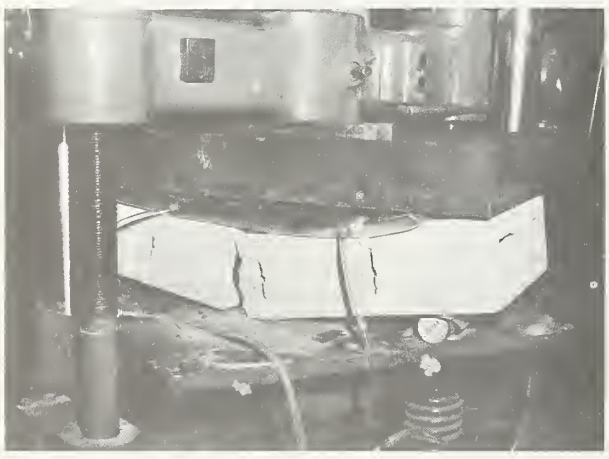

FIGURE 6.24. *Failure of hollow concrete block prism in flexure.*

PRISM SPECIMEN 3A3

FIGURE 6.25. *Typical failure of composite prisms with flat ends under vertical compression.*

FIGURE 6.26. *Typical failures of composite prisms under eccentrically applied compressive loads.*

FIGURE 6.27. *Typical failures of composite prisms under eccentrically applied compressive loads.*

6.3. Wall Test Results

A summary of test results for wall specimens is given in tables 6.4 and 6.5. The results in table 6.4 are for walls tested in vertical compression. The results in table 6.5 are for walls tested under various combinations of vertical compressive and transverse uniform loads. Included in the latter group are specimens, of each of the three types of masonry construction, that were subjected only to transverse loads in order to determine the modulus of rupture.

In some of the tests, the midspan deflections at the actual time of failure were not recorded since instrumentation was removed prior to this stage to avoid possible damage. For each of these specimens, the value of the largest measured midspan deflection and the corresponding load value are shown in both tables. Specimens in which deflections were recorded for the entire loading range are identified by the fact that the magnitude of the load tabulated in the last column is equal to the magnitude of the tabulated load at failure. In these instances the tabular value of the midspan deflection occurs at the maximum tabulated load level. The vertical load eccentricities for the composite specimens listed in table 6.4 are measured from the centroid of the transformed section having the properties given in figure 4.1.

The tests for each of two concentrically loaded composite walls are shown in table 6.4. Both tests were terminated after the 600-kip capacity of the testing machine was reached without failure of either specimen. Figures 6.28 through 6.31 are plots of transverse, or vertical, load versus the mean transverse midspan deflection for the wall specimens of each of the three types of masonry construction.

TABLE 6.4. *Summary of vertical compression tests for walls*

Wall designation	End condition	Age days	Maximum Axial Load		Largest measured midspan deflection in	Corresponding vertical load kip
			Magnitude kip	Eccentricity in		
4-in Brick						
4A7	Flat	128	501.0	0	0.220	375
4A8	Flat	132	500.0	0	.168	420
4A1	Pin	92	307.0	0	.206	255
4A2	Pin	94	321.5	0	.147	200
4A9	Pin	164	168.5	0.297	.380	150
4A10	Pin	133	167.3	.297	.410	140
4A3	Pin	113	108.0	.593	.159	60
4A4	Pin	106	112.0	.593	.213	80
4A5	Pin	113	39.9	1.187	.178	35
4A6	Pin	123	23.0	1.187	.220	20
6-in Hollow block						
4B8	Flat	154	130.0	0	.015	130
4B9	Flat	154	148.0	0	.007	148
4B1	Pin	96	137.0	0	.033	102
4B2	Pin	110	128.2	0	.186	123
4B3	Pin	109	133.5	0.467	.100	80
4B4	Pin	110	119.3	.467	.162	100
4B5	Pin	126	93.2	.933	.210	60
[b]4B7	Pin	129	57.0	.933	.212	57
4B11	Pin	72	120.0	.933	.164	59
4B12	Pin	77	99.0	1.400	.270	80
4B15	Pin	76	99.8	1.400	.273	70
4B13	Pin	78	60.0	1.867	.340	60
4B14	Pin	79	72.0	1.867	.440	72
4B23	Pin	91	105.0	$e_{top} =$ 1.867	.330	105
4B24	Pin	92	100.0	$e_{bot} =$ 0	.336	100
4B25	Pin	94	80.0	$e_{top} =$ 1.867	.044	80
4B26	Pin	94	110.1	$e_{bot} = -$ 1.867	.013	110.1
4B27	Pin	97	111.4		.060	111.4
10-in Composite walls						
4C1	Pin	112	> 600	0	0.198	600
4C2	Pin	110	> 600	0	.060	600
4C3	Pin	113	320.0	[a]$e_c = 1.550$	.112	240
4C4	Pin	113	351.0	$e_c = 1.550$	.136	260
4C5	Pin	132	541.5	[a]$e_c = 0.820$	.264	390
4C6	Pin	128	596.0	$e_b = 0.820$	.227	450
4C7	Pin	159	170.0	$e_c = 3.100$	.163	150
4C8	Pin	160	190.0	$e_c = 3.100$	.145	152

[a] The notation e_c and e_b designates eccentricities of vertical load from the centroid of the composite section towards the concrete block and brick faces, respectively.

[b] Specimen damaged during handling and moving.

TABLE 6.5. *Summary of combined load tests for walls*

Wall designation	End conditions	Age days	Vertical compressive load			Maximum transverse load psi	Largest measured midspan deflection in	Corresponding transverse load psi
			Magnitude kip	Eccentricity in	Midspan deflection in			
4-in. Brick								
4A11	Pin	147	0	—	—	0.200	0.050	0.200
4A15	Pin	152	0	—	—	.085	.260	.085
4A13	Pin	160	70	0	0	2.660	.450	2.660
4A14	Pin	165	70	0	0	2.400	.306	2.400
6-in. Hollow block								
4B10	Pin	71	0	—	—	0.090	.030	0.088
4B16	Pin	78	0	—	—	.200	.030	.200
4B17	Pin	82	20	0	0	1.770	.136	1.770
4B18	Pin	83	20	0	0	1.780	.068	1.700
4B21	Pin	89	20	1.400	0.004	.730	.148	.730
4B22	Pin	90	20	1.400	.050	.700	.220	.700
4B19	Pin	85	40	0	0	3.240	.248	3.240
4B20	Pin	87	40	0	0	3.000	.246	3.000
10-in. Composite								
[a]4C2	Pin	290	0	—	—	3.18	.072	3.18
[a]4C9	Pin	97	0	—	—	2.28	.066	2.25
[b]4C10	Pin	99	0	—	—	1.04	.150	1.04
[b]4C11	Pin	100	0	—	—	1.08	.038	1.08
[b]4C12	Pin	106	80	0	0.009	7.15	.290	6.96
[b]4C13	Pin	108	80	0	010	7.00	.290	6.96
[b]4C14	Pin	109	160	$e_b^c = 0.800$	.076	6.30	.550	6.30
[b]4C15	Pin	111	160	$e_b = 0.800$	.063	6.60	.570	6.60

[a] Transverse uniform load applied to the hollow block face.
[b] Transverse uniform load applied to the brick face.
[c] The notation e_b designates eccentricity of vertical load from the centroid of the composite section towards the brick face.

6.4. Description of Wall Failures

Wall failures are described in this section according to type of construction and type of loading. As indicated previously, walls were loaded in vertical compression, transverse flexure, or a combination of both.

6.4.1. Brick Walls

Walls tested in vertical compression generally failed by sudden crushing and collapse. Concentrically loaded specimens exhibited face spalling and vertical cracking across the thickness. Increased load eccentricity caused greater shattering of specimens at failure. Typical compression failures are shown in figure 6.32.

Under transverse loads, or combined vertical and transverse loads, tensile bond-failure occurred between the mortar and the brick along horizontal joints near mid-height. A typical failure is shown in figure 6.33. This wall was subjected to a 70,000-lb compressive axial load applied prior to and maintained during the application of transverse uniform load.

6.4.2. Block Walls

Hollow concrete block walls, tested in vertical compression, generally developed vertical cracks in the web or in the face shell with failure being accompanied by crushing and spalling of the blocks usually in the three top and bottom courses of the specimen. Vertical loads applied at large eccentricities caused horizontal splitting along mortar joints near wall mid-height, together with vertical splitting of the webs extending from the bottom courses upward. Typical wall failures under vertical compressive loads are shown in figure 6.34.

Under transverse loads, failure occurred by cracking along a horizontal joint near wall mid-height in specimens with little or no vertical load. Larger vertical loads caused substantial web splitting, usually in the lowest three or four courses of the specimen. A typical failure of a horizontal joint at mid-height under combined loading is shown in figure 6.35. This wall was under a 40,000-lb compres-

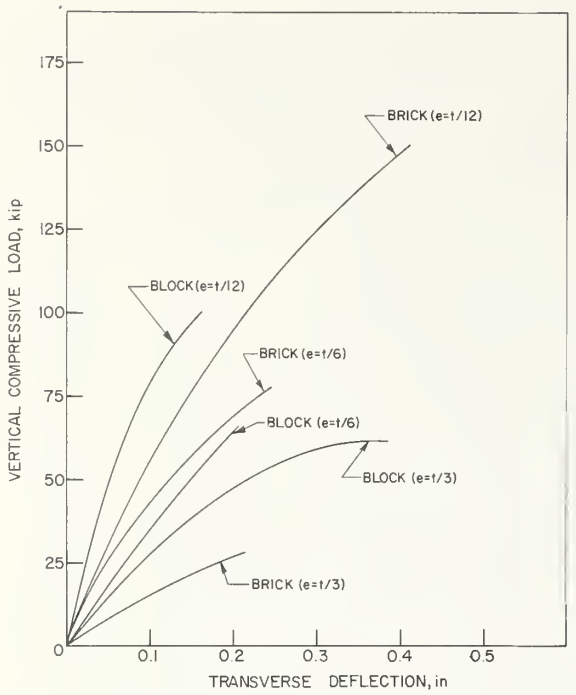

FIGURE 6.28. *Relationship between vertical compressive load and transverse midspan deflection for brick and hollow block walls.*[a]

[a] Each curve represents the mean of the results of two tests.

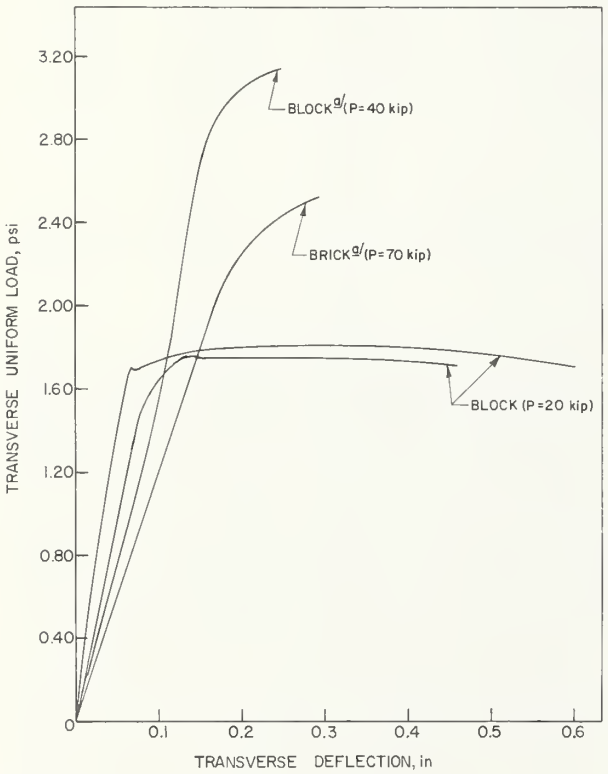

FIGURE 6.30. *Relationship between transverse uniform load and transverse midspan deflection for brick and hollow block walls.*

[a] Each curve represents the mean of the results of two tests.

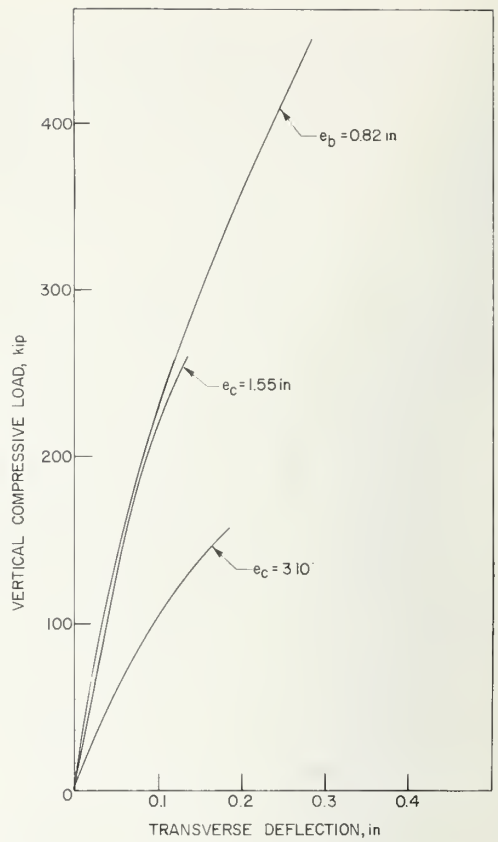

FIGURE 6.29. *Relationship between vertical compressive load and transverse midspan deflection for composite walls.*[a]

[a] Each curve represents the mean of the results of two tests.

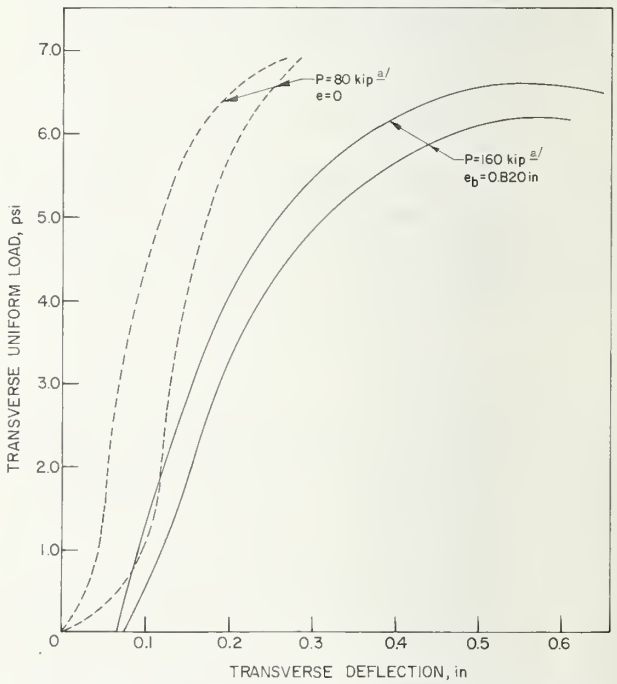

FIGURE 6.31. *Relationship between transverse uniform load and transverse midspan deflection for composite walls.*[a]

[a] Transverse uniform load applied to the brick face.

WALL SPECIMEN 4A1

WALL SPECIMEN 4A7

FIGURE 6.32. *Failure of brick walls under vertical compression.*

WALL SPECIMEN 4A14

FIGURE 6.33. *Failure of brick wall under combined vertical and transverse loading.*

sive load during the application of the transverse uniformly distributed load.

6.4.3. Composite Walls

As in the case of composite prisms, composite walls under axial compression supported the 600-kip capacity load of the testing machine without complete failure. At this load level, web cracking was observed in the edge blocks at the lowest three courses of the specimens as shown in figure 6.36 (4C2). Specimen 4C2 was later tested in transverse flexure. Specimens in which the eccentricity of vertical loading was toward the block face, exhibited sudden failure by vertical splitting in the webs of blocks at the top or bottom three courses of the specimens as shown in figure 6.36 (4C7). Specimens tested with eccentric load applied near the brick face, failed by sudden crushing of the brick. Examination of failures of specimens loaded in vertical compression did not reveal any significant cracking or separation occurring at the interface between brick and block. In specimens tested under transverse load, failure occurred in bond between mortar and masonry units along horizontal joints near mid-height of the walls as shown in figure 6.37. This mode of failure was also observed in transversely loaded specimens under an 80-kip axial load. Specimens under a 160-kip vertical load, and subjected to transverse uniform load applied to the brick face, failed by crushing of the brick and tensile cracking of the block at mid-height as shown in figure 6.38.

593-885 O - 76 - 5

WALL SPECIMEN 4B8 WALL SPECIMEN 4B12

FIGURE 6.34. *Failure of concrete hollow block walls in vertical compression.*

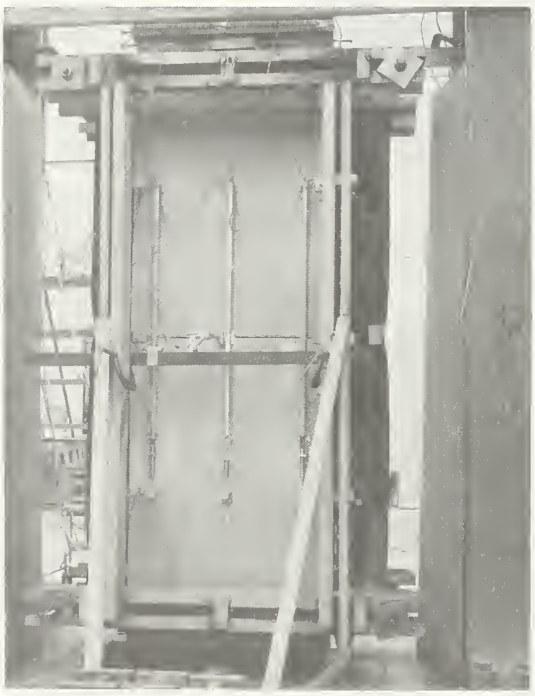

WALL SPECIMEN 4B19

FIGURE 6.35. *Failure of concrete hollow block masonry wall under vertical and transverse loading.*

WALL SPECIMEN 4C2

WALL SPECIMEN 4C7

FIGURE 6.36. *Failure of composite walls loaded in vertical compression.*

WALL SPECIMEN 4C9

WALL SPECIMEN 4C10

FIGURE 6.37. *Failure of transversely loaded composite walls.*

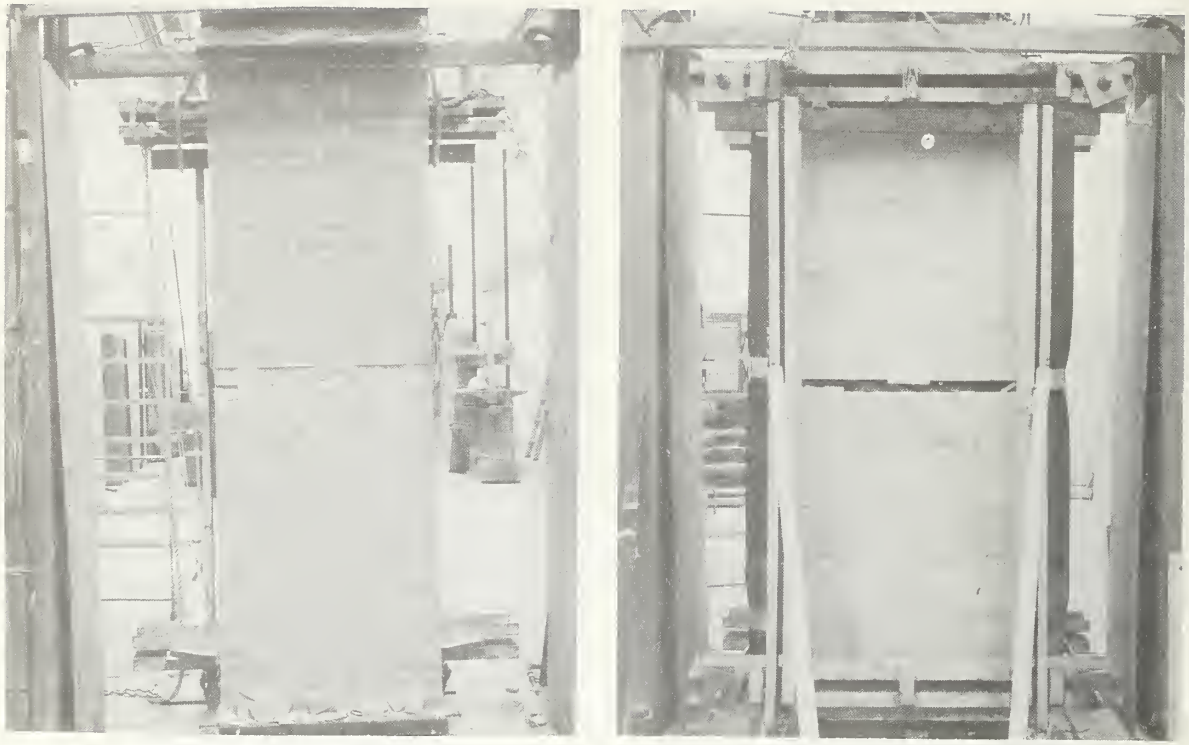

FIGURE 6.38. *Failure of composite walls under transverse and vertical loads.*

7. Analysis and Synthesis of Test Results

7.1. Introduction

In this section, the experimental results are interpreted and compared with analytical results based on failure theory for masonry walls under the simultaneous action of bending and compression. The constitutive relations for brick, concrete block and composite masonry specimens used in the tests are discussed in section 7.2. The interaction relations between compressive axial load and bending moment for short masonry piers are discussed in section 7.3. In section 7.4 the effect of wall slenderness on these interaction relations is discussed.

7.2. Constitutive Relations

7.2.1. Brick Masonry

Average stress-strain curves obtained from the axial compression tests of brick masonry specimens are shown in figure 7.1. These curves have been developed on the basis of average calculated stresses on the sections specified in figure 4.1 and of average strains obtained by dividing measured vertical deformations by the corresponding gage lengths of the recording instruments.

In figure 7.1, it is shown that the average stress-strain relations for prism and wall specimens with flat end supports[6] (curves A and B, respectively) are approximately linear and virtually identical up to a stress level which is about 50 percent of the calculated average failure stress of the prisms. Above that level, the prisms as a group developed less stiffness than the walls although this divergence does not appear to be very significant. As shown in figure 6.1, the test results from individual prisms were reasonably consistent with somewhat greater scatter at higher loads.

Curves C and D in figure 7.1 show average stress-strain relationships for prism and wall specimens with pinned supports. The average stress-strain curve for 4 × 32 × 16-in prisms had a noticeably lower slope in comparison with the rest of the curves. A possible source for this discrepancy is the influence of end effects, such as localized conditions at the ends of the specimens due to lack of fit between load bearing surfaces, and stress concentration under the line loading. These effects would be more pronounced in specimens with low aspect ratios such as the 4 × 32 × 16-in prisms and would be more evident when the deformation gages are mounted close to the ends of the specimens.

[6] The test setup designed to inhibit end rotations is described in section 5.3 and illustrated in figure 5.2.

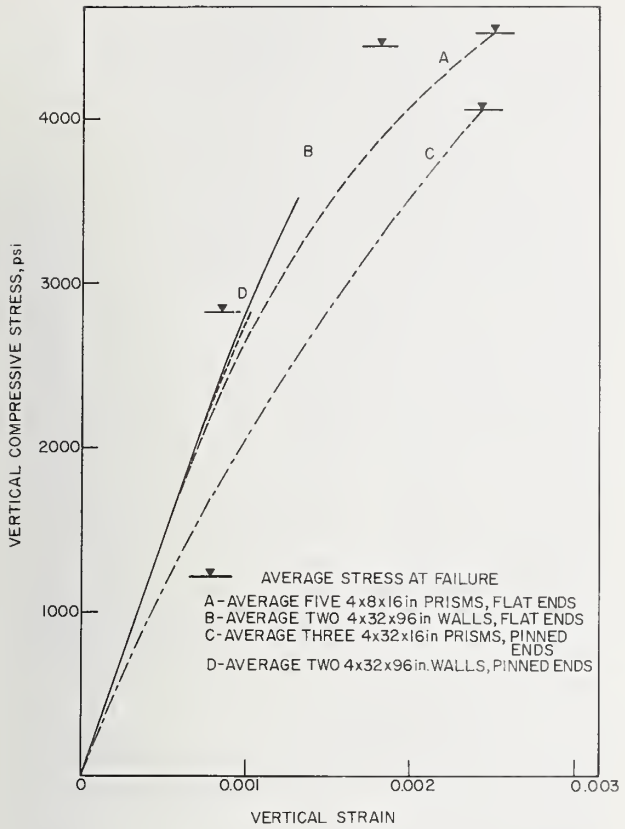

FIGURE 7.1. *Relationship between vertical compressive stress and vertical strain of axially loaded brick specimens.*

The proximity of curves B and D is probably due to the gage points being sufficiently remote from the end plates of the walls to minimize the effect of such end conditions on deformation measurements.

The elastic moduli derived from axial compression tests on brick specimens are summarized in table 7.1. The notation E_i, E_s, and E_t has been introduced to designate the initial tangent modulus of elasticity, the secant modulus of elasticity at failure, and the tangent modulus of elasticity at failure, in that order; f'_m designates the average compressive strength as determined by tests on axially loaded prisms with flat supports (4515 psi). The secant and tangent moduli at failure for the wall specimens could not be obtained from test results since instrumentation was removed before the masonry developed its capacity. The tabulated values for masonry walls with flat supports were estimated at the highest load level prior to such removal. As will be explained later, walls with pinned supports failed by instability. For these walls, the tangent modulus of elasticity at failure shown in table 7.1 was calculated using the Euler buckling formula

$$P_c = \frac{\pi^2 E_t I}{h^2} \tag{7.1}$$

where P_c is the Euler buckling load, h is the height of the wall and I is the moment of inertia of the cross section about its centroidal axis. The values of E_s and E_t are both dependent on the stress level at failure.

In order to investigate stress-strain relationships in flexure where a strain gradient is present on the section, a series of eccentric load tests was conducted on short prisms in which the effect of transverse deflections on cross-sectional stress distribution is of second order magnitude and can therefore be neglected.

Figures 6.3 through 6.6 show a family of curves relating vertical loads to vertical strains derived from test results on eccentrically loaded brick prisms with pinned support conditions. The vertical loads were applied at four, equal top and bottom, eccentricities (producing single curvature) of $t/12$, $t/6$, $t/4$, and $t/3$, where "t" is the thickness of the specimen. At each eccentricity, prisms were tested in triplicate and the results were averaged to develop curves for outer fibers at opposite faces of the specimen. In each figure, the curve on the right refers to the face subjected to maximum vertical compressive strain while the curve on the left refers to the opposite face. Generally, these

TABLE 7.1. *Modulus of elasticity of axially loaded brick masonry specimens ($f'_m = 4515$ psi)*

Description of specimen	$E_i \times 10^{-6}$ psi	$\frac{E_i}{f'_m}$	$E_s \times 10^{-6}$ psi	$\frac{E_s}{f'_m}$	$E_t \times 10^{-6}$ psi	$\frac{E_t}{f'_m}$
4 × 8 × 16-in Prisms flat ends	2.8	620	1.8	400	0.8	180
4 × 32 × 96-in Walls, flat ends	2.8	620	2.4	530	1.7	376
4 × 32 × 16-in Prisms, pinned ends	2.3	510	1.6	350	1.2	270
4 × 32 × 96-in Walls, pinned ends	2.8	620	2.5	550	2.2	490

curves are linear for loads of up to about 40 to 50 percent of capacity and are similar to those derived from axial loading (fig. 7.1), indicating, at first glance, that the stress-strain characteristics of brick masonry are not materially altered by the presence of a strain gradient. Assuming a linear stress-strain relationship and an uncracked section, stresses at the opposite faces of a specimen may be obtained using superposition of flexural and axial stresses as follows:

$$f = \frac{P}{A} + \frac{(Pe)c}{I} \tag{7.2}$$

where A = net area of cross section
I = moment of inertia about centroidal axis of net cross section
e = eccentricity of applied load from centroidal axis
c = distance from centroidal axis to outer fibers
P = compressive load
= stress at outer fibers.

In eq (7.2), c is positive if it is on the same side of the centroidal axis as e. Also, f and P are taken to be positive when compressive. For masonry with no tensile strength or negligible tensile strength eq (7.2) is valid only when the vertical load eccentricity is equal to or less than the kern eccentricity (fig. 7.2b). Since a load applied at the kern produces zero stress in the outer fibers on one side of the section, the magnitude of the kern eccentricity e_k may be obtained from eq (7.2),

$$e_k = \frac{I}{Ac} \tag{7.3}$$

For a solid rectangular section eqs (7.2) and (7.3) assume the simpler form,

$$\left.\begin{aligned} f_{max} &= \frac{P}{A}\left(1 + \frac{6e}{t}\right) \\ f_{min} &= \frac{P}{A}\left(1 - \frac{6e}{t}\right) \end{aligned}\right] \tag{7.4}$$

$$e_k = \frac{t}{6}. \tag{7.5}$$

For vertical loads applied at eccentricities greater than the kern eccentricity, the section will be partially cracked and, assuming tensile strength is negligible, the stress distribution will be as shown in figure 7.2c. In this case, the maximum stress for a solid rectangular section and a linear stress block is given by the equation,

$$f_{max} = \frac{P}{A} \cdot \frac{4/3}{1 - (2e/t)}. \tag{7.6}$$

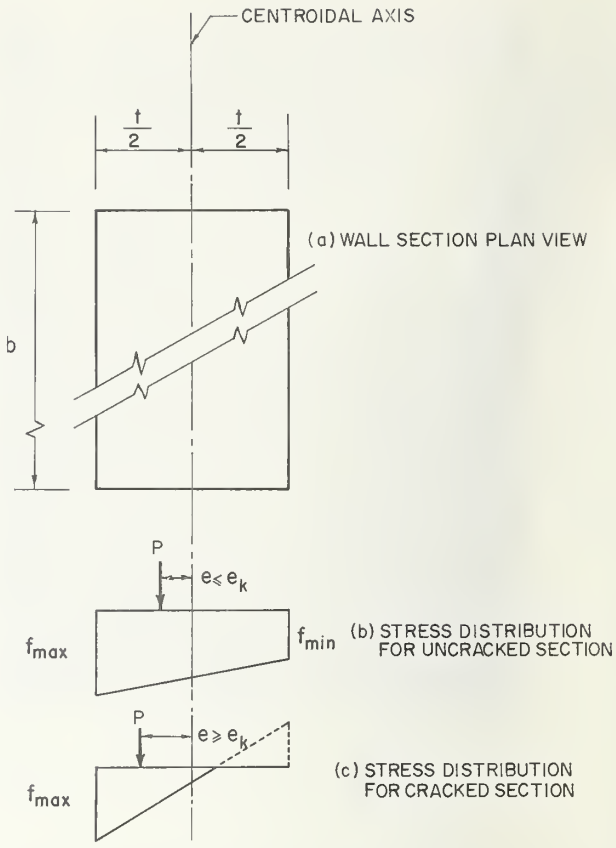

FIGURE 7.2. *Stress distribution.*

Initial tangent moduli of elasticity may be computed from the linear portion of load-strain relationships and eqs (7.4) or (7.6). The following tabulated values were derived in this manner.

TABLE 7.2. *Initial modulus of elasticity of eccentrically loaded brick prisms* ($f'_m = 4515$ *psi*)

Vertical load at eccentricity	$t/12$	$t/6$	$t/4$	$t/3$
$E_i \times 10^{-6}$ psi	2.5	2.3	1.9	2.6
$\frac{E_i}{f'_m}$	550	510	420	580

Table 7.2 indicated an average initial tangent modulus of elasticity in flexure of about 2.3×10^6 psi which is equal to the value derived for the axially loaded prisms (table 7.1). It should be noted, however, that values derived from eccentric load tests tend to become more sensitive to factors such as accidental deviations in eccentricity, degree

of precision of deformation measurements and specimen imperfections. Since the ratio of strains at opposite outer fibers is constant in the linear range, actual eccentricities may be estimated using the curves in figures 6.3 to 6.6 on the basis of the assumption that the combined effect of other factors is not significant. For instance, at an intended load eccentricity of $t/4$, the magnitudes of strains[7] at opposite face fibers of the specimens should have a ratio of 3. The ratio of 2.4, derived from figure 6.5, indicates a probable actual eccentricity larger than $t/4$. Likewise, the actual strain ratio obtained from figure 6.6 is 1.2 compared with a ratio of 1 which would result from an eccentricity of $t/3$. The initial tangent modulus of elasticity calculated on the basis of actual test-derived strain ratios would be about 2.1×10^6 psi in both of these cases.

While results of eccentric-load tests can be utilized to develop stress-strain curves for nonlinear regions, the procedure would be approximate because the curves often fall short of the ultimate load level, and would involve construction of partially nonlinear stress blocks in a manner that would satisfy the equilibrium conditions. Nonetheless, to establish some basis of comparison with axial load test results, the stress-strain curve for the full loading range was developed for prisms loaded at an eccentricity of $t/12$. The resulting approximate secant and tangent moduli of elasticity at failure were 1.7×10^6 psi and 1.1×10^6 psi respectively. These values compared closely with the corresponding values of 1.6×10^6 psi and 1.2×10^6 psi indicated in table 7.1, which were derived from axial load tests of prisms of similar geometry, composition and end support conditions.

Elastic moduli of slender masonry walls subjected to eccentric compressive loads may also be derived from available test data on load-deflection relationships. Average plots of eccentric load versus midspan transverse deflection for $4 \times 32 \times 96$- in high brick walls pinned at the ends, are shown in figure 6.28. The wall specimens were tested in duplicate at load eccentricities of $t/12$, $t/6$, and $t/3$.

Yokel [15] obtained an analytical solution for walls of solid rectangular cross section subjected to compressive loads applied at equal top and bottom eccentricity. The graphical form of that solution, relating vertical load to midspan deflection, is shown in figure 7.3 for ready reference. Relevant notation is defined in the same figure. The derivation is based on the assumption of a constant modulus of elasticity in compression and zero tensile strength for the material, and is valid in the region $t/6 \leq e < t/2$. It was subsequently shown [16] that for practical purposes the relationship provides a good approximation in the region $0 \leq e \leq t/6$. The following tabulation of initial tangent moduli of eccentrically loaded walls was derived using the load-deflection curves from individual wall tests and the analytically derived curve of figure 7.3.

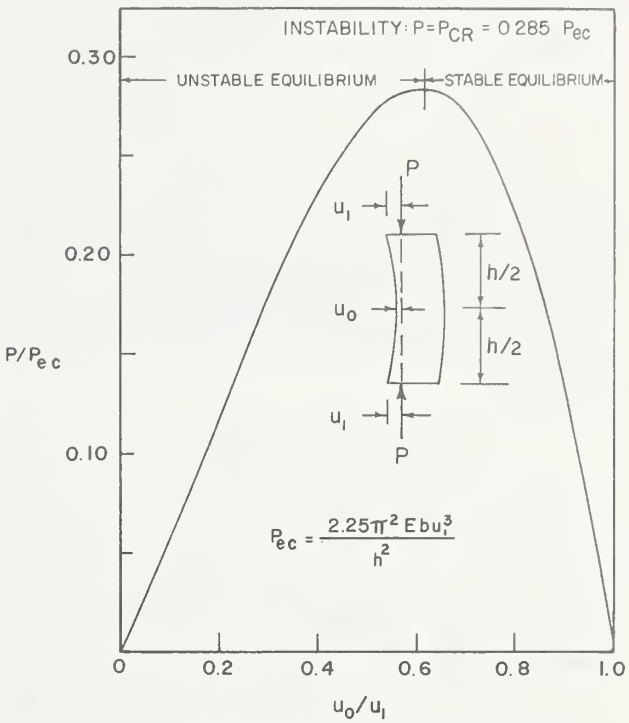

FIGURE 7.3. *Graphical presentation of brick wall failure by instability.*

Note that the values of elastic moduli, predicted on the basis of load-deflection curves for walls with load eccentricities equal to or less than the kern eccentricity, fell within the range of values predicted on the basis of vertical deformations. At greater load eccentricities, it becomes virtually impossible to obtain meaningful estimates since slight deviations in eccentricity, either as a result of lack of planeness or inaccurate positioning of test specimens, are likely to produce a significant change in deflection and wall capacity as evidenced by the test results from walls 4A5 and 4A6 shown in table 6.4. In addition, larger load eccentricities will produce an apparent increase in the modulus of elasticity (table 7.3) since, in this range, tensile strength significantly influences stiffness and the curve in figure 7.3 was derived for the case of zero tensile strength.

Elastic properties of masonry walls may also be derived from the test results of wall specimens subjected, simultaneously, to axial load and trans-

[7] The word "strain" as applied to a cracked surface is used here to designate average vertical deformation per unit length, even though cracks actually represent discontinuous localized length changes.

TABLE 7.3. *Initial modulus of elasticity of eccentrically loaded brick walls ($f'_m = 4515$ psi)*

Vertical load eccentricity	Wall designation	$E_i \times 10^{-6}$ psi	$\frac{E_i}{f'_m}$
$t/12$	4A9	2.3	510
	4A10	2.2	490
$t/6$	4A3	2.8	620
	4A4	2.9	640
$t/3$	4A5	8.1	1790
	4A6	3.4	750

verse uniform load. Figure 7.4 shows the deflected shape of a wall under combined loads. The broken curve designates the deflection under uniformly distributed transverse load w, while the solid curve designates the deflection produced by the simultaneous action of axial load P and transverse load w. The latter, acting alone, produces the following deflections:

$$\Delta_w = \Delta_1 + \Delta_2 = \frac{5wL^4}{384EI} + \frac{wL^3}{48EI}(h - L). \quad (7.7)$$

The addition of axial load P produces the deflected shape given by the solid curve, which is also the shape of the moment diagram produced by the axial load. Assuming the moment curve to be parabolic,[8] the deflection, produced by the axial load, is given by [2]

$$\Delta_P = \frac{5P\Delta h^2}{48EI}. \quad (7.8)$$

Noting that

$$\Delta = \Delta_w + \Delta_P \text{ and } \frac{48EI}{5h^2} = \frac{\pi^2 EI}{h^2} = P_c$$

where P_c is defined by eq (7.1), the total midspan deflection relative to the ends of the wall is approximately given by

$$\Delta \simeq \frac{1}{1 - \frac{P}{P_c}} \Delta_w. \quad (7.9)$$

Using Δ_w, obtained from tests on brick walls loaded transversely and with a 70-kip axial load (fig. 6.33), eq (7.9) gives an average initial modulus of elasticity of 3.0×10^6 psi. This value is in good agreement with 2.9×10^6 psi in table 7.3 obtained from test results of walls subjected to loads applied at the kern, and with 2.8×10^6 psi in table 7.1 obtained from test results for axially loaded walls.

[8] A parabolic curve is a close approximation to the actual deflection curve.

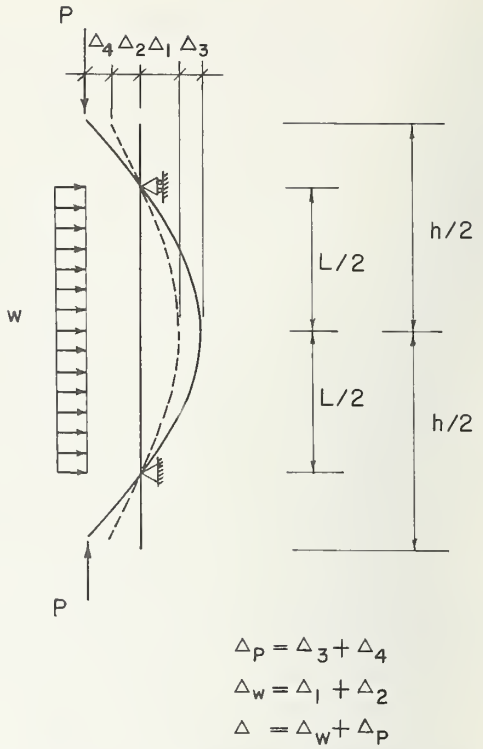

FIGURE 7.4. *Wall deflection under combined loads.*

On the basis of the information discussed in this section, the brick masonry used in this program developed an average initial modulus of elasticity of approximately $620 f'_m$ or 2.8×10^6 psi. This value is corroborated by data derived from a variety of test loading conditions producing flexural as well as axial deformations. The current issue of "Building Code Requirements for Engineered Brick Masonry" developed by BIA (formerly SCPI) [12] stipulates a design modulus of elasticity of $1000 f'_m$ with an upper limit of 3×10^6 psi for inspected brick masonry construction. This discrepancy does not necessarily apply to all brick masonry since the modulus of elasticity is dependent on many parameters. However, results from previous tests [17] on brick masonry, involving other types of brick and mortar, confirm the experimental trend of a lower modulus of elasticity than that presently stipulated by BIA.

7.2.2. Summary of Findings and Conclusions

(1) The brick masonry specimens used in this program developed an average initial modulus of elasticity of 2.8×10^6 psi or $620 f'_m$. This was considerably less than that stipulated by the present BIA Standard [12]. A similar trend has also been

observed in the results of previous tests [17]. Since a reliable prediction of the modulus of elasticity is essential in brick masonry design which generally requires consideration of deflections and slenderness effects, there is a need to reconcile provisions of the present standard with experimental evidence.

(2) The initial modulus of elasticity of brick masonry walls can be reasonably predicted on the basis of axial load tests on companion prisms with flat ends and of the same material composition as the walls. The method has particular merit in view of the relative simplicity of the testing procedure and because errors due to accidental load eccentricity or geometric imperfections can be effectively controlled by averaging deformations of the outer fibers at opposite faces of the specimens.

(3) Flexure-induced strain gradients had no appreciable effect on the stress-strain characteristics of brick masonry walls.

(4) Prisms with the smaller height-to-width ratio ($h/w = 1/2$) developed a lower modulus of elasticity in relation to the other specimens. This is probably attributed to the influence of localized stress conditions at the supports. Mounting of instrumentation in a manner that would keep vertical deformation measurements free of end zone effects would require test specimens to have a greater height-to-width ratio than that of the $4 \times 32 \times 16$-in prisms.

(5) The specimens exhibited nearly linear stress-strain properties under load intensities of up to approximately 50 percent of the load at failure. Thus, the value of the initial modulus of elasticity would provide a reasonably good estimate of the modulus of elasticity within the region of practical design loads. The average secant and tangent moduli of elasticity at failure for the axially loaded specimens were approximately in the order of 80 and 50 percent, respectively, of the value of the initial modulus of elasticity.

7.2.3. Concrete Block Masonry

Figure 7.5 shows average stress-strain relations for prisms and walls of hollow concrete block masonry tested in axial compression. The curves shown are based on the idealized sectional properties of figure 4.1 and test data relating vertical deformations to applied loads. Figures 6.7 and 6.8 show average results derived from individual prism tests.

A comparison of the curves in figures 7.1 and 7.5 indicates a common trend in shape and degree of linearity of compressive stress-strain curves of brick and of concrete block masonry specimens. There are other similarities. Note, for instance, the lack of stiffness exhibited by the pin ended 24-in prisms relative to the other specimens and the good agreement between the initial elastic moduli of the flat ended 24-in prisms and wall panels.

Table 7.4 gives a summary of elastic moduli of axially loaded concrete block specimens. The values

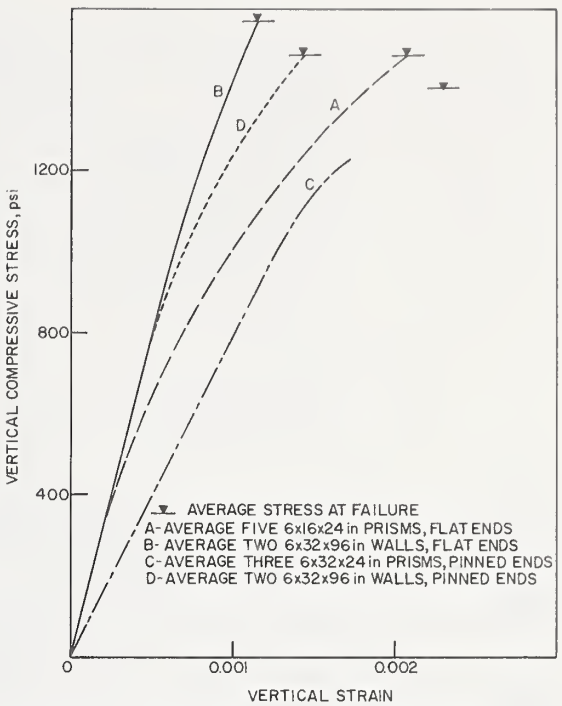

FIGURE 7.5. *Relationship between vertical compressive stress and vertical strain of axially loaded concrete block specimens.*

of E/f'_m appearing in the table have been calculated using an average compressive strength $f'_m = 1473$ psi for prisms with flat ends (table 6.1). Due to the absence of test data on displacements near peak loads, tangent and secant moduli at failure could not be predicted for the prisms with pinned supports.

The results of eccentric load tests on $6 \times 32 \times 24$-in hollow concrete block prisms were used to derive the curves shown in figure 6.9 through 6.12 which relate the compressive loads to the vertical strains in the outer fibers. The vertical loads were applied at equal (single curvature) top and bottom eccentricities of $t/12$, $t/6$, $t/4$, and $t/3$ where t designates the thickness of the specimens. In each figure the curve on the right represents outer fibers under maximum compression and the curve on the left represents outer fibers on the opposite face of the specimens.

The test data from $6 \times 32 \times 24$-in eccentrically loaded prisms provide a means of examining compressive stress-strain characteristics of concrete block masonry in flexure. In the region where the strain is proportional to the external load, the maximum fiber stress may be calculated using eq (7.2) provided the load is applied within the kern of the section. An exact continuous equation for the maximum stress of cracked hollow sections cannot be derived because of discontinuities in sectional geometry. For such cases maximum fiber stress may

TABLE 7.4 *Modulus of elasticity of axially loaded concrete block masonry specimens ($f'_m = 1473$ psi)*

Description of specimen	$E_i \times 10^{-6}$ psi	$\frac{E_i}{f'_m}$	$E_s \times 10^{-6}$ psi	$\frac{E_s}{f'_m}$	$E_t \times 10^{-6}$ psi	$\frac{E_t}{f'_m}$
6 × 16 × 24-in Prisms flat ends	1.5	1020	0.7	480	0.3	200
6 × 32 × 92-in Walls flat ends	1.5	1020	1.4	950	1.0	680
6 × 32 × 24-in Prisms pinned ends	0.8	540	–	–	–	–
6 × 32 × 96-in Walls pinned ends	1.5	1020	1.0	680	0.5	340

be calculated by trial and error procedures using equilibrium of the resultant of a linear stress block on the cracked section with the external load.

Stresses calculated in the manner described above and the corresponding strains obtained from figures 6.9 through 6.12 have been used to evaluate the initial elastic moduli in table 7.5. While these average values are consistently smaller than the initial elastic modulus of like-size prisms tested in axial compression (table 7.4), the elastic modulus appears to be independent of load eccentricity which is a measure of the flexural strain gradient on the cross section. Secant and tangent moduli at failure cannot be reliably predicted on the basis of available test data on eccentrically loaded prisms because of nonlinear effects and, in certain instances, absence of deformation measurements near peak loads. However, the shapes of the curves shown in figure 6.9 through 6.12 suggest that for all practical purposes, it would be reasonable to assume stress-strain characteristics of concrete block masonry in flexure to be similar to those under axial compression.

TABLE 7.5. *Initial modulus of elasticity of eccentrically loaded 6 × 32 × 24-in concrete block prisms* ($f'_m = 1473$ *psi*)

Vertical load at eccentricity	$t/12$	$t/6$	$t/4$	$t/3$
$E_i \times 10^{-6}$ psi	1.0	1.2	1.1	1.0
$\frac{E_i}{f'_m}$	680	810	750	680

Test results of eccentrically loaded masonry walls provide an alternate means of deriving the modulus of elasticity of concrete block masonry in compression. For the case where $e \neq 0$, eq (7.9) applies with the following modification:

$$\Delta = \frac{1}{1 - \frac{P}{P_c}} \Delta_m \tag{7.10}$$

where

$$\Delta_m = \frac{Peh^2}{8EI} \tag{7.11}$$

is the deflection produced by two equal and opposite moments of magnitude Pe applied at the ends of the specimen. The derivation of eq (7.10) is similar to that of eq (7.9) except that eq (7.7) is replaced by eq (7.11).

Table 7.6 lists the initial modulus of elasticity of concrete block walls as determined by equations (7.10) and (7.11) and load-deflection test data. The values obtained are generally in good agreement with test results of walls under axial compression and higher than those derived from eccentrically load prisms having pinned supports.

TABLE 7.6. *Initial modulus of elasticity of eccentrically loaded concrete block walls* ($f'_m = 1473$ *psi*)

Vertical load eccentricity	Wall designation	$E_i \times 10^{-6}$ psi	$\frac{E_i}{f'_m}$
$t/12$	4B3	1.4	950
	4B4	1.4	950
	Avg.	1.4	950
$t/6$	4B5	1.2	810
	4B7	1.3	880
	4B11	1.4	950
	Avg.	1.3	880
$t/4$	4B12	1.8	1220
$t/3$	4B13	1.6	1090
	4B14	1.8	1220
	Avg.	1.7	1150

Concrete block masonry other than the pinned prisms developed an initial modulus of elasticity of $810 f'_m$ to $1220 f'_m$ with an average value of $1020 f'_m$ based on the average compressive strength of 1473 psi obtained from axial tests on prisms with flat support conditions. The values derived from the pinned prism tests were, on the average, about 30 percent less. The current edition of NCMA Specification for Concrete Masonry [13] recommends a modulus of elasticity of $1000 f'_m$ with a specified upper limit of 3×10^6 psi. NCMA recommends a compressive strength which is the test strength modified by a correction factor. This factor is dependent on the height-to-thickness ratio of the test specimen. If a compressive strength of 1768 psi ($= 1473 \times 1.2$, [13]) calculated in accordance with this provision is used as a basis of comparison, the initial modulus of elasticity obtained from tests would be between $675 f'_m$ and $1200 f'_m$ with an average of $850 f'_m$. Thus, for the masonry used in this investigation, the modulus of elasticity derived in accordance with NCMA is, on the average, 17 percent greater than the experimentally derived values.

7.2.4. Summary of Findings and Conclusions

The following conclusions can be drawn on the elastic properties of hollow concrete block masonry specimens:

(1) On the average, the concrete block masonry specimens developed an initial modulus of elasticity which was significantly less ($\cong 15\%$) than that prescribed by the present edition of the NCMA Standard [13]. Thus, it appears, there is a need to reconcile present provisions with experimental evidence.

(2) The initial modulus of elasticity of walls can be reasonably predicted on the basis of load-deformation relationships of prisms with flat ends tested in axial compression. The size and geometry of these specimens should be governed by requirements of a minimum height-to-width ratio (preferably greater than ⅔ which is that of the $6 \times 32 \times 24$ in prisms) that would keep the influence of end zone effects on test results within tolerable limits.

(3) Flexure-induced strain gradients have no appreciable effect on the stress-strain relations of concrete block walls as evidenced by eccentric load tests on the prisms.

7.2.5. Composite Masonry

The composite masonry used in this program consisted of a 4-in-thick brick wythe and a 6-in-thick hollow concrete block wythe. Galvanized steel ties and mortar-filled collar joints were used to insure integral action in flexure. Inspection of test specimens during and after failure indicated that the assembly performed monolithically.

In order to study the capacity of composite walls a knowledge of the stiffness parameters (elastic constants and sectional properties) of its constituents is required. Based on test results of brick and concrete block specimens, a modular ratio of 2.6 has been assumed for the purpose of developing the transformed section used in this investigation. This value falls within the limiting modular ratios of 2.9 for the pinned prisms and 1.9 for all the other specimens (consult tables 7.1 and 7.4). The sectional properties of composite walls listed in figure 4.1 have been determined in accordance with this ratio. The kern eccentricities relative to the centroid of the transformed section are $e_{kc} = 2.04$ in and $e_{kb} = 0.92$ in so that a vertical load applied at e_{kc} (the kern nearest the block face) or at e_{kb} (the kern nearest the brick face) should produce zero stress in the extreme brick fibers, respectively.

Figures 6.14 through 6.18 show a family of curves developed from tests on composite prisms subjected to vertical loads applied at various eccentricities. Noting that load eccentricities close to the kern eccentricities of the section (i.e.,: $e_b = 0.82$ in versus $e_{kb} = 0.92$ in, and $e_c = 1.55$ in versus $e_{kc} = 2.04$ in) produce near zero strains in respective opposite fibers, the assumed transformed section appears to be reasonable. It should also be noted that the results of $10 \times 16 \times 32$-in composite prism tests shown in figure 6.13 are not indicative of the true strains in these specimens because during testing the specimens could not be prevented from partially rotating at the top. This condition, which resulted in variable curvature along the height, is taken into consideration in section 7.3.4 where the correlation of the interaction diagram of composite specimens with test data is interpreted.

The eccentric load tests of composite prisms offer an alternate means to check the initial elastic moduli of masonry. In the region $e_{kb} \geq e \geq e_{kc}$, the maximum fiber stress is determined using the sectional properties of the uncracked section shown in figure 4.1. When the vertical load is applied outside the kern, the maximum fiber stress may be determined on the basis of a cracked section analysis using a linear stress distribution on the uncracked portion of the cross section. These stresses and the corresponding strains obtained from figures 6.14 through 6.18 were used to derive the elastic moduli listed in table 7.7. These values are higher than indicated for the non-composite prisms of similar size and end condition (consult tables 7.1, 7.2, 7.4, and 7.5), while the modular ratio of 2.1 is less than 2.6 (which was based on all the prism tests) used in its derivation.[9] Despite these differences, the computed values in table 7.7 suggest the feasibility of developing criteria for predicting composite behavior from tests of non-composite constituents if a more substantial bank of experimental research data were to become available.

[9] Successive trials made these modular ratios converge to a value of about 2.4 (i.e.: an assumed ratio less than 2.6 yields a computed ratio greater than 2.1, etc.) so that the computed elastic moduli of brick and block were respectively higher and lower than the values appearing in table 7.7.

TABLE 7.7. *Initial modulus of elasticity of eccentrically loaded composite prisms*

Prism designation	Vertical load eccentricity in	$E_i \times 10^{-6}$ psi
3B1–3B3	$e_b = 0.82$ (uncracked)	3.0 (brick)
3B10–3B12	$e_b = 1.64$ (cracked)	2.8 (brick)
3B4–3B6	$e_c = 1.55$ (uncracked)	1.6 (block)
3B7–3B9	$e_c = 3.10$ (cracked)	1.4 (block)
3B14, 3B15	$e_c = 4.65$ (cracked)	1.3 (block)

7.2.6. Flexural Rigidity of Masonry

A reliable prediction of the modulus of elasticity of masonry is essential in the analysis of composite sections or in calculations involving the axial rigidity EA and the flexural rigidity EI of the section. The magnitude of EI depends on the intensity and distribution of stresses on the cross section; the modulus of elasticity decreasing with increasing stress; and the moment of inertia I decreasing with flexural cracking.

An empirical expression for EI which accounts for change in E, as well as in I, is given by

$$EI = E_i I_n \left(0.2 + \frac{P}{P_0} \right) \leq 0.7\, E_i I_n \qquad (7.12)$$

where I_n designates the moment of inertia of an uncracked net section, P designates the compressive load at failure, and P_0 is the axial load capacity derived from prism tests with flat support conditions. This equation was proposed in a study on the capacity of brick masonry walls tested under various combinations of flexure and axial compression [2]. The authors demonstrated that the proposed expression will adequately approximate a substantial amount of test data on brick walls over the entire range of vertical loads. The accuracy of eq (7.12) for short-wall sections of brick and possible application to concrete block masonry can be examined in relation to the curves for eccentrically loaded prisms from this experimental investigation (figs. 6.3 through 6.6 and 6.9 through 6.12). In short walls, the moment $P\Delta$ produced by vertical load P acting on transverse deflection Δ, is negligible compared to the moment Pe and therefore the specimens may be assumed bent in constant curvature. From moment-curvature relation the following equation for the flexural rigidity at failure is derived:

$$EI = \frac{Pet}{\epsilon_1 - \epsilon_2} \qquad (7.13)$$

where ϵ_1 and ϵ_2 designate maximum (compressive) and minimum strains associated with the two opposite face fibers of the specimen. The values of EI obtained for brick and concrete block specimens in this manner are plotted on the nondimensional chart shown in figure 7.6 which also shows a plot of eq (7.12). It is noted that better agreement with brick prism data are obtained while EI for concrete block prisms is underestimated. Obviously, these results should be viewed in light of the limited available test data, particularly in the region where $P/P_0 < 0.50$. In the subsequent sections (7.4.1) and (7.4.2) it is demonstrated that the use of the bilinear curve for EI given by eq (7.12) results in moment amplification factors which, when applied to brick as well as concrete block prism test data, give wall capacities comparable to those obtained from tests of large-size wall specimens in which stability effects are not insignificant.

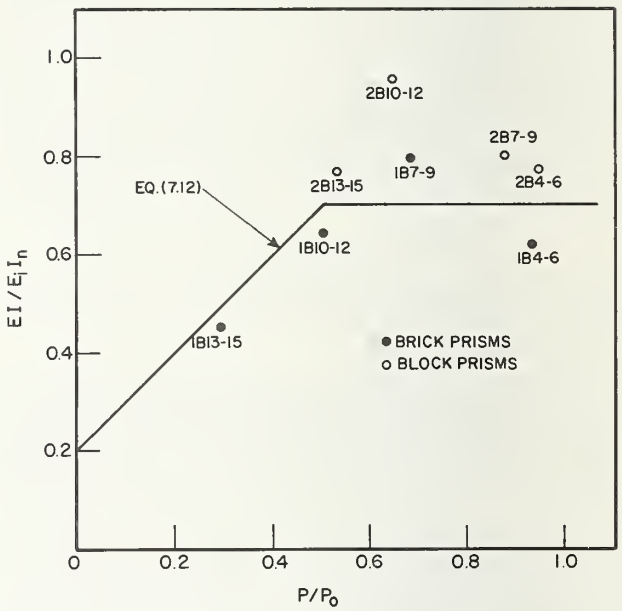

FIGURE 7.6. *Flexural rigidity of brick and concrete block prisms at failure.*

7.3. Capacity of Short Wall Sections

In order to investigate the strength of full-scale wall panels, it is first necessary to consider the capacity of short prisms in which deflections are small. In this section, the test results of prisms are discussed and compared with an analytical approach which closely parallels the procedure used to predict the test results of other experimental programs [1, 2]. A summary of the interactive relations between compression and flexure at failure, from these previous studies, is given in section 9.1 for convenient reference.

7.3.1. Analytical Basis

The analytical approach described in section 9.1 has been developed to predict the capacity of masonry piers under various configurations of load-

ing producing compression and flexure. Equations (9.1) through (9.8) have been derived from consideration of equilibrium conditions and are based on the assumption that the stress-strain relationships for masonry are approximately linear and therefore the stress distribution on the critical section at failure can be approximated reasonably well by a linear stress block. The test results from previous experimental programs [1, 2, 17, 19] have been used to demonstrate that cross-sectional capacity determined in accordance with the proposed analytical approach is in close agreement with that developed from test data.

The constitutive relationships discussed in section 7.2 provide a means to examine the approximation involved in the assumption of linear stress distribution across the section at failure. In connection with the curves shown in figures 7.1 and 7.5, it is observed that the lower halves of the stress-strain curves for brick and concrete block masonry are approximately linear. While the upper halves of these curves are, in general, not linear, a linear approximation for the entire loading region would not depart significantly from these curves. It is noted that a stress block at failure, similar in shape to the area under the actual stress-strain curve, can be closely approximated by a statically equivalent linear stress block without significantly changing the position of the resultant force. In the following sections, it is shown that such an approximation gives predicted capacities which are reasonably consistent with the test results.

7.3.2. Capacity of Brick Prisms

A total of fifteen $4 \times 32 \times 16$-in prisms were tested under vertical loads applied at equal top and bottom eccentricities of 0, $t/12$, $t/6$, $t/4$, and $t/3$ in a manner that would permit end rotations (pinned ends). In addition, five prisms were tested in axial compression in a manner that would inhibit end rotation (flat ends), and ten $4 \times 8 \times 24$-in prisms were tested as beams subjected to transverse loading.

Figure 7.7 shows plots from individual test results of eccentrically loaded prisms. The compressive loads at failure are taken from table 6.1 while the moments are computed from the product $M = Pe$. The 509-kip load plotted on the P-axis is the equivalent average failure load of five stacked-bond prisms tested in axial compression, the equivalence being established on the basis of common cross-sectional area.

It is evident, from figure 7.7 and table 6.1, that the apparent compressive strength of masonry in flexure is significantly greater than that in axial compression. A similar behavior of clay masonry has been reported in references [1] and [2] which introduced the coefficient "a" to distinguish compressive strength in flexure, designated by af'_m, from the compressive strength f'_m, obtained from

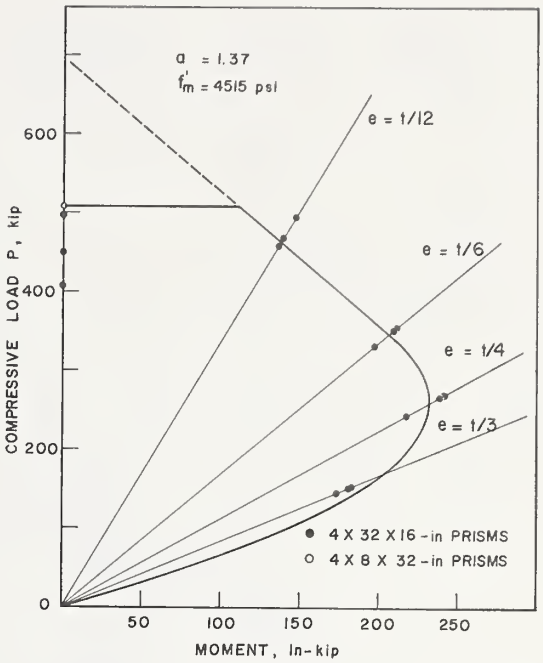

FIGURE 7.7. *Cross-sectional capacity of brick prisms.*

axial load tests on prisms with flat supports. The values of "a" given in table 7.8 have been calculated by taking the ratio of flexural compressive strength to axial compressive strength. It is interesting to note that "a" is approximately constant for vertical load eccentricities of $t/4$ or less, and decreases by only about 14 percent at $e = t/3$. Thus, the statement in reference [2] that "a" appears to increase with eccentricity is not substantiated by these test results.

TABLE 7.8. *Coefficient* "a" *for brick prisms*

e/t	1/12	1/6	1/4	1/3
"a" for $f'_m = 4515$ psi (flat ends)	1.40	1.37	1.36	1.18
"a" for $f'_m = 4016$ psi (pinned ends)	1.57	1.54	1.53	1.32

The solid curve shown in figure 7.7 is a theoretical interaction curve developed from eqs (9.5) and (9.6) and the average compressive strength under kern loading (i.e., $af'_m = 1.37 \times 4515 = 6140$ psi). The solid line $e = t/6$ marks the boundary between cracked and uncracked sections. Note that the theoretical interaction curve is in good agreement with test results for $e \geq t/12$ but slightly over-

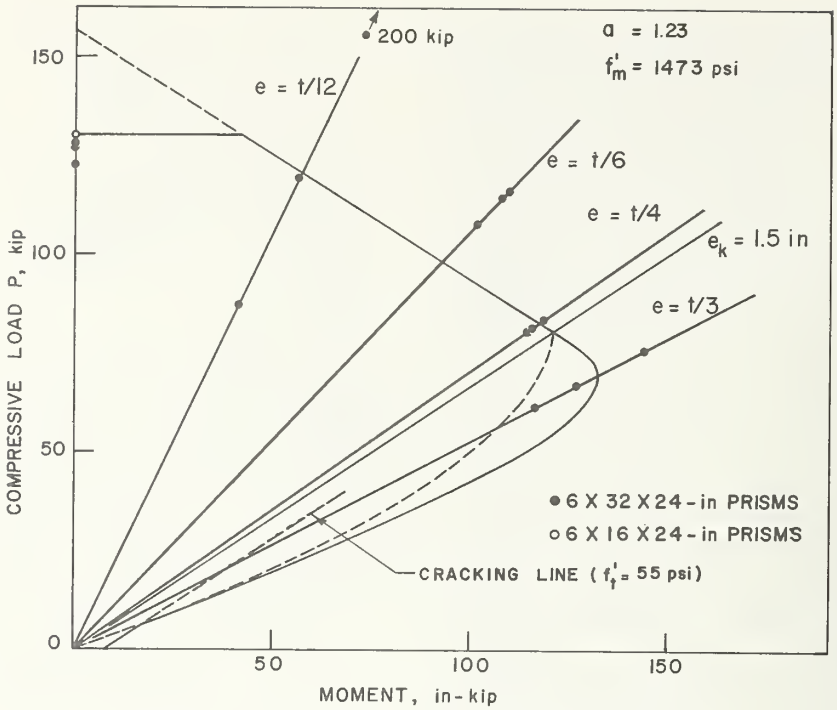

FIGURE 7.8. *Cross-sectional capacity of concrete block prisms.*

estimates the capacity at $e=t/3$. It should also be pointed out that the theoretical interaction curve overestimates axial load capacity in situations where coefficient "a" is greater than unity (since by definition $a=1$ for axial loading). From a practical viewpoint, this inconsistency may be readily resolved by limiting the compressive load capacity to that obtained from axial load tests of prisms with flat supports. This criterion would then confine the interaction diagram to the portion below the solid horizontal line passing through the hollow circular point on the P-axis shown in figure 7.7.

The specimens tested as beams developed an average tensile capacity of 128 psi under transverse concentrated loads applied at third points of the span and 111 psi under transverse uniform loads. The results for the individual specimens are listed in table 6.3. Since these values correspond to a moment capacity of about 2 in-kip, which is very small, the cracking line for $f_t' \neq 0$ has been omitted in figure 7.7.

7.3.3. Capacity of Concrete Block Prisms

Fifteen $6\times32\times24$-in prisms were tested with pinned support conditions under vertical loads applied at equal top and bottom eccentricities of 0, $t/12$, $t/6$, $t/4$, and $t/3$. Five $6\times16\times24$-in prisms were tested under axial compression and with flat support conditions. Flexure tests included five $6\times16\times16$-in prisms tested in accordance with ASTM−E149 [3] and ten $6\times16\times32$-in prisms tested as horizontal beams.

Figure 7.8 shows plots from individual test results of eccentrically loaded prisms using failure loads from table 6.1 and corresponding moments, Pe. The average 130-kip failure load of the five $6\times16\times24$-in specimens with flat ends, computed on an equal area basis, is plotted on the same figure.

Considering the results in figure 7.8 and table 6.1, once again it is evident that a significant increase in the apparent compressive strength occur as a result of flexure. Magnitudes of coefficient "a" calculated for various vertical load eccentricities are shown in table 7.9.

TABLE 7.9. *Coefficient "a" for concrete block prisms*

e/t	1/12	1/6	1/4	1/3
"a" for $f_m'=1473$ psi (flat ends)	1.23	1.41	1.23	1.21
"a" for $f_m'=1405$ psi (pinned ends)	1.29	1.48	1.29	1.27

The solid curve shown in figure 7.8 is a theoretical interaction diagram based on the compressive strength under kern loading (i.e., $e_k \sim t/4$, $af'_m = 1.23 \times 1473 = 1814$ psi). The portion of the curve above the cracking line $e_k = 1.50$ in, is developed from eq (9.6) which applies to uncracked sections; the curved portion below the cracking line is obtained from equilibrium of the resultant of a linear stress block on the uncracked portion of the cross section with external loads: the straight portion shown intersecting the moment axis near the origin is the cracking line developed from eq (9.8) assuming an average modulus of rupture $f'_t = 55$ psi, for the small specimens tested in bending (table 6.3). For comparison, the approximate interaction equation (9.5) for the cracked section is indicated by the broken curve on the same figure. This approximation introduces a maximum error in the moment of about 11 percent and is on the conservative side. Equation (9.5) offers the added advantage of being much simpler to use for design purposes than a cracked section analysis.

Consistent with the approach considered for brick masonry, the compressive load capacity of the section may be conservatively assumed to be limited to the capacity developed by the axially loaded prisms with flat ends. The solid horizontal line shown in figure 7.8 would then be considered as the maximum useful capacity of the section.

7.3.4. Capacity of Composite Prism

Fifteen $10 \times 32 \times 32$-in composite prisms were tested under vertical loads applied at equal top and bottom eccentricities (including $e = 0$) in a manner that would permit rotation at the supports. In addition, ten $10 \times 16 \times 32$-in prisms were tested as horizontal beams and five $10 \times 16 \times 32$-in prisms were tested under axial compression. The intended test setup for the latter specimens was one that would simulate flat support conditions. As previously noted (sec. 7.2.5), these specimens could not be entirely constrained against rotation at the top while testing was in progress, and therefore, the effective load eccentricity at the top is not known precisely. In table 6.2, the maximum compressive stress at failure for specimens 3A1 through 3A5 was calculated using an estimated eccentricity of $e_c = 1.23$ in derived by linear interpolation between compressive load capacities at $e = 0$ and $e_c = 1.55$ in, taking into account the difference in cross-sectional areas.

Figure 7.9 shows plots from individual test results of eccentrically loaded composite prisms obtained from the failure loads listed in table 6.2 and the corresponding moments calculated from the product Pe. The results of $10 \times 16 \times 32$-in prism compression tests are also plotted on the basis of an estimated eccentricity of $e_c = 1.23$ in and a common equivalent area of 394.8 in^2 (fig. 4.1). Note that one of the three specimens loaded at $e_b = 0.82$ in and one of the two specimens loaded at $e = 0$ did not fail under the 600-kip capacity of the testing machine. This condition is indicated by arrows drawn at the appropriate points in the figure.

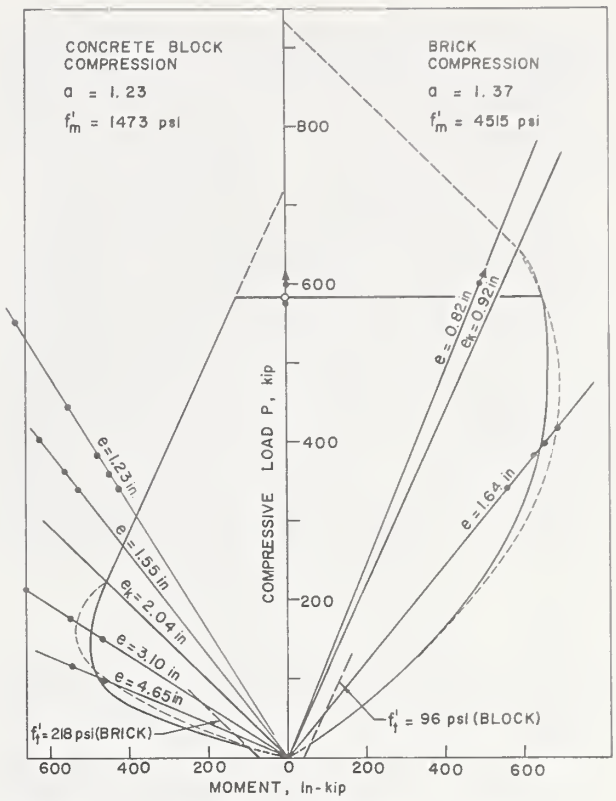

FIGURE 7.9. *Correlation of wall strength with prism strength of composite masonry.*

The analytical prediction of the sectional capacity of short composite walls in accordance with the equations in section 9 requires the use of compressive strength values in flexure for the brick and concrete block masonry components. The theoretical interaction diagram shown by the solid lines in figure 7.9 is based on the respective compressive strengths of brick and concrete block prisms under kern loading as previously determined (figs. 7.7 and 7.8). The plot on the right applies to moments that cause compression in the brick, and the plot on the left applies to moments that cause compression in the block. The diagram for eccentricities smaller than the kern eccentricity ($e_{kc} = 2.04$ in and $e_{kb} = 0.92$ in) is developed from eq (9.2) applicable to uncracked sections. The curved portions of the diagrams for larger eccentricities are obtained by statics assuming a linear stress block on the uncracked portion of the cross section. The two moment capacities based on flexural tensile strength lines for $f'_t \neq 0$, shown intersecting the interaction curves at low compressive loads, are developed from eq (9.4). The intercepts of these lines with the moment axis are calculated on the basis of average

f_t' values obtained from flexure tests of brick and block prisms (table 6.3). Interaction curves for the cracked section developed from the approximate simplified equation (9.1), are shown by the broken curves. It is noted that in this case the approximation slightly overestimates the capacity, the maximum error introduced being less than 10 percent.

Figure 7.9 indicates that, in general, when failure occurs in the brick there is good agreement between the analytically derived capacity and the test results. On the other hand, at certain eccentricities ($e_c = 1.55$ in, for instance), the block side of the composite wall developed capacities considerably in excess of those predicted on the basis of tests on block prisms. This increased capacity is probably attributable to the confining effects of the brick wythe and the ties and should be further investigated. It should be pointed out that at $e_c = 1.55$ in and, in general, at small load eccentricities towards the block face, failure occurred by vertical cracking in the web of the block, indicating the type of tensile failure mode described in section 7.3.4.

At $e_b = 0.82$ in, the theoretical capacity was probably in excess of the average test capacity (600 kip or greater) by a small margin. The average axial load capacity was greater than 590 kip. This is slightly more than the average capacity of 582 kips which is equal to the product of the compressive capacity of concrete block specimens ($f_m' = 1473$ psi) and the transformed concrete area of the composite section (394.8 in^2), but it is probably less than the average capacity of 685 kip which is equal to the product of the compressive capacity of brick specimens ($f_m' = 4515$ psi) and the transformed brick area (394.8/2.6 = 152 in^2) of the same composite section.

By reference to figure 7.9, it is noted that the condition of dual axial load capacities occurs as a result of having used different values of coefficient "a" for the brick and concrete block components of the composite section. In addition, as in the case for the noncomposite prisms, the use of $a > 1$ gives theoretical capacities in excess of the test values at small or zero eccentricities. In a practical design situation these conditions may be satisfactorily and conservatively resolved by requiring the compressive load capacity not to exceed the axial load capacity of the weaker component (583 kips in this case). This limit is displayed in figure 7.9 by the horizontal lines intersecting the ordinate at $P = 582$ kip.

7.3.5. Failure Hypothesis for Hollow Concrete Block

In the foregoing analysis it was demonstrated that interaction curves based on a flexural compressive strength coefficient "a" evaluated at the kern eccentricity, provide reasonably good approximation to short wall capacity except that in cases where the compressive load is applied at small or zero eccentricity the capacity is overestimated since "a" is greater than unity. It should be noted that eqs (9.2) and (9.6) are based on the premise that failure will occur when the maximum stress in the extreme fiber equals the apparent compressive strength in flexure, af_m', derived from an assumed linear stress distribution on the cross section. Hollow concrete block walls built with face shell mortar typically fail by vertical tensile splitting of the web under compressive loads applied axially or at small eccentricity (figs. 6.22 and 6.23, and fig. 6.19 of ref. [2]). Furthermore, a substantial body of experimental evidence from this and previous studies (figs. 7.7 and 7.8 and refs. [1, 2]) indicates that compressive load capacity is not significantly altered by variations in positioning of vertical load at small eccentricities when the characteristic failure mode is tensile.

To study the behavior of a hollow block unit in compression, a finite element analysis is presented in section 9.2 using a 100-kip load placed at various eccentricities on the 6×32-in section shown in figure 4.1. The load was assumed to be transmitted to the face shells and through shear action to the webs. The numerical results are shown in figures 9.3 through 9.8.

Subject to the limitations of the idealized model described in section 9.2, certain inferences may be drawn from these results. For instance, it is observed that a condition of maximum uniaxial tensile stress exists at the top of the web midway between the two face shells under a concentrically applied load (fig. 9.3). According to maximum normal stress failure theory, initiation of failure by cracking of the web at this location might therefore be expected. This prediction would corroborate the observed mode of failure of hollow block masonry test specimens. It is further noted, by reference to figures 9.4 to 9.7, that increasing the vertical load eccentricity does not appreciably alter the magnitude of this tensile stress; a condition which may explain the insensitivity of the average sectional capacity to variations in the positioning of vertical loads within the central third region of the specimen as indicated in figure 7.8 ($e = \pm t/6$). At larger eccentricities, the maximum positive normal strain near the face shell (element 1) is considerably in excess of the maximum uniaxial tensile strain in the web (figs. 9.7 to 9.9). This condition could cause initiation of web failure near the face shell junction.

The foregoing example was used to provide qualitative information on the behavior of masonry specimens built with hollow block units and face shell mortar. The procedure can be effectively utilized to study parametric relationships to better predict the cross-sectional capacity on the basis of experimentally observed failure mechanisms. Furthermore, a study on the optimum shape of a hollow block unit could offer the potential of improvements in the strength characteristics of concrete block masonry construction.

7.3.6. Summary of Findings and Conclusions

The following compares analytically predicted and experimentally derived properties of short wall sections obtained from the current test series and relates to similar documented studies based on previous test results [1, 2, 17, 19].

(1) The moment capacity of short masonry walls under compressive loads can be reliably predicted by rational analysis based on linearly elastic behavior at failure. This conclusion is consistent with that drawn from the previous studies. The constitutive relations developed in section 7.2 provide further indication that the response of masonry walls at failure may be considered as being essentially linear.

(2) The previous studies indicated an apparent increase in the compressive strength of masonry from f'_m under axial compression to af'_m under combined compression and flexure, where "a" is a coefficient greater than unity. The results from the current test series corroborate this trend. For instance, within the range of eccentricities used ($t/12 \leq e \leq t/3$), and on the basis of f'_m derived from axial tests on prisms with flat supports, the average value of coefficient "a" was 1.33 for the brick specimens and 1.27 for the concrete block specimens, with the values at other eccentricities not being appreciably different from these averages. Thus, the hypothesis advanced in the previous studies that compressive strength increases with flexural strain gradient was not corroborated by the current test results.

(3) The theoretical interaction diagrams for brick and concrete block prisms were developed on the basis of the corresponding compressive strengths at the kern eccentricities, noting that the values of 1.37 and 1.23 of coefficient "a" at these eccentricities (shown underlined in tables 7.8 and 7.9), were nearly equal to the respective average values. The feasibility of a standard prism test using kern loading to evaluate coefficient "a" has considerable practical significance in the design of masonry walls on the basis of ultimate strength theory. Since "a" is greater than unity, however, an ultimate design approach should simultaneously stipulate limitation of the maximum compressive load capacity at the level obtained from standard prism tests under axial loading.

(4) The possibility of a tensile failure mode in the web of concrete block units in compression specimens constructed with face shell bed mortar was explored by means of a finite element analysis. The results indicated that when the axial compressive load is transmitted to the units through the face shells, peak uniaxial tensile stress conditions develop near the unmortared top and bottom surfaces of the web. This situation could account for the vertical cracking pattern frequently observed in compression tests of small specimens. The analysis also indicated that the same load applied at a range of eccentricities (approximately confined within the kern of the section) did not appreciably alter the magnitude of the peak tensile stress in the web. Thus, a tensile mode of failure would provide a plausible explanation of the experimental trend of undiminished compressive strength of prisms within a certain range of low vertical load eccentricities.

(5) The interaction diagram for the composite specimens developed on the basis of noncomposite prism test data, generally showed good correlation with composite test results. However, when the strength of the composite section was governed by compressive failure of the concrete block wythe, analytically predicted values tended to become quite conservative at small load eccentricities. This trend is probably attributed to an increase in the strength of the concrete block component as a result of its confinement by the brick and the presence of horizontal steel ties in the assembly.

7.4. Wall Capacity

In section 7.3, the test results of short wall sections were predicted reasonably well by the analytical approach discussed in section 9.1. In this section, the interaction diagrams developed in that analysis are compared with the experimentally observed load capacity of 8-ft wall panels, taking into consideration the additional effects of wall slenderness.

7.4.1. Capacity of Brick Walls

A total of sixteen $4 \times 32 \times 96$-in brick walls were tested under various loading conditions. The test results for walls subjected to vertical loads are given in table 6.4. The test results for walls subjected to concentric load and transverse uniform load are listed in table 6.5. The load-deflection curves of brick walls are plotted in figures 6.28 and 6.30.

Walls tested under transverse uniform load and zero vertical load developed moments of 5.4 in-kip and 2.3 in-kip corresponding to flexural tensile strengths of 80 psi and 34 psi, respectively. These values compare with an average tensile strength of 120 psi developed by the $4 \times 8 \times 27$-in beam specimens. Thus, on the average, the walls developed about 50 percent of the tensile strength obtained from prism tests.

The correlation between prism strength and wall strength is shown in figure 7.10. The part of the moment attributed to horizontal deflection is shown by a horizontal line. The left end of this line represents the maximum moment excluding the effect of the vertical load acting on the horizontal deflection. Where the line is solid, the right-hand end represents the total maximum moment at failure. Thus, the length of the solid horizontal line is a measure of the magnitude of the slenderness effect. The right-hand end of the solid horizontal lines should be compared to the solid interaction curve on the

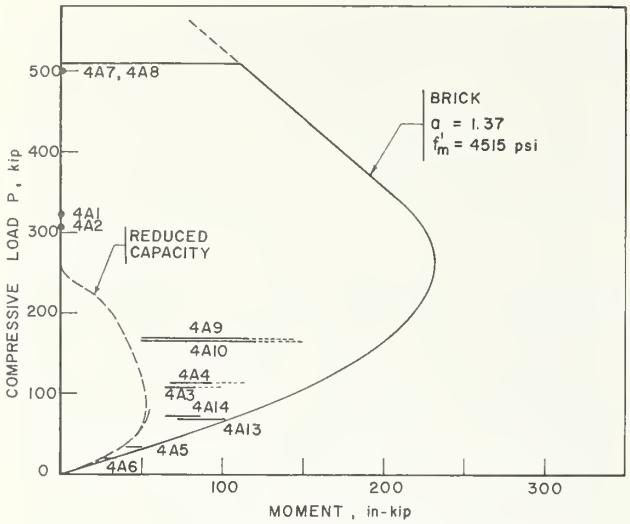

FIGURE 7.10. *Correlation of wall strength with prism strength of brick masonry.*

right which was derived from the prism tests. However, by reference to table 6.4, it is noted that instrumentation on all specimens tested under vertical load was removed prior to failure. For such cases the solid portion of the horizontal line is the magnitude of the added moment at the last measured deflection while the dotted line merely indicates that such removal occurred. Therefore, in general, a direct comparison with prism moment capacity represented by the solid interaction curve cannot be made.

As an alternate basis of comparison between prism and wall strength, the theoretical interaction diagram for the prisms may be modified by using a moment magnification factor [2]. The modified interaction diagram shown by the dotted curve on the left-hand side in figure 7.10 is developed using reduced moments calculated from the following equations:

$$M_0 = M_e \left(1 - \frac{P}{P_{cr}} \right) \tag{7.14}$$

$$P_{cr} = \frac{\pi^2 EI}{h^2} \tag{7.15}$$

where M_e is the moment capacity of the prisms obtained from eqs (9.5) and (9.6), M_0 is the reduced moment capacity, P_{cr} is the Euler buckling load for specimens pinned at the ends, h is the height of the wall and EI is the flexural rigidity determined from eq (7.12). The value of $E_i = 2.8 \times 10^6$ psi used in eq (7.12) was taken from table 7.1.

The reduced interaction curve developed in this manner should be compared with the left ends of the solid horizontal lines. Figure 7.10 indicates generally good correlation between theory and experimental results.

The walls with flat end supports developed a 500-kip axial load capacity. This compares closely with the 500-kip equivalent average axial capacity of the prisms with flat end supports and is about 10 percent greater than the average value of 452 kip developed by the prisms with pinned support conditions. The fact that these walls could develop the full short wall capacity is attributed to the rotational constraints induced by the flat support condition at the ends. The axially loaded walls with pinned support conditions failed by stability-induced compression at an average load of 314 kip. The moment capacity of all other walls except the two specimens with zero axial load was significantly reduced by slenderness effects.

7.4.2. Capacity of Concrete Block Walls

Twenty-six $6 \times 32 \times 96$-in hollow block masonry walls were tested under various load combinations. Table 6.4 shows the test results of 18 walls subjected to compressive loads applied at the specified eccentricities. The remaining eight walls were subjected to various combinations of transverse uniform load and vertical load. These results are shown in table 6.5. The load-deflection history of block walls is illustrated by the curves shown in figures 6.28 and 6.30.

The two walls tested under transverse uniform load and zero axial load developed tensile strengths of 18 psi and 40 psi. The $6 \times 16 \times 32$-in prisms, tested as beams, developed average tensile strengths of 51 psi under uniform loading and 38 psi under third-point concentrated loads. Thus the full-scale walls developed, on the average, approximately 60 percent of the average tensile strength of the prisms although the number of replicate wall tests (two specimens) was too small to permit a stochastic assessment of scatter which appears to be considerable in this case.

In order to compare wall strength to the interaction curves for the prisms, the additional moment attributable to the wall slenderness must be taken into consideration. Figure 7.11 correlates the strength of the full-scale wall specimens to the predicted strength of the prisms. The moment attributable to wall slenderness effect is given by the product of the maximum vertical load and the corresponding maximum transverse midheight deflection in the wall and is shown by the horizontal lines in the figure. In cases where such deflection measurement is not available, the solid portion of the horizontal line is the magnitude of the added moment at the last measured deflection.

The solid curve in figure 7.11 is the interaction curve previously developed for concrete block prisms (fig. 7.8). The broken curve is the reduced interaction curve developed from eqs (7.12), (7.14), and (7.15) and an initial modulus of elasticity of $E_i = 1.5 \times 10^6$ psi as previously derived in section 7.2.3 and listed in table 7.4. The predicted moment

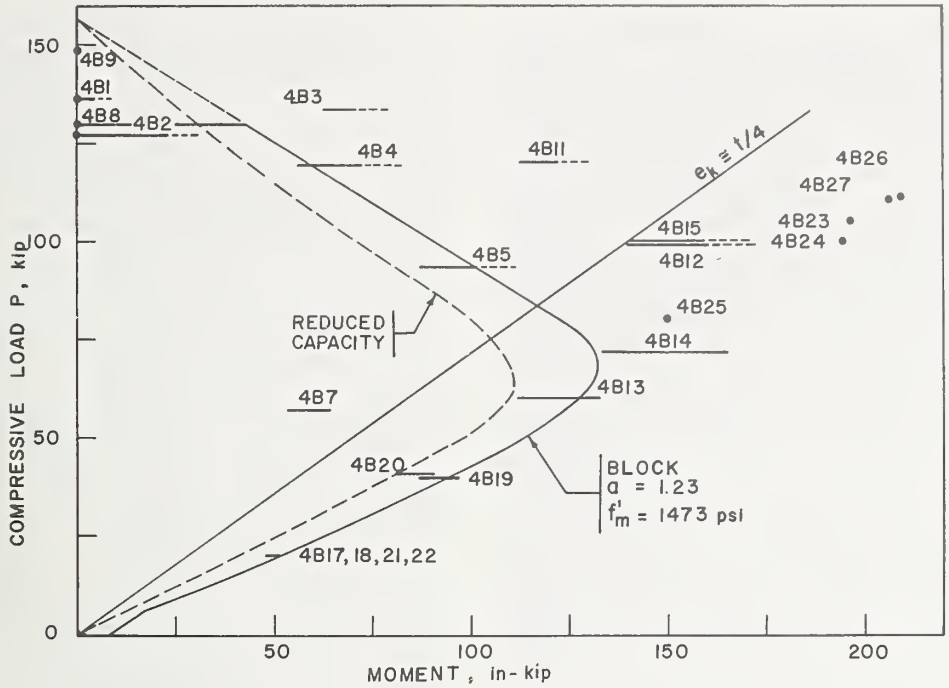

FIGURE 7.11. *Correlation of wall strength with prism strength of hollow concrete block masonry.*

attributed to wall slenderness, which is represented by the horizontal interval bounded by the original and reduced interaction curves at any particular load level, is, in general, reasonably consistent with the magnitude of the corresponding measured value from wall test results as indicated in the figure by the length of the solid horizontal lines.

In the region below the cracking line, $e \simeq t/4$, the short-wall interaction curve closely predicts wall capacity. Above this line, wall capacity exceeded predicted values, often by considerable margins. This difference is probably attributed to a tensile mode of failure prevalent at smaller eccentricities as described in section 7.3.5. Also, the walls were tested at twice the average age at which the prisms were tested and it is likely that some strength gain occurred as a result of this difference. It should be noted that specimen 4B7 was damaged during handling and, therefore, its strength should not be considered indicative of wall strength at $e = t/6$. Walls tested in axial compression developed a strength equal to or greater than the average axial load capacity of the prisms.

The wall tests included two sets of specimens which were subjected to compressive loads applied at unequal top and bottom eccentricity. In specimens 4B23 and 4B24, the top and bottom eccentricities were 1.867 in and zero, respectively. In specimens 4B25 through 4B27, the top and bottom eccentricities of 1.867 in were equal, but opposite, causing the walls to bend in double or reverse curvature. Since, in all these specimens, the maximum moment occurred at the ends, their capacity was not altered by slenderness effects. Figure 7.11 compares the test values plotted as points with the short-wall interaction curve. It is seen that all but one specimen tested more than twice the predicted moment capacity. However, since the critical section at the supports is laterally confined by the steel bearing plates, the capacity of the section, as governed by tensile splitting of the web, would increase significantly. The cracked specimen shown in figure 6.22 provides corroborative, visual evidence on the extent of lateral confinement at the ends.

7.4.3. Capacity of Composite Walls

Sixteen $10 \times 32 \times 96$-in brick and hollow concrete block composite wall were tested under various load combinations. Table 6.4 shows the test results for eight composite walls subjected to vertical loads applied at the designated eccentricities. The test results for walls under combined transverse and axial loads (including $P = 0$) are shown in table 6.5. Figures 6.29 and 6.31 show plots of transverse deflection versus vertical load and transverse uniform load, respectively.

The two composite walls tested in axial compression did not fail under the 600-kip load capacity of the testing machine. As previously noted, one of the composite prisms also did not fail at this load level while the other prism developed an axial load capacity of 577 kip. The two walls, tested under a transverse uniform load applied to the hollow block face and zero vertical load, developed tensile

strengths of 104 psi and 74 psi. These should be compared to the average value of 218 psi obtained from tests of similarly loaded composite prisms, and to the average value of 120 psi obtained from beam tests of brick prisms. Note that the walls developed 74 percent of the average tensile strength of brick prisms and 41 percent of the tensile strength of the brick component of composite prisms. The two composite walls under uniform transverse load and zero vertical load developed almost equal tensile strengths of about 76 psi, which is equal to the average tensile strength of concrete block prisms tested in accordance with ASTM E149 [3], but greater than the average values of 38 psi and 51 psi derived from respective concrete block beam tests under third-point concentrated loads and transverse uniform loads. This strength is about 79 percent of the average tensile strength of the block component of composite prisms tested as beams.

The moment amplification approach may also be used to compare composite wall strength to predicted short-wall capacity. The slenderness effect is small in the composite masonry walls because they are stiffer than either the brick or the concrete block walls.

In figure 7.12, the strength of full-scale walls is compared with the predicted strength of the prisms. Again, the moments attributed to wall slenderness are indicated by horizontal lines, the solid portion of which is the moment increment corresponding to the last measured deflection or the deflection at maximum load at failure in cases when such deflection measurement is available.

The outer solid curves in figure 7.12 represent the interaction diagram of the composite prisms (fig. 7.9). This diagram was developed on the basis of different compressive strengths for the brick and concrete block components of the composite section. The inner broken curves represent the reduced interaction diagram developed from eqs (7.12), (7.14), and (7.15) and an initial elastic modulus of $E_i = 1.5 \times 10^6$ psi for concrete to account for the effect of wall slenderness. A comparison of the reduced diagram with the ends of the horizontal lines closest to the load axis (unamplified moment capacities of the walls derived from tests) indicates a smaller predicted capacity than that derived from wall tests in cases where failure was governed by the compressive strength of the concrete block masonry component. As noted earlier, the increased capacity of the concrete block component is probably attributed to the confinement effect of the brick wythe and the metal ties used in the construction of composite specimens. When failure was governed by the compressive strength of the brick component, the capacity of the section was predicted more closely but somewhat less conservatively. The maximum difference occurred for specimen 4C5, with the predicted test-derived moment capacity exceeding the (unamplified) test-derived moment

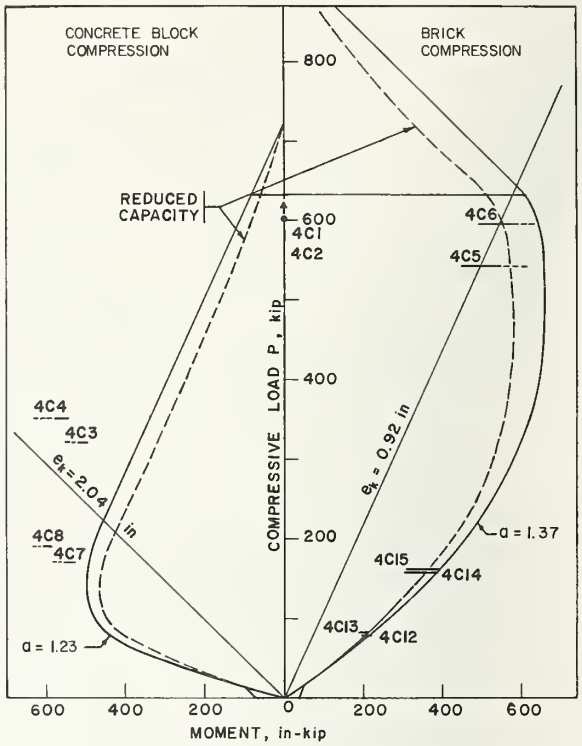

FIGURE 7.12. *Correlation of wall strength with prism strength of composite masonry.*

capacity by about 26 percent. This is probably attributed to the considerable difference in strength and in stiffness between the brick and concrete block components. Under certain loading conditions, the flexural compressive strength in the concrete fibers interfacing with the brick may develop before the outer face fibers in the brick attain their maximum compressive strength, and thereby contribute to the reduction in the load capacity of the composite assembly.

7.4.4. Summary of Findings and Conclusions

The following conclusions are drawn from the test results of the three types of masonry walls subjected to various combinations of vertical and transverse loads:

(1) The capacity of brick walls was closely and conservatively predicted by analytically derived interaction equations for short-wall sectional capacity, modified in accordance with eqs. (7.12), (7.14), and (7.15) to account for the effect of wall slenderness. This agreement is rather significant in view of the substantial reduction in moment capacity caused by wall slenderness and demonstrates the feasibility of utilizing the approximate moment amplification factor given by eq (7.14) together with the empirical relationship (7.12) for estimating the flexural rigidity of the wall.

(2) The reduction in capacity attributable to slenderness effects was also evident in the results of tests on full-size concrete block wall specimens. However, compared to the brick walls, the influence of wall slenderness was small. This is attributable to the fact that the compressive strength and height-to-thickness ratio of concrete block walls were less than the corresponding values for brick walls. Nevertheless, the trend of the experimental results for the concrete masonry walls was correctly predicted on the basis of the same analytical approach as was used for the brick walls. The moment capacity derived from theory and experiment were in close agreement in the region of small compressive loads, while at larger loads, the test-derived capacity of the walls, which often exceeded that of the comparable prisms, were conservatively predicted. As noted elsewhere in the report, the average age of the walls was twice that of the prisms. Thus, to a certain extent, the observed strength gain of the walls is probably attributed to this age difference.

(3) Generally, good agreement was obtained between predicted and test-derived capacities of brick-block composite walls. The experimental trend in composite construction, both in the prisms and the walls, seemed to indicate a definite increase in the strength of the concrete block component and a slight decrease in the strength of the brick component, in relation to the values indicated by independent tests of each component. Since the theoretical interaction diagram was developed on the basis of noncomposite prism tests, the predicted capacity tends to be more conservative when failure is governed by the strength of the concrete block constituent.

(4) On the average, the walls subjected to lateral loads and zero axial compression developed approximately 50 percent of the flexural tensile strength of the prisms. This size effect would be significant in design which, from a practical standpoint, will probably have to be based on tensile bond strength measurements obtained from small prism tests with appropriate modifications to account for wall size. However, the results indicate the need for additional test replication of large-scale specimens to permit a more reliable assessment of this trend.

8. Conclusions and Recommendations

8.1. Conclusions

The diverse combinations of loads and the different types and sizes of masonry specimens used in this experimental program provided the means for a comprehensive study of the constitutive relationships of masonry. Initial elastic moduli of brick and concrete block specimens, developed independently from prism and wall test results, showed generally good agreement but were consistently smaller than those stipulated by the current masonry standards [12, 13, 22]. The difference was sufficiently significant to indicate the need to reconcile current practice with experimental evidence.

The stress-strain curves developed from compressive tests on prisms were observed to be insensitive to flexure-induced strain gradients on the cross section. The initial modulus of elasticity of masonry walls was reliably predicted on the basis of axial load test results on prisms with flat support conditions but was consistently greater than that obtained from prisms with pinned support conditions. The tangent modulus of elasticity at failure was of the order of 30 to 50 percent of the initial elastic modulus. In general, the stress-strain relationships were sufficiently linear to permit a close analytical prediction of test-derived sectional capacity by assuming a linear stress block on the cross-section at failure.

An empirical relationship for the flexural rigidity EI, proposed by the authors of reference [2] for brick masonry, was checked for correlation with prism test data for brick as well as concrete block masonry. It was subsequently shown that the use of this expression in the analytical derivation of sectional capacity gives predicted values which are consistent with experimental results for the three types of masonry walls considered in this program.

In previous experimental studies [1, 2] the observation was made that compressive strength in flexure (af'_m) derived from a linear stress distribution in the cross section at failure, exceeds the compressive strength (f'_m) developed in axial compression by a significant margin. This observation was quantitatively corroborated by the results of the present experimental program. In the case of kern loading, for instance, coefficient "a" was calculated as 1.23 and 1.37 for the respective concrete block and brick specimens using f'_m of flat-ended prisms as a datum; an increase of 23 and 37 percent in respective strengths. It was further observed that these values did not significantly change at other eccentricities, and, therefore, a prism test with kern loading should permit a reliable calculation of coefficient "a".

With certain modifications proposed in this study, the theoretical approach developed by the authors of reference [2] was used to predict the capacity of short masonry walls. The modifications were introduced in order to take full advantage of the increased compressive strength in flexure. Specifically, the theoretical interaction diagrams for short wall capacity of brick and concrete block masonry were developed using a constant coefficient $a > 1$, based on the compressive strength of the prisms loaded at the kern or at the centroid, whichever resulted in a smaller total axial load capacity. In general, the interaction curves developed in this manner showed consistently good agreement with experimentally derived short-wall capacity. In the case of brick-block composite construction, the interaction curves, developed on the basis of flexural compressive

strengths of the respective brick and concrete block components, showed reasonably good correlation with test data on component wall strength.

The capacity of full-size, brick, concrete block and brick-block composite walls was reasonably predicted by means of short-wall interaction relationships modified to account for amplification of internal moments attributed to slenderness effects [2]. In the case of walls where flexure was induced by lateral loads singly or in combination with eccentrically applied compressive loads, the agreement between theory and experiment constitutes a generalization of the basic theory proposed in the earlier studies [1, 2, 17, 19].

Brick masonry specimens under compressive loads applied at small or zero eccentricity typically failed by in-plane vertical cracking. Similarly loaded concrete block masonry specimens failed by vertical cracking through the webs. The stresses in the webs of a hollow concrete block masonry unit under face-shell compression were investigated by means of a finite element analysis. The results of this analysis indicated probable locations of critical tensile regions in the web that would cause a tensile failure mode similar to that observed experimentally, particularly in cases where the applied eccentricity was close to the centroid of the section.

8.2. Recommendations

A substantial body of structural test data on masonry, acquired through three separate experimental research programs at the National Bureau of Standards, has been utilized to develop a rational analytical procedure for the prediction of the capacity of masonry walls under diverse configurations of transverse and compressive loads. The approach was found to be applicable to all the types of clay, concrete block and composite masonry tested. From a practical design standpoint, the proposed analytical approach offers the following advantages:

(1) It provides a consistent and unified method for ultimate design of masonry.
(2) The method is based on the same principles of elastic analysis that are used in working stress design recommended by the present masonry codes and standards, and a moment amplification factor similar to that now used in concrete and steel design.
(3) The method lends itself to direct consideration of the increased compressive strength of masonry in flexure and of requirements for consistent safety margins against failure.

In view of the large body of corroborative experimental data, the inclusion of the proposed analytical approach in masonry design standards should be given serious consideration. It is also recommended that the present provisions for determination of the modulus of elasticity of masonry be revised to reflect the findings of this study.

9. Appendix

9.1. Flexure–Compression Interaction

The equations in this section have been developed by the authors of reference [2] to predict the moment capacity of short masonry walls subjected to compression and bending. The governing equations are given without derivation.

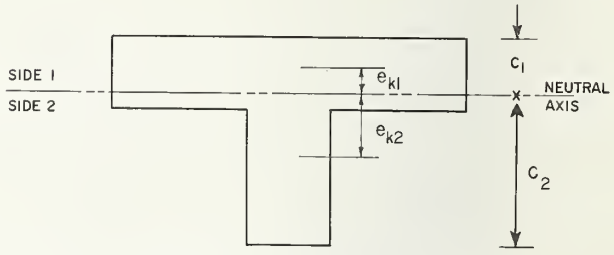

FIGURE 9.1. *Asymmetrical section.*

Assuming masonry has no tensile strength, the approximate flexure-compression interaction equations for the general case of nonsymmetric transformed section shown in figure 9.1 (masonry units of dissimilar composition), are given by the following equations:

For a cracked section

$$\left.\begin{aligned} M_{e1} &= Pc_1\left(1 - g_1 \cdot \frac{P}{aP_0}\right) \\ M_{e2} &= Pc_2\left(1 - g_2 \cdot \frac{P}{aP_0}\right) \\ g_1 &= \frac{aP_0}{P_{k1}}\left(1 - \frac{e_{k1}}{c_1}\right) \\ g_2 &= \frac{aP_0}{P_{k2}}\left(1 - \frac{e_{k2}}{c_2}\right) \\ P_{k1} &= \frac{aP_0}{1 + \frac{c_1}{c_2}} \\ P_{k2} &= \frac{aP_0}{1 + \frac{c_2}{c_1}} \\ e_{k1} &= \frac{I}{Ac_2} \\ e_{k2} &= \frac{I}{Ac_1} \\ P_0 &= Af'_m \end{aligned}\right\} \quad (9.1)$$

where

a = Flexural compressive strength coefficient defined below
A = Net area of transformed section
c_1, c_2 = Distances from neutral axis to outermost fibers in maximum compression
e_{k1}, e_{k2} = Kern eccentricities from centroid of transformed section in directions 1 and 2, respectively
f'_m = Compressive strength of masonry under axial load
I = Moment of inertia of net transformed section about its centroidal axis
M_{e1}, M_{e2} = Moment capacity of masonry, producing maximum compressive stress in outer fibers on sides 1 and 2, respectively
P = Axial compressive load on the cross section
P_{k1}, P_{k2} = Compressive loads capacity of masonry applied at kern eccentricities e_{k1} and e_{k2}, respectively
P_0 = Axial load capacity of masonry.

A note of explanation is needed with regard to the compressive strength f'_m. For a composite construction, such as a brick-block wall assembly, the axial compressive strengths of the two wythes may have different values. The lower of these two values defines f'_m to be used in these equations.

Coefficient "a" is a factor equal to, or greater than, unity to account for an apparent increase in masonry compressive strength from f'_m under axial compression to af'_m under combined flexure and compression. The expressions for P_{k1} and P_{k2} in eqs (9.1) are based on the simplifying assumption that the ratio of the moduli of elasticity of the two materials comprising the composite section is the same as the ratio of the flexural compressive strengths. In addition, the expressions for M_{e1} and M_{e2} in eqs (9.1) are approximate when the load is applied at an eccentricity greater than the kern eccentricity. However, for the case of solid rectangular section of noncomposite masonry, g assumes a value of 4/3 and the expression for M_e is no longer approximate.

For an uncracked section

$$\left.\begin{aligned} M_{e1} &= P_{k1}e_{k1}\frac{aP_0 - P}{aP_0 - P_{k1}} \\ M_{e2} &= P_{k2}e_{k2}\frac{aP_0 - P}{aP_0 - P_{k2}} \cdot \end{aligned}\right\} \tag{9.2}$$

The cracking line which separates the uncracked and cracked regions is defined by the equations

$$M_{k1} = M_{k2} = P_{k1}e_{k1} = P_{k2}e_{k2} \cdot \tag{9.3}$$

Equations (9.1) are applicable in the regions $P \leq P_{k1}$ and $P \leq P_{k2}$ and equations (9.2) are applicable in the regions $P \geq P_{k1}$ and $P \geq P_{k2}$. An interaction diagram based on $a = 1$ for an asymmetric composite section of 4-in brick and 4-in hollow block is reproduced from reference [2] and is shown in figure 9.2. Note that the M_e curve for a cracked section, obtained from eq (9.1), agrees reasonably well with the solid curve developed from cracked section theory.

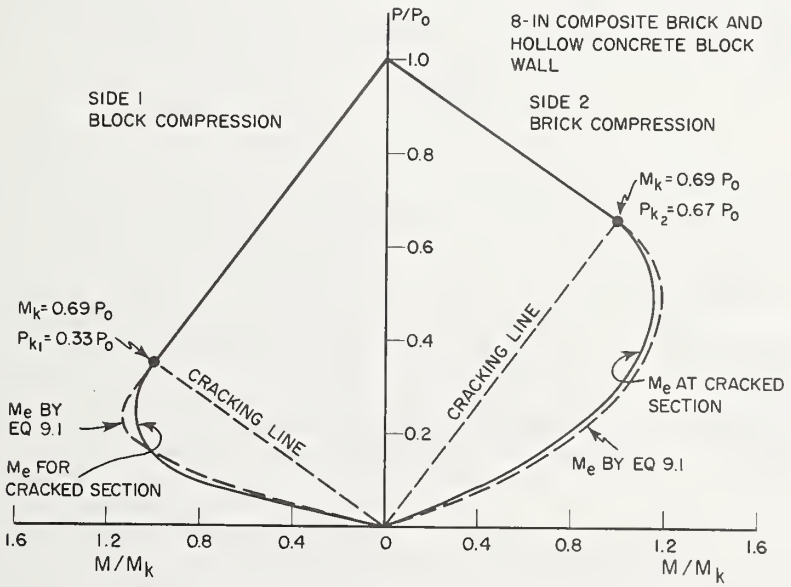

FIGURE 9.2. *Cross-sectional moment capacity of asymmetrical section.*

Equations (9.1) were derived on the basis of zero tensile strength of masonry. For large M/P ratios, failure will occur when the maximum flexural tensile strength of the specimen is developed. Assuming a nonzero tensile strength for masonry, the expressions for the cracking lines will become,

$$\left.\begin{aligned} M_{e1} &= \frac{f'_{t2} I}{c_2} + P e_{k1} \\ M_{e2} &= \frac{f'_{t1} I}{m c_1} + P e_{k2} \\ m &= \frac{E_1}{E_2} \end{aligned}\right\} \qquad (9.4)$$

where,

f'_{t1}, f'_{t2} = Flexural tensile strength of masonry on sides 1 and 2, respectively

E_1, E_2 = Modulus of elasticity in direction normal to bed joints of masonry on sides 1 and 2, respectively.

The moment capacity for the cracked section is the larger of the two values determined from eqs (9.1) and (9.4).

For a symmetric section, the interaction equations become considerably simpler. Thus, for a cracked section,

$$\left.\begin{aligned} Me &= Pc\left(1 - g\frac{P}{aP_0}\right) \\ g &= 2\left(1 - \frac{4I}{At^2}\right) \\ P_k &= \frac{aP_0}{2} \\ e_k &= \frac{I}{Ac} \\ P_0 &= Af'_m \end{aligned}\right\} \qquad (9.5)$$

and, for an uncracked section,

$$M_e = \frac{I}{Ac}(aP_0 - P). \qquad (9.6)$$

The cracking line is given by

$$M_k = P_k e_k \qquad (9.7)$$

or, in the case where $f'_t > 0$, by

$$M_e = \frac{f'_t I}{c} + P e_k. \qquad (9.8)$$

The moment capacity for the cracked section is the larger of the two values obtained from eqs (9.5) and (9.8).

9.2. Numerical Analysis of Hollow Concrete Block Unit in Compression

A finite element analysis of a hollow concrete block unit is made using a 100-kip compressive load applied at various eccentricities to the 6×32-in section shown in figure 4.1. The load is assumed to be transmitted from the face shells to the web through shear action. A Poisson ratio of 0.2 is assumed for the material. The results are displayed in figures 9.3 to 9.8.

The analytical model for the upper half of a block unit consists of 12 face shell beam elements and 48 rectangular plane stress web elements of equal size as indicated in figure 9.3. The web thickness is equal to the sum of web thicknesses of the actual section. Principal stresses and their orientation are plotted at the centroids of web elements as shown. Stresses are expressed in psi units and tension is assumed positive. The following differences between the idealized model and the actual specimen should be taken into consideration in the interpretation of the numerical results:

(1) In an actual block, face shell and web thickness varies with height and is on the average about 25 percent greater than assumed in the idealized model.

(2) Mortar was assumed to be confined to the face shell area. Examination of actual test specimens indicates a 25 to 50 percent mortar penetration over the web area.

(3) In an actual block, the joints between face shells and webs have smooth transitional fillets which were not considered in the idealized model.

In general, these assumptions will tend to overestimate and somewhat distort stresses in the web. In particular, the second assumption will amplify tension at the top while the effect of the third assumption would be to amplify stresses near the face shells relative to stresses elsewhere.

Figure 9.3 shows principal stresses in the web under concentric loading. At the top of the block, the two outer shells are under equal compression. Through shear transfer, a near uniform compression develops on the entire section halfway down the block as indicated by the lower stress diagram. The diagram on the right shows the stress distribution on the vertical plane of symmetry and describes a condition analogous to flexure in deep beams of rectangular cross section reinforced with vertical flanges at the supports [18]. The minimum principal tensile stress occurs at the top of the web in the horizontal direction midway between the two

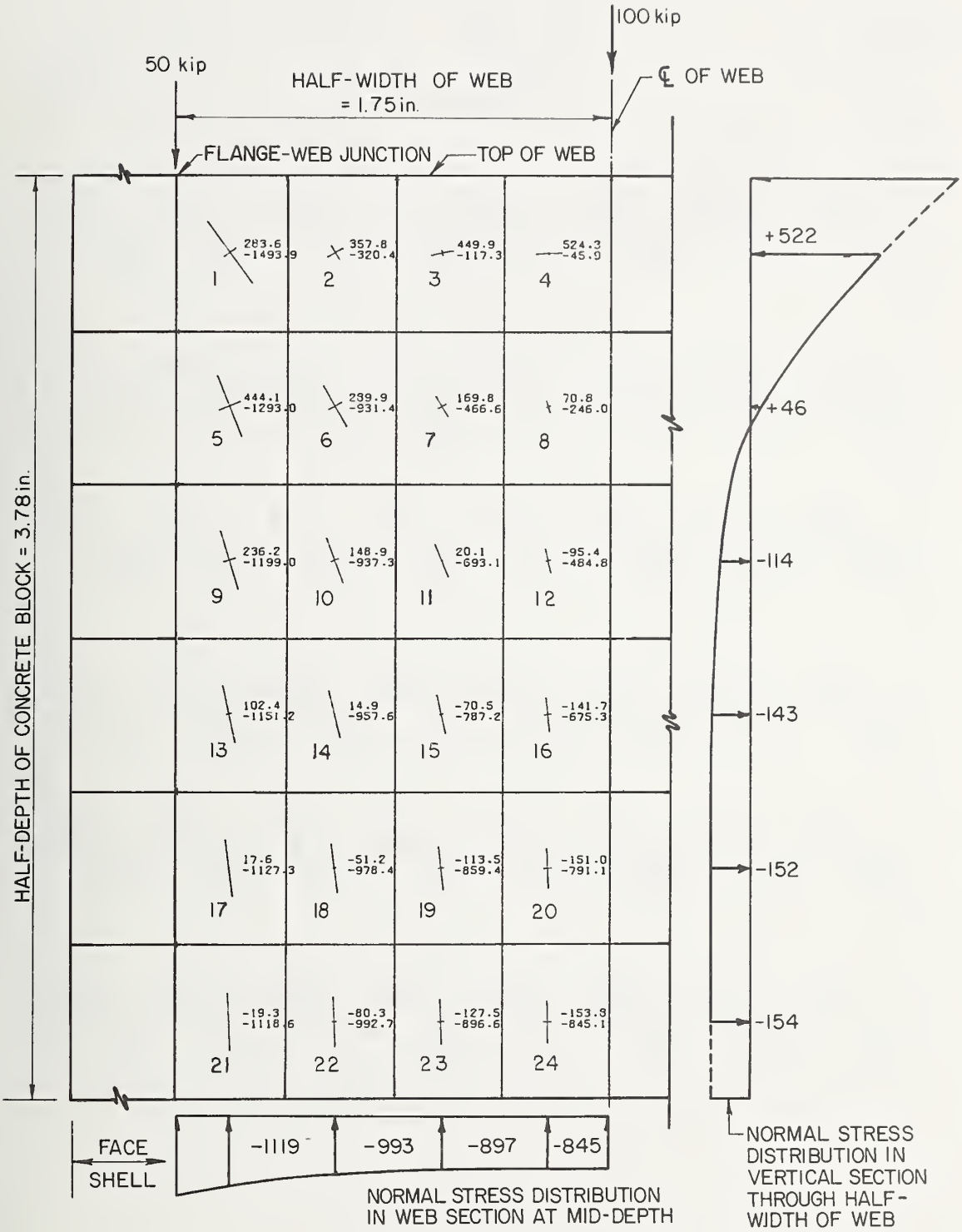

FIGURE 9.3. *Stress distribution in concrete web block at* e = 0.

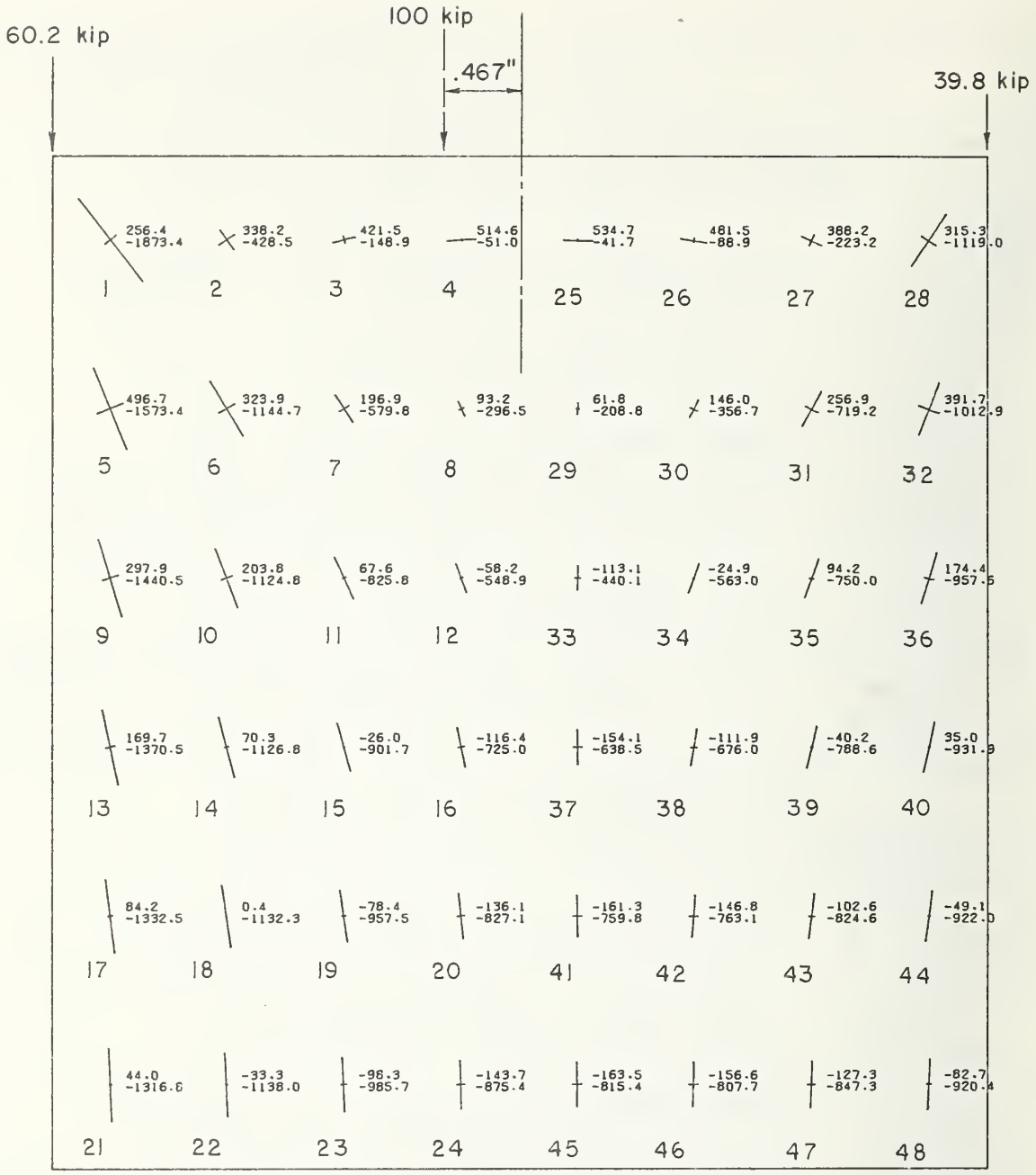

FIGURE 9.4. *Stress distribution in concrete block web at* e = *0.467 in.*

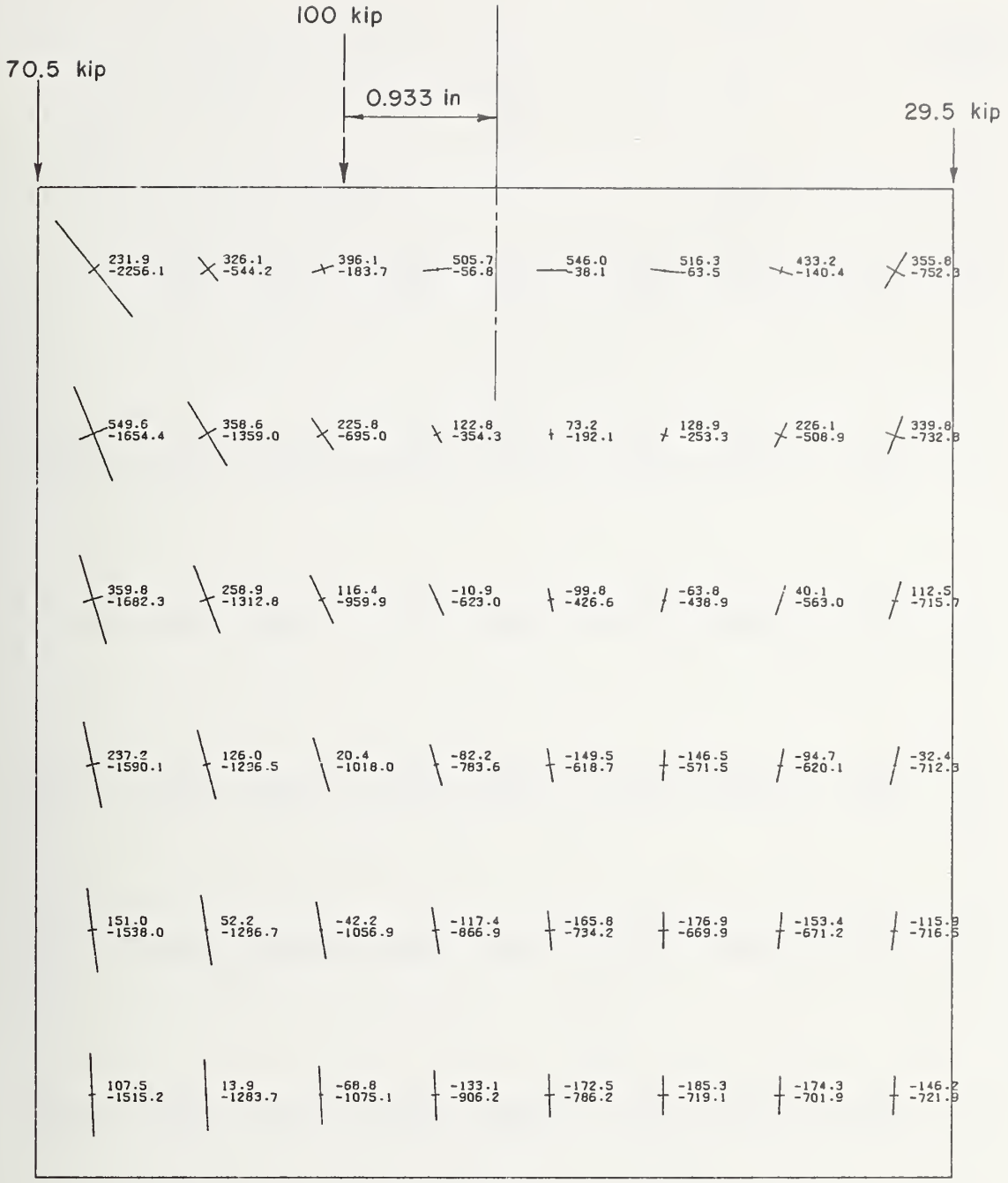

FIGURE 9.5. *Stress distribution in concrete block web at* e = *0.933 in.*

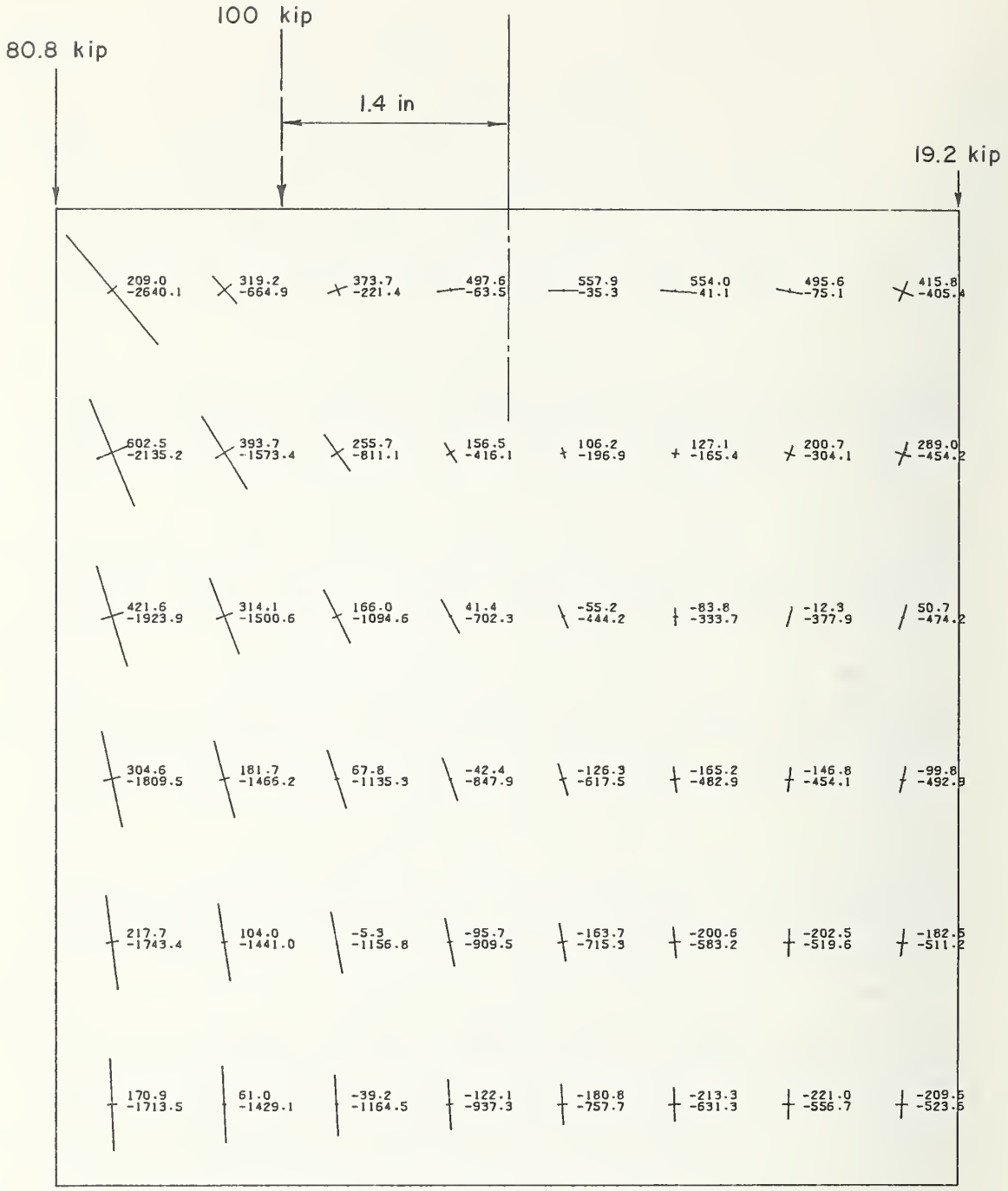

FIGURE 9.6. *Stress distribution in concrete block web at e=1.4 in.*

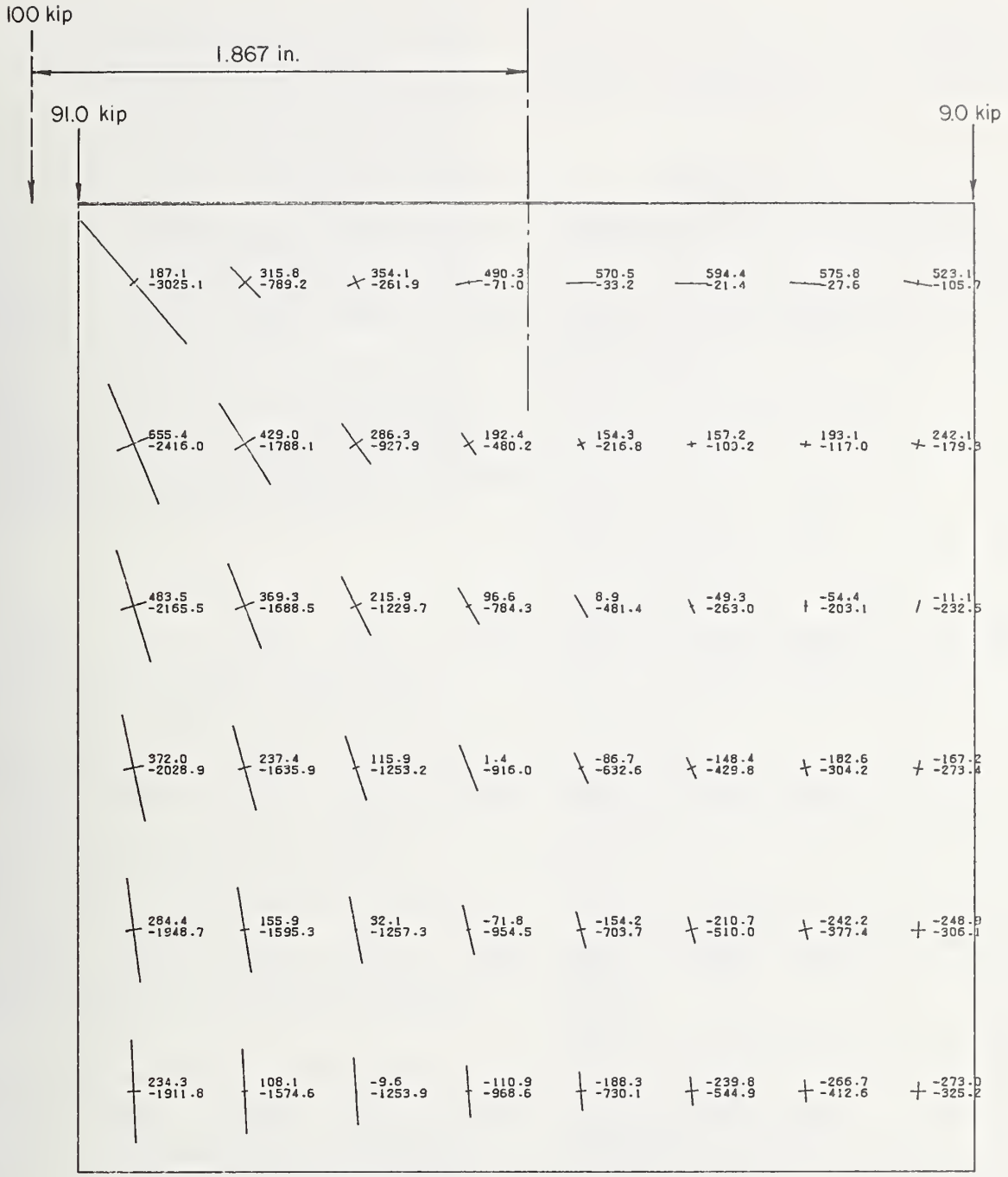

FIGURE 9.7. *Stress distribution in concrete block web at* e = *1.867 in.*

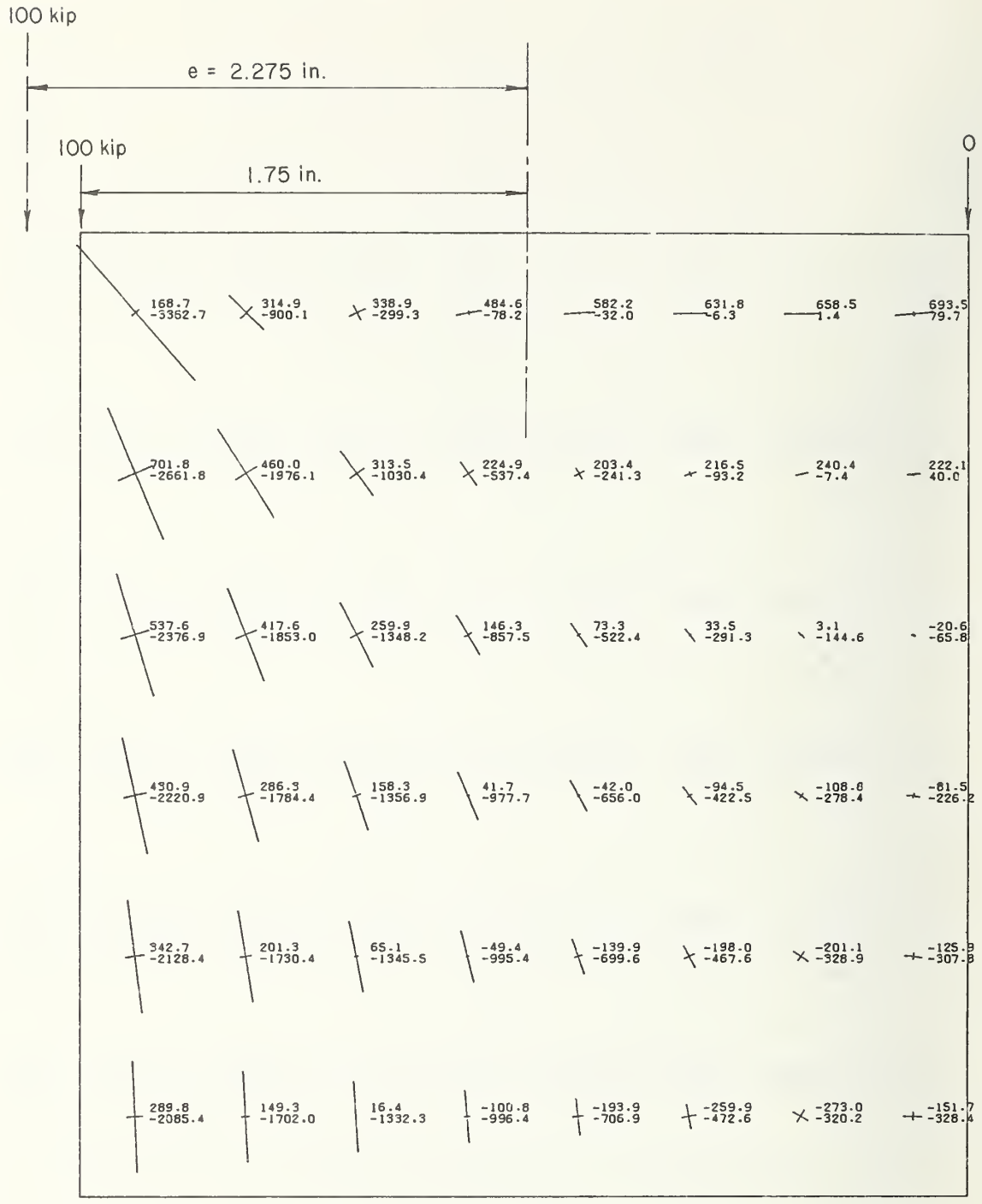

FIGURE 9.8. *Stress distribution in concrete block web at* e=2.275.

face shells. The maximum positive normal strain (extension) also occurs at the top of the web but near the face shell junction (element 1).

Figures 9.4 to 9.8 show the effect of eccentricity on the stress distribution in the web. Within the range of eccentricities considered, the change in the maximum tensile stress is small while a substantial increase in the maximum compressive stress occurs (element 1) with increasing eccentricity. Because tensile stresses are affected by factors such as partial presence of mortar on the web and possible dimensional differences in the blocks, considerable scatter could occur in tested capacity such as those observed in figures 7.8 and 7.9, and figure 6.3 of reference [1].

It is noted that with increasing eccentricity the maximum compressive stress in the web (element 1) increases at a much faster rate than the maximum tensile stress. Therefore, at larger load eccentricities, the maximum positive normal strains near the face shells are considerably in excess of normal tensile strain away from the face shells.

The contributions made by the following persons are gratefully acknowledged by the authors:

Robert D. Dikkers planned and executed the research program, and critically reviewed the report.

Felix Y. Yokel participated in the analysis of test results and critically reviewed the report.

Robert A. Crist, H. S. Lew, and Norman F. Somes critically reviewed the report.

Robert Livingston, from the Brick Institute of America, was the mason in charge of the construction of specimens.

Frank A. Rankin was in charge of all laboratory testing activities.

James Seiler, James Warfield, Lymus Payton, Mark LeMay, David Eichman, Harvey Shirley, Edward Butler, and Michael Hawkins collaborated in the testing of specimens.

Charles Bulik was responsible for coordination of instrumentation and data acquisition activities.

Randolph Williams was in charge of computer data processing.

William Appleton, Thomas Ruschell, and James Owen collaborated on electronic instrumentation.

Connie Roth, and Becky Hocker typed the several drafts of the report manuscript.

10. References

[1] Yokel, F. Y., Mathey, R. G., Dikkers, R. D., Compressive strength of slender concrete masonry walls, Nat. Bur. Stand. (U.S.), Bldg. Sci. Ser. 33, 32 pages (1970).

[2] Yokel, F. Y., Mathey, R. G., Dikkers, R. D., Strength of masonry walls under compressive and transverse loads, Nat. Bur. Stand. (U.S.), Bldg. Sci. Ser. 34, 74 pages (1971).

[3] Standard Method of Test for Bond Strength of Mortar to Masonry Units, ASTM E149–66 (1966).

[4] Standard Methods of Sampling and Testing of Brick, ASTM C67–66 (1966).

[5] Tentative Methods of Sampling and Testing Concrete Masonry Units, ASTM C140–65 (1965).

[6] Standard Specifications for Mortar for Unit Masonry, ASTM C270–68 (1968).

[7] Standard Specifications for Portland Cement, ASTM C150–70 (1970).

[8] Standard Specifications for Hydrated Lime for Masonry Purposes, ASTM C207–49 (1949).

[9] Standard Specifications for Aggregate for Masonry Mortar ASTM C144–70 (1970).

[10] Standard Method of Test for Air Content of Hydraulic Cement Mortar, ASTM C185–59 (1959).

[11] Standard Method of Test for Air Content of Freshly Mixed Concrete by the Pressure Method, ASTM C231–68 (1968).

[12] Structural Clay Products Institute, Building Code Requirements for Engineered Brick Masonry (August 1969).

[13] National Concrete Masonry Association, Specifications for the Design and Construction of Load-Bearing Concrete Masonry (1970).

[14] Standard Methods of Test for Compressive Strength of Masonry Assemblages, ASTM E447–72 (1972).

[15] Yokel, F. Y., Stability of Load Capacity of Members with No Tensile Strength, Journal of the Structural Division, Proceedings of the American Society of Civil Engineers (July 1971).

[16] Yokel, F. Y., Closure on Stability and Load Capacity of Members with No Tensile Strength, Journal of the Structural Division, Proceedings of the American Society of Civil Engineers (April 1973).

[17] Yokel, F. Y., Dikkers, R. D., Strength of Load Bearing Masonry Walls, Journal of the Structural Division, Proceedings of the American Society of Civil Engineers (May 1971).

[18] Leonhardt, F., Walther, R., Versuche an Wandartigen Trägern mit Unterschiedlicher Belastung, Lagerung und Bewehrung mit Schlussfolgerungen, Wilhelm Ernst & Sohn, Berlin (1966).

[19] Yokel, F. Y., Dikkers, R. D., Fattal, S. G., Closure on Strength of Load Bearing Masonry Walls, Journal of the Structural Division, Proceedings of the American Society of Civil Engineers (May 1973).

[20] Hilsdorf, H. K., Investigation into the Failure Mechanism of Brick Masonry Loaded in Axial Compression, International Conference on Masonry Structural Systems, University of Texas, Austin (1967).

[21] American Concrete Institute, Committee 531, Concrete masonry structures—design and construction, J. Am. Concr. Inst. **67**, Nos. 5 and 6 (1970).

[22] Uniform Building Code, International Conference of Building Officials, Whittier, California (1973).

[23] Standard Method of Test for Flexural Bond Strength of Masonry, ASTM E 518–74 (1974).

NBS-114A (REV. 7-73)

U.S. DEPT. OF COMM. BIBLIOGRAPHIC DATA SHEET	1. PUBLICATION OR REPORT NO. NBS-BSS 73	2. Gov't Accession No.	3. Recipient's Accession No.

4. TITLE AND SUBTITLE

Structural Performance of Masonry Walls Under Compression and Flexure

5. Publication Date June 1976

6. Performing Organization Code

7. AUTHOR(S) S. G. Fattal and L. E. Cattaneo

8. Performing Organ. Report No.

9. PERFORMING ORGANIZATION NAME AND ADDRESS

NATIONAL BUREAU OF STANDARDS
DEPARTMENT OF COMMERCE
WASHINGTON, D.C. 20234

10. Project/Task/Work Unit No. 4615130

11. Contract/Grant No.

12. Sponsoring Organization Name and Complete Address *(Street, City, State, ZIP)*

Brick Institute of America, McLean, Va. 22101
National Bureau of Standards, Washington, D. C. 20234
National Concrete Masonry Assoc., Arlington, Va.
The Departments of the Army, the Navy and the Air Force, Washington, D. C.

13. Type of Report & Period Covered Final

14. Sponsoring Agency Code

15. SUPPLEMENTARY NOTES

Library of Congress Catalog Card Number: 75-619305

16. ABSTRACT *(A 200-word or less factual summary of most significant information. If document includes a significant bibliography or literature survey, mention it here.)*

Ninety-five prisms and fifty-six walls of brick, concrete block and composite brick and block masonry construction were tested under various combinations of compressive and transverse loads. Constitutive relations for masonry are developed from test results. By using rational analysis it is shown that prism strength can be predicted on the basis of linear behavior at failure. It is also shown that wall strength can be predicted on the basis of prism strength when an appropriate allowance is made for the effect of wall slenderness on sectional capacity.

17. KEY WORDS *(six to twelve entries; alphabetical order; capitalize only the first letter of the first key word unless a proper name; separated by semicolons)* Brick; buckling; composite walls; compressive strength; concrete block; constitutive relations; flexural strength; masonry; masonry walls; mortar; slenderness ratio; standards; stiffness; structural stability; walls.

18. AVAILABILITY

[X] Unlimited

[ ] For Official Distribution. Do Not Release to NTIS

[X] Order From Sup. of Doc., U.S. Government Printing Office Washington, D.C. 20402, SD Cat. No. C13.29/2:73

[ ] Order From National Technical Information Service (NTIS) Springfield, Virginia 22151

19. SECURITY CLASS (THIS REPORT) UNCLASSIFIED

21. NO. OF PAGES 65

20. SECURITY CLASS (THIS PAGE) UNCLASSIFIED

22. Price $1.25

USCOMM-DC 29042-P74

(cut here)

ANNOUNCEMENT OF NEW PUBLICATIONS IN BUILDING SCIENCE SERIES

Superintendent of Documents,
Government Printing Office,
Washington, D.C., 20402

Dear Sir:

Please add my name to the announcement list of new publications to be issued in the series: National Bureau of Standards Building Science Series.

Name----------

Company----------

Address----------

City----------State----------Zip Code----------

(Notification key N-339)

U. S. GOVERNMENT PRINTING OFFICE : 1976 O - 593-885

NBS TECHNICAL PUBLICATIONS

PERIODICALS

JOURNAL OF RESEARCH reports National Bureau of Standards research and development in physics, mathematics, and chemistry. It is published in two sections, available separately:

• **Physics and Chemistry (Section A)**

Papers of interest primarily to scientists working in these fields. This section covers a broad range of physical and chemical research, with major emphasis on standards of physical measurement, fundamental constants, and properties of matter. Issued six times a year. Annual subscription: Domestic, $17.00; Foreign, $21.25.

• **Mathematical Sciences (Section B)**

Studies and compilations designed mainly for the mathematician and theoretical physicist. Topics in mathematical statistics, theory of experiment design, numerical analysis, theoretical physics and chemistry, logical design and programming of computers and computer systems. Short numerical tables. Issued quarterly. Annual subscription: Domestic, $9.00; Foreign, $11.25.

DIMENSIONS/NBS (formerly Technical News Bulletin)—This monthly magazine is published to inform scientists, engineers, businessmen, industry, teachers, students, and consumers of the latest advances in science and technology, with primary emphasis on the work at NBS. The magazine highlights and reviews such issues as energy research, fire protection, building technology, metric conversion, pollution abatement, health and safety, and consumer product performance. In addition, it reports the results of Bureau programs in measurement standards and techniques, properties of matter and materials, engineering standards and services, instrumentation, and automatic data processing.

Annual subscription: Domestic, $9.45; Foreign, $11.85.

NONPERIODICALS

Monographs—Major contributions to the technical literature on various subjects related to the Bureau's scientific and technical activities.

Handbooks—Recommended codes of engineering and industrial practice (including safety codes) developed in cooperation with interested industries, professional organizations, and regulatory bodies.

Special Publications—Include proceedings of conferences sponsored by NBS, NBS annual reports, and other special publications appropriate to this grouping such as wall charts, pocket cards, and bibliographies.

Applied Mathematics Series—Mathematical tables, manuals, and studies of special interest to physicists, engineers, chemists, biologists, mathematicians, computer programmers, and others engaged in scientific and technical work.

National Standard Reference Data Series—Provides quantitative data on the physical and chemical properties of materials, compiled from the world's literature and critically evaluated. Developed under a world-wide program coordinated by NBS. Program under authority of National Standard Data Act (Public Law 90-396).

NOTE: At present the principal publication outlet for these data is the Journal of Physical and Chemical Reference Data (JPCRD) published quarterly for NBS by the American Chemical Society (ACS) and the American Institute of Physics (AIP). Subscriptions, reprints, and supplements available from ACS, 1155 Sixteenth St. N. W., Wash. D. C. 20056.

Building Science Series—Disseminates technical information developed at the Bureau on building materials, components, systems, and whole structures. The series presents research results, test methods, and performance criteria related to the structural and environmental functions and the durability and safety characteristics of building elements and systems.

Technical Notes—Studies or reports which are complete in themselves but restrictive in their treatment of a subject. Analogous to monographs but not so comprehensive in scope or definitive in treatment of the subject area. Often serve as a vehicle for final reports of work performed at NBS under the sponsorship of other government agencies.

Voluntary Product Standards—Developed under procedures published by the Department of Commerce in Part 10, Title 15, of the Code of Federal Regulations. The purpose of the standards is to establish nationally recognized requirements for products, and to provide all concerned interests with a basis for common understanding of the characteristics of the products. NBS administers this program as a supplement to the activities of the private sector standardizing organizations.

Federal Information Processing Standards Publications (FIPS PUBS)—Publications in this series collectively constitute the Federal Information Processing Standards Register. Register serves as the official source of information in the Federal Government regarding standards issued by NBS pursuant to the Federal Property and Administrative Services Act of 1949 as amended, Public Law 89-306 (79 Stat. 1127), and as implemented by Executive Order 11717 (38 FR 12315, dated May 11, 1973) and Part 6 of Title 15 CFR (Code of Federal Regulations).

Consumer Information Series—Practical information, based on NBS research and experience, covering areas of interest to the consumer. Easily understandable language and illustrations provide useful background knowledge for shopping in today's technological marketplace.

NBS Interagency Reports (NBSIR)—A special series of interim or final reports on work performed by NBS for outside sponsors (both government and non-government). In general, initial distribution is handled by the sponsor; public distribution is by the National Technical Information Service (Springfield, Va. 22161) in paper copy or microfiche form.

Order NBS publications (except NBSIR's and Bibliographic Subscription Services) from: Superintendent of Documents, Government Printing Office, Washington, D.C. 20402.

BIBLIOGRAPHIC SUBSCRIPTION SERVICES

The following current-awareness and literature-survey bibliographies are issued periodically by the Bureau:

Cryogenic Data Center Current Awareness Service

A literature survey issued biweekly. Annual subscription: Domestic, $20.00; foreign, $25.00.

Liquefied Natural Gas. A literature survey issued quarterly. Annual subscription: $20.00.

Superconducting Devices and Materials. A literature survey issued quarterly. Annual subscription: $20.00. Send subscription orders and remittances for the preceding bibliographic services to National Bureau of Standards, Cryogenic Data Center (275.02) Boulder, Colorado 80302.

Electromagnetic Metrology Current Awareness Service Issued monthly. Annual subscription: $24.00. Send subscription order and remittance to Electromagnetics Division, National Bureau of Standards, Boulder, Colo. 80302.

U.S. DEPARTMENT OF COMMERCE
National Bureau of Standards
Washington, D.C. 20234

OFFICIAL BUSINESS

Penalty for Private Use, $300

POSTAGE AND FEES PAID
U.S. DEPARTMENT OF COMMERCE
COM-215

U.S.MAIL

SPECIAL FOURTH-CLASS RATE
BOOK

AMERICAN REVOLUTION BICENTENNIAL 1776-1976

75 YEARS NBS 1901-1976